ABSTRACT

Detailed Molecular and Isotopic Characterization of Carbonaceous Aerosols to Assess Air Quality Issues in Urban Areas: the San Francisco Bay Area and the Houston Metropolitan Area

Subin Yoon, Ph.D.

Mentor: Rebecca J. Sheesley, Ph.D.

The objective of this dissertation is to provide detailed characterization of carbonaceous organic aerosols to better understand major sources of particulate matter (PM) and their atmospheric formation in an oxidizing and highly complex urban atmosphere. For this dissertation, optimized radiocarbon (^{14}C) and source characterization techniques were applied to PM samples from the Houston Metropolitan Area and the San Francisco Bay Area.

The San Francisco Bay area study was focused on identifying seasonal trends (winter and non-winter) and sources of elemental carbon (EC). The study required isolation of EC for ^{14}C-based source apportionment. Chemical mass balance model (CMB) of EC and ^{14}C-based total organic carbon (TOC; OC + EC) were also included for comparison of source apportionment methods and different carbonaceous aerosol fractions, respectively. Sources of EC and TOC were similar at most of the sites while a few sites (e.g. San Francisco and Napa) were distinctively more impacted by fossil fuel or contemporary/biomass burning sources. The winter season had significantly larger TOC

concentration due to meteorological conditions and changes in emissions (e.g. increased residential wood smoke). Relatively good agreement between the ^{14}C-EC- and CMB-EC- was observed for both seasons.

The first and second Houston studies focused on identifying diurnal and temporal trends of aerosols using both fine and coarse PM and contribution of secondary organic carbon during periods of poor air quality (i.e. high ozone and PM), respectively. The largest concentrations of fine EC and BC concentrations occurred during the mornings while periods of enhanced TOC was driven by an increase in the fine PM. Interestingly, a relatively large contribution of coarse EC was measured in Houston. Based on the ^{14}C and CMB analysis, Houston's carbonaceous aerosols are largely from secondary biogenic sources while secondary fossil contribution was highly variable. Furthermore, the poor air quality period in the Houston metropolitan area was driven by favorable meteorological conditions (i.e. Bay Breeze) providing stagnant atmospheric conditions, allowing for accumulation and photooxidation of fossil fuel emissions.

Overall, the study results provided up-to-date characterization and source apportionment of less studied carbonaceous aerosols fractions at two major U.S. urban coastal regions.

Detailed Molecular and Isotopic Characterization of Carbonaceous Aerosols to Assess Air Quality Issues in Urban Areas: The San Francisco Bay Area and the Houston Metropolitan Area

by

Subin Yoon, B.A.

A Dissertation

Approved by the Department of Environmental Science

_____

George P. Cobb, Ph.D., Chairperson

Submitted to the Graduate Faculty of
Baylor University in Partial Fulfillment of the
Requirements for the Degree
of

Doctor of Philosophy

Approved by the Dissertation Committee

_____

Rebecca J. Sheesley, Ph.D., Chairperson

_____

Sascha Usenko, Ph.D.

_____

Erica D. Bruce, Ph.D.

_____

William Hockaday, Ph.D.

_____

James Fulton, Ph.D.

Accepted by the Graduate School

August 2020

_____

J. Larry Lyon, Ph.D., Dean

Page bearing signatures is kept on file in the Graduate School.

TABLE OF CONTENTS

LIST OF FIGURES

LIST OF TABLES

LIST OF ABBREVIATIONS

$\Delta^{14}C_{cont}$	contemporary end member
$\Delta^{14}C_{fossil}$	fossil end member
µg	micrograms
µL	microliter
µm	micrometers
^{12}C	most abundant stable carbon isotope; carbon-12
^{14}C	radiocarbon
%BB	percent biomass burning
%Cont	percent contemporary
A	afternoon
ACSM	aerosol chemical speciation monitor
AGL	above ground level
AK	Alaska
AMS	accelerator mass spectrometry
BAAQMD	Bay Area Air Quality Management District
BAAQMD-EI	Bay Area Air Quality Management District Emission Inventory for $PM_{2.5}$
BB	biomass burning
BBOA	biomass burning organic aerosol
BC	black carbon
BI	Bethel Island
BSTFA-TMCS	*N*,*O*-bis(trimethylsilyl)trifluoroacetamide trimethylchlorosilane
BT	back trajectory
BVOC	biogenic volatile organic carbon
C	light scattering
CA	California
CAMS	Continuous Ambient Monitoring Stations
CAMx	Comprehensive Air Quality Model with Extensions
CARB	California Air Resources Board
CARB-EI	California Air Resources Board Black Carbon Emission Inventory
CBSA	core based statistical areas
CC	carbonate carbon
CH	Switzerland
Cl	chloride
CMB	chemical mass balance
CN	China
CO	carbon monoxide
Con	Concord
CR	Conroe
Cup	Cupertino
D	day

DISCOVER-AQ	Deriving Information on Surface Conditions from Column and Vertically Resolved Observations Relevant to Air Quality
EC	elemental carbon
EI	emissions inventory
EPA	U.S. Environmental Protection Agency
ES	Spain
ESE	east-southeast
f_{cont}	fraction contemporary carbon
f_{fossil}	fraction fossil carbon
F_M	fraction of modern carbon
GC-ARCH	Gulf Coast Aerosol Research and Characterization
GC-MS	gas chromatography mass spectrometry
h	hour
HCl	hydrochloric acid
HDD	heavy duty diesel
HGB	Houston-Galveston-Brazoria
HOA	hydrocarbon-like organic aerosol
HR-ToF-AMS	high resolution – time of flight – aerosol mass spectrometer
HSC	Houston Shipping Channel
HYSPLIT	Hybrid Single Particle Lagrangian Integrated Trajectory
IC	ion chromatography
IN	India
IS	internal standards
IT	Italy
K	potassium
LO-OOA	less oxidized oxygenated organic aerosol
LP	La Porte
MAQL	mobile air quality laboratory
MC	Manvel Croix
MO-OOA	more oxidized oxygenated organic aerosol
MS	mass spectrometry
MT	Moody Tower
MV	Maldives (Chapter 2)
MV	medium volume (Chapter 3)
MVE	motor vehicle exhaust
m/z	mass-to-charge ratios
N	night
Nap	Napa
NASA	National Aeronautics and Space Administration
NIOSH	National Institute of Occupational Safety and Health
NNE	north-northeast
NO	nitric oxide
NO	Norway (Chapter 2)
NO_x	nitrogen oxides; nitric oxide and nitrogen dioxide
NO_2	nitrogen dioxide
NO_3	nitrate

NR-PM_1	non-refractory submicron particulate matter
NOSAMS	National Ocean Sciences Accelerator Mass Spectrometry
NW	non-winter
nss K	non sea salt potassium
O_3	ozone
OA	organic aerosols
OC	organic carbon
OC/EC	organic carbon to elemental carbon ratio
OOA	oxygenated organic aerosol
PAH	polycyclic aromatic hydrocarbon
PM	particulate matter
PM_{TSP}	total suspended particulate matter
$PM_{TSP-2.5}$	coarse particulate matter calculated taking the difference between TSP and fine particulate matter
$PM_{2.5}$	fine particulate matter with an aerodynamic diameter smaller than 2.5 µm
PM_{10}	coarse particulate matter with an aerodynamic diameter smaller than 10 µm
PyrC	pyrolyzed OC
PMF	positive matrix factorization
POA	primary organic aerosol
POC	primary organic carbon
QFF	quartz fiber filter
r^2	coefficient for linear least squares regression
R(ATN)	shadowing effect
RU	Russia
S	south
SE	southeast (Chapter 3)
SE	Sweden (Chapter 2)
SF	San Francisco
SHARP	Study of Houston Atmospheric Radical Precursors
SOA	secondary organic aerosol
SOC	secondary organic carbon
SP	San Pablo
SR	San Rafael
SSA	single scattering albedo
SV-OOA	semi-volatile organic aerosol
TEOM	tapered element oscillating microbalance
TexAQS	Texas Air Quality Study
TCEQ	Texas Commission on Environmental Quality
TOC	total organic carbon; organic and elemental carbon
TOR	thermal optical reflectance
TSP	total suspended particulate
TX	Texas
U.S.	United States
UT	Utah

VOC	volatile organic carbon
W	winter

ACKNOWLEDGMENTS

Most importantly, I would like to thank Dr. Sheesley for her mentorship, support, and encouragement throughout my graduate career. Truly, through her supervision and patience was I able to complete this doctorate degree. A special thanks to Dr. Sascha Usenko for his support and guidance. Additionally, I would like to acknowledge my committee members including Dr. Erica Bruce, Dr. Jamie Fulton, and Dr. Bill Hockaday for their insightful comments and guidance through this doctorate journey.

I would like to recognize Baylor University's Department of Environmental Science, especially Mrs. Kristie Curttright and Mr. Doug Nesmith for their generous support and assistance. I would also like to recognize the institutions that provided the financial support which made my research possible. These agencies include the Texas Commission on Environmental Quality Air Quality Research Program, the C. Gus Glasscock Jr. Endowed Fund for Excellence in Environmental Science, and the Bay Area Air Quality Management District.

I would like to acknowledge my previous and current Environmental Science colleagues including Dr. Tate E. Barrett, Dr. Adelaide Clark, Stephanie Ortiz, Claire Moffett, Sujan Shrestha, Zach C. Winfield, Farzaneh Mansouri, Marie Stephensen, Sarah Guberman VerPloeg, Meghan Guagenti, Dr. Jing Lui and Abhilasha Acharya. Also, a special thanks to Grace Aquino for the many hours she spent editing and re-editing my manuscripts. Thank you all for your support, guidance, knowledge, expertise, time, and friendship! My Waco friends have been a wonderful support system during my graduate career including Elissa Henry, Solange Balikunde, Pastor Jo and the members of Korean

Church of Waco. Thank you all for your love, prayers, and friendships. I will cherish them always.

Lastly, I would like to express my deepest gratitude to my amazing family for the many years of support, encouragement and at times reprieve during this arduous and at times very lonely journey. You guys have been my rock through it all! Thanks Mom, Dad and Billy! And a final shout out to Ben Yoo: my study buddy, therapist, uber driver, life coach, cheer leader and comedian extraordinaire! You're the best!

ATTRIBUTIONS

Subin Yoon assisted with the conceptualization, methodology, validation, formal analysis, investigation, data curation and visualization for the Houston and San Francisco Bay Area studies. She also wrote, reviewed and edited the *Biomass and Fossil Fuel Combustion Contributions to Elemental Carbon across the San Francisco Bay Area* (Chapter Two), *Fine and Coarse Carbonaceous Aerosol in Houston, TX during DISCOVER-A* (Chapter Three) and *Apportioned Primary and Secondary Organic Aerosol During Pollution Events of DISCOVER-AQ Houston* (Chapter Four). Dr. Rebecca J. Sheesley assisted with conceptualization, supervision, project administration and funding acquisition for the Houston and San Francisco Bay Area studies. She has also assisted in the review and editing processes for the *Biomass and Fossil Fuel Combustion Contributions to Elemental Carbon across the San Francisco Bay Area* (Chapter Two), *Fine and Coarse Carbonaceous Aerosol in Houston, TX during DISCOVER-A* (Chapter Three) and *Apportioned Primary and Secondary Organic Aerosol During Pollution Events of DISCOVER-AQ Houston* (Chapter Four).

Dr. Sascha Usenko assisted with conceptualization and funding acquisition for the Houston studies. He has also assisted in the review and editing processes for *Fine and Coarse Carbonaceous Aerosol in Houston, TX during DISCOVER-A* (Chapter Three) and *Apportioned Primary and Secondary Organic Aerosol During Pollution Events of DISCOVER-AQ Houston* (Chapter Four). Dr. Tate E. Barrett assisted with the investigation and data curation for the Houston and San Francisco Bay Area studies. He has also assisted in the review and editing process for the manuscripts *Biomass and*

Fossil Fuel Combustion Contributions to Elemental Carbon Across the San Francisco Bay Area (Chapter Two) and *Apportioned Primary and Secondary Organic Aerosol During Pollution Events of DISCOVER-AQ Houston* (Chapter Four). Stephanie M. Ortiz and Dr. Adelaide E. Clark contributed with the investigation and data curation for the Houston studies. They have also assisted in the review and editing process for the manuscript *Apportioned Primary and Secondary Organic Aerosol during Pollution Events of DISCOVER-AQ Houston* (Chapter Four).

Dr. Rachelle M. Duvall and Dr. Lea Hildebrandt-Ruiz assisted on the conceptualization of the Houston studies and the review and editing process for the manuscript *Apportioned Primary and Secondary Organic Aerosol during Pollution Events of DISCOVER-AQ Houston* (Chapter Four). Dr. James H. Flynn III, Dr. Robert J. Griffin, Dr. Jeffrey K. Bean, Dr. Cameron B. Faxon and Dr. Yu Jun Leong have all assisted in the review and editing process for the manuscript *Apportioned Primary and Secondary Organic Aerosol during Pollution Events of DISCOVER-AQ Houston* (Chapter Four). Dr. Barry L. Lefer assisted in funding acquisition for the Houston study.

DEDICATION

To my formidable but always loving grandmother, Sunjung Lee.

CHAPTER ONE

Introduction

Particle pollution is a major concern in urban areas where exposure to particulate matter (PM) can be significant due to densely populated and industrialized cities. Respirable PM, which includes fine PM ($PM_{2.5}$; particulates with an aerodynamic diameter less than 2.5 μm) and coarse PM (PM_{10}) is known to negatively impact human health causing respiratory (Dockery and Pope, 1994), cardio-pulmonary (Brook et al., 2010; Pope III et al., 2002) diseases, and overall increase in mortality (Laden et al., 2000). Extreme particle pollution during favorable atmospheric conditions can also produce "haze" events causing poor visibility and sharp spikes in respiratory-related hospital visits (Gao et al., 2015). For instance, the health-related economic costs due to particle pollution in Shanghai (Kan and Chen, 2004), Beijing (Gao et al., 2015), and the state of Washington (2009) are estimated to be at least $625, $254, and $190 million U.S. dollars per year, respectively. Carbonaceous aerosols are a significant component of respirable PM (Jimenez et al., 2009; Kanakidou et al., 2005), however, its formation processes are not well understood and it is difficult to chemically characterize this fraction of PM. Understanding the sources and formation processes of PM is vital for more effective management and to understand the impact of PM on other criteria air quality pollutants like ozone.

Aside from the negative influence to human health, atmospheric aerosol also affects Earth's radiative budget and impacts climate change (Andreae and Gelencsér, 2006; Chung et al., 2012; Hansen et al., 1997). Aerosols can directly impact radiative

forcing via absorption and scattering of incoming radiation (Fraser and Kaufman, 1985; Moise et al., 2015), or indirectly through cloud interactions (Novakov and Penner, 1993). The critical gaps in our understanding of the sources, processes, and optical properties of these carbonaceous aerosols are also uncertainties in global climate models.

The resultant air quality of an area is dependent on several factors which include emission sources, meteorology, the region's topography, and ecology. Urban areas have a plethora of anthropogenic emission sources and certain major U.S. urban areas are also near vegetated areas producing a mix of anthropogenic air masses with biogenic emissions. Recent observational studies have found that areas intersecting anthropogenic- and biogenic-heavy emissions experience significant contribution from secondary organic aerosols (SOA) (Bean et al., 2016; Gunsch et al., 2018; Xu et al., 2015). SOA constitutes a substantial fraction of carbonaceous aerosols (Hodzic et al., 2015; Kleindienst et al., 2007). However, there are unique challenges to characterizing and apportioning urban SOA. Similarly, biomass burning can be a major component of urban air pollution and poses challenges in terms of quantifying the impact across metropolitan areas. This dissertation work aims to identify the impact of secondary processes and biomass burning on Houston air quality and to improve our laboratories' ability to characterize both urban sources using a combination of analytical and statistical methods. The sample sites in this dissertation include several cities across the San Francisco Bay Area and Houston Metropolitan Area. Both metropolitan areas are some of the most populous in the U.S. and, based on ozone (O_3) and PM pollution, ranked as having the poorest air quality in the U.S. (Nolen et al., 2017).

Carbonaceous Aerosols

Carbonaceous organic aerosols refer to organic components (i.e. organic carbon; OC) and elemental carbon (EC, also referred to as black carbon, BC). These aerosols are a significant contributor to $PM_{2.5}$ mass (Jimenez et al., 2009; Kanakidou et al., 2005) and can be studied to better characterize PM sources and formation processes. In the U.S., major sources of anthropogenically produced OC and EC include industry (e.g. petrochemical processes, refineries, etc.), exhaust from gasoline and diesel vehicles and cooking. Major sources of naturally produced OC and EC include emissions from biogenic and marine sources. Biomass burning sources which include agricultural burning, wood smoke from residential wood burning and wildfires can be from either anthropogenic or natural sources. OC can be emitted by both combustion and non-combustion sources, while EC is specific to combustion processes. EC is the refractory carbon fraction of total organic carbon (TOC; OC+EC) and is highly light absorbing. Though EC and BC have been used interchangeably, the difference between the two is based on their measurement protocol: a thermal-optical method is used for measurement of EC (Chow et al., 2001) while an optical approach is used for BC (Hansen et al., 1983). The OC fraction is more susceptible to thermal degradation and volatilization during transport in the urban atmosphere. The OC fraction is composed of thousands of different polar and non-polar organic compounds including alkanes, polycyclic aromatic hydrocarbons, hopanes, steranes, acids, aldehydes, ketones, humic-like substances, cellulose. However, only 10-20% of the organic carbon compounds have been identified (El Haddad et al., 2011; Rogge et al., 1993).

Organic aerosols (OA) can also be distinguished based on their formation process. Primary organic aerosol (POA) are aerosols that are emitted directly into the atmosphere from their emission sources. Major sources of POA include motor vehicle exhaust (e.g. diesel and gasoline), coal combustion, industrial processes, meat cooking, biomass burning and emissions from biogenic sources. SOA is formed from the oxidation of volatile, or gas-phase, organic compounds; the new organic compounds have added oxygenated functional groups making the compounds more polar and lower in vapor pressure than their volatile precursors. These SOA compounds can form new particles or condense onto pre-existing PM (Kleindienst et al., 2007; Kroll and Seinfeld, 2008; Pandis et al., 1992). The SOA precursors are from biogenic or anthropogenic sources.

Bulk Carbon Measurements

The OC and EC concentrations were measured with a Sunset Laboratory's Carbon Analyzer (Tigard, OR, USA) using either the National Institute for Occupational Safety and Health (NIOSH) (Birch and Cary, 1996) or the Interagency Monitoring of Protected Visual Environments (IMPROVE) protocol (Chow et al., 1993). For this bulk carbon measurement method, a known filter area of a sampled quartz fiber filter is exposed to different atmospheres and temperature ranges while the carbon analyzer continuously monitors the transmittance or reflectance of light on the filter. A helium-neon (He-Ne) laser (at 678nm) is used as the light source in the carbon analyzer.

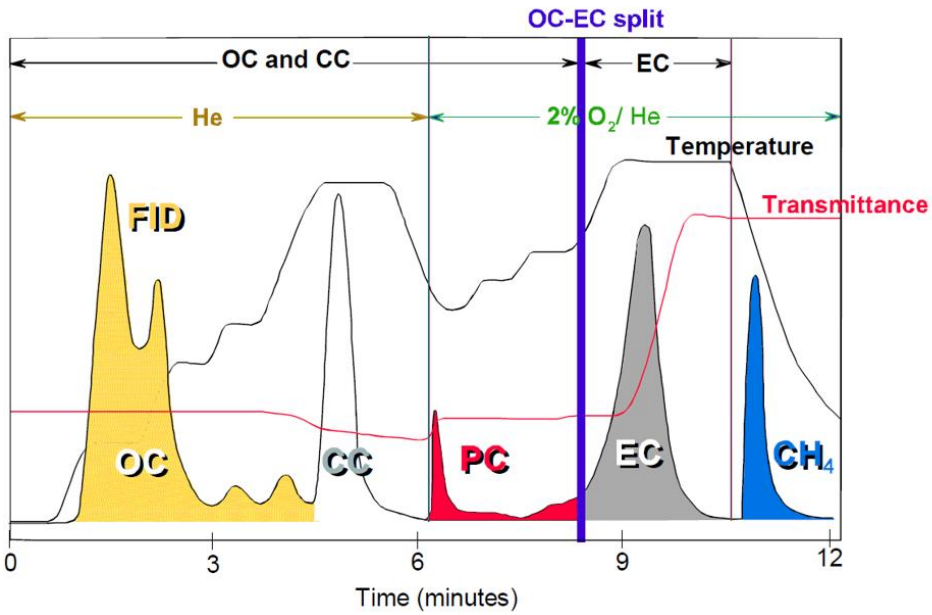

Figure 1.1. Thermogram of sample containing OC, calcium carbonate (CC), pyrolytic carbon (PyrC), and EC. Final peak is methane calibration peak. Also includes temperature ramp.

The NIOSH and IMPROVE protocols have three major steps. In the first step, the filter is exposed to a helium (He) atmosphere and the temperature is ramped up in four stages. For the NIOSH protocol the temperatures are 250°C (OC1), 500°C (OC2), 650°C (OC3), 820°C (OC4) and then drops down to 525°C. For the IMPROVE protocol the temperature is 120°C (OC1), 250°C (OC2), 450°C (OC3), and 550°C (OC4). Before the second set of temperature ramps the oven switches into a 10% oxygen/helium atmosphere mixture. For the NIOSH protocol the temperature is ramped to 650°C (EC1), 750°C (EC2), and 850°C (EC3). For the IMPROVE protocol the temperature is ramped to 550°C (EC1), 700°C (EC2), and 850°C (EC3). As the temperature drops, the final step is a methane (CH_4) spike that is injected into the FID after each run for calibration purposes. During the first two steps, carbon is desorbed from the QFF filters, oxidized to CO_2 by manganese dioxide, reduced to CH_4 in a methanator oven, and quantified using a

flame ionization detector (FID). The first step measures OC and potential concentrations of calcium carbonate (CC). During the first step, EC can be produced on the filter due to charring of OC on the filter. This charred carbon is referred to as pyrolytic carbon (PyrC) in this methodology. The PyrC is volatized from the filter in the 10% oxygen/helium atmosphere with the EC. Once this PyrC is volatilized, the transmittance (NIOSH) or reflectance (IMPROVE) value from the filter will return to its original value, which we define as the "split-point" or "split-time". Carbon evolving prior and post the split-point is considered OC and EC, respectively. The CC is sourced from mineral dust and is not likely to be in fine atmospheric aerosol samples. Though some Mediterranean studies have observed enhanced contribution of CC in their fine and coarse PM samples due to street abrasion or construction activities near their sampling sites(Perrone et al., 2011), samples from our study observed minimal contribution of CC (Yoon et al., 2018). Instruments blanks, sucrose standards, and triplicates are run regularly on the instrument for quality assurance/ quality control (QA/QC) purposes.

Isolation of EC Fraction

For radiocarbon (^{14}C) analysis of a TOC sample, an aliquot of the filter, or filters for a composite sample, is acidified, dried and sent for isotope analysis. The amount of filter needed is dependent on the filter loading, as the isotope analyses requires a minimum amount of carbon mass.

However, for ^{14}C analysis of an EC sample, the EC needs to be physically isolated from the bulk TOC. There are a couple of published methods for this EC isolation (Gustafsson et al., 2009; Szidat et al., 2004), this thesis work used the Gustafsson et al method of EC isolation. This method uses the multi-level temperature step NIOSH

protocol with a thermal optical transmittance instrument, as described in *Bulk Carbon Measurements* section, to determine the split-time and collect the EC from filter-based samples. To harvest the EC fraction preliminary OC-EC runs, using the carbon analyzer, are completed to establish the split-time for each sample. A split-time marks the transition of OC to EC during carbon analysis (Figure 1.1). This method operates under the assumption that PyrC volatilizes prior to native EC. Sensitivity analysis is typically conducted to assess the potential impact of the PyrC on ^{14}C of the EC (Barrett et al., 2015) Using the split-time, which is specific to each sample, a protocol is generated to volatilize all OC and PyrC leaving behind only the EC on the filter (i.e. EC harvest) (Figure 1.1). Even though there is typically minimal contribution of calcium carbonate (CC) in ambient PM samples, the EC isolated filters are acid fumigated using 1N HCl for removal of any CC contribution.

Source Apportionment Models

Current source apportionment methodologies include bottom-up approaches which uses emission factors, inventories and dispersion models to estimate ambient PM concentration. The top-down source apportionment methods use measurement and statistical treatment of ambient pollutants in models to identify and quantify contribution of pollution sources. There is great interest in assessing top-down approaches to apportion sources of POA and SOA. Some of these models include principal component analysis (PCA), positive matrix factorization (PMF) and chemical mass balance (CMB) model. The PCA and PMF methods apportion sources based on observations at the receptor site, however, they result in components or factors (e.g. less oxidized – oxygenated OA vs. more oxidized-oxygenated OA) (Jimenez et al., 2009; Leong et al.,

2017). Because these factors are calculated based on components that trend together in the ambient datasets, these can represent a single emission source, an aged source, or sources that are transported together.

The CMB model is a receptor based mathematical model produced by the Environmental Protection Agency (EPA) to use for air quality purposes (Coulter, 2004). The model combines chemical and physical characteristics of particles or gases at the sources and the receptor location to identify the presence of different sources and their contributions to concentrations at the receptor site. When there are *s* ambient aerosol samples, the model uses the following mathematical equation to calculate c_{ik} which is the concentration of component *i* in sample *k*.

$$c_{ik} = \sum_{j=1}^{m} f_{ij} g_{jk} \quad i = 1,2, \dots n \ \ and \ \ k = 1,2, \dots s$$

The g_{jk} is the contribution of emission source *j* to the total PM concentration during the *k*th sampling period. Assuming that the source signature f_{ij}, which is fraction of component *i* in emission source *j*, is not modified by processes occurring during atmospheric transport between the sources and at the receptor site. For the CMB studies in this dissertation, the components, *i*, used as tracers will include organic, inorganic and trace gas compounds. CMB analysis requires knowledge of the individual chemical tracer profiles for all relevant emission sources and does not account for chemical changes that might occur from the profile from the emitter and the receptor. Though CMB is a robust receptor model for POA in urban centers (Schauer et al., 1996), the model is not as easily applied for SOA apportionment.

^{14}C-based Source Apportionment

Another key tool for apportionment includes utilizing ^{14}C analysis. In fields like archeology and geology, ^{14}C analysis is widely used as a dating tool, determining the age of objects containing organic material (Stuiver and Polach, 1977). ^{14}C is naturally produced in the upper atmosphere by the interaction of atmospheric nitrogen and cosmic rays. The produced ^{14}C combines with atmospheric oxygen to form radioactive carbon dioxide (CO_2). Through carbon fixation, living organic materials retain a similar ^{14}C abundance to atmospheric CO_2, especially for newer biogenic sources (e.g. grass pruning, agricultural products) (Levin et al., 2010; Zotter et al., 2014). With the known half-life of ^{14}C (i.e. 5700 ± 40 years) ^{14}C dating of organic materials are possible.

For tracer-based analysis, ^{14}C is regarded as a robust tracer as the carbon isotope can retain its identity throughout atmospheric processes and transport (Lewis et al., 2004). In atmospheric chemistry studies, ^{14}C measurement is utilized as an apportioning technique to distinguish contributions of fossil to non-fossil fuel sources in carbonaceous aerosols (Al-Naiema et al., 2018; Barrett et al., 2015; Bean et al., 2016; Bernardoni et al., 2013; Sheesley et al., 2012; Yoon et al., 2018). Fossil fuel sources are depleted in ^{14}C (-1000‰) as the fuel is composed of dead organic material generally millions of years while contemporary biogenic sources have a ^{14}C abundance similar to ^{14}C abundance of atmospheric CO_2. For contemporary biogenic sources, it is important to consider the alteration of atmospheric ^{14}C abundances due to two major human influenced effects: the Suess and bomb pulse effects. The Suess effect is from increased fossil fuel burning causing dilution of atmospheric ^{14}C (Baxter and Walton, 1970). The bomb pulse effect is from nuclear weapons testing during the 1950-60s causing enhanced atmospheric ^{14}C

abundances due to additional neutron production in the atmosphere (Heal, 2014; Reimer et al., 2004). To account for these effects, ^{14}C abundances are commonly reported as a fraction modern carbon ($F^{14}C$) where the ratio of ^{14}C to ^{12}C is normalized to the defined "modern" standard (Heal, 2014).

The CO_2 and $\Delta^{14}C$ end-member values have been derived from previous tree growth models and measurements range between +28.1‰ and +107.5‰ for newer and older biogenic sources, respectively (Pye and Seinfeld, 2010; Tsigaridis et al., 2014). For TOC samples, the contemporary fraction includes primary biogenic emissions, biomass combustion, and secondary organic carbon from biogenic and biomass combustion precursors. The contemporary fraction of EC or BC, is from biomass burning sources(e.g. wood smoke, agricultural burning, etc.).

Air Quality in the San Francisco Bay Area

The state of California has historically been progressive with air quality research and regulation in the U.S. However, many of its cities and counties are regarded as having the worst air quality in the U.S. (Nolen et al., 2017). In the San Francisco Bay Area, regulation efforts have focused on reducing PM, specifically BC, by reducing fossil fuel combustion sources including implementing exhaust filters on diesel vehicles at the Port of Oakland and prohibiting prolonged idling of commercial diesel vehicles (~5min) (CARB). However, another significant source of aerosols has been from residential fires. Approximately 64% of households in the area contain at least one fireplace, pellet stove or wood stove (McLarney and Sarles, 2005). There has also been an emphasis on controlling aerosol emissions from residential biomass burning by implementing "no burn" days (McLarney and Sarles, 2005). With the implementation of these regulation,

there is interest to understand the efficacy of diesel regulations and their impact to the biomass burning in the region.

Air Quality in the Houston Metropolitan Area

Houston, TX is the fourth most populous city in the U.S. with approximately 2.3 and 6.9 million residents living in the city and metropolitan area, respectively (2019c). The city is home to dense industrial zones which include refineries, scrap metal yards, power plants, and cement factories. The Houston Ship Channel (HSC), the busiest seaport in the U.S., is also a large part of Houston's economic base, bringing in an average of 200 million tons of cargo per year (2019b). The area near the HSC is also lined with dense industrial zones housing petrochemical refineries, chemical plants, and heavy duty diesel traffic (Wallace et al., 2018). With this sprawling economic industry, Houston has seen a 20% population increase in the last decade (2019a). The city also has heavy traffic with averages of 173 million miles driven per day (Lubertino, 2019). Aside from the anthropogenic emissions, the Houston metropolitan area also includes biogenic sources from heavily forested/vegetated areas outside of the city and also has significant land coverage of urban forest canopy (~20%) within the city (Nowak et al., 2017). The complex mixture of natural and anthropogenic emission sources makes this city a prime location to study urban air quality.

References

Reduction Airborne Toxic Control Measure to Limit Diesel-Fueled Commerical Motor Vehicle Idling, California Air Resources Board.

2009. Health Effects and Economic Impacts of Fine Particle Pollution in Washington. Washington State Department of Ecology.

2019a. Houston Facts, Greater Houston Partnership.

2019b. Port Houston Overview, Port Houston: The International Port of Texas.

2019c. United States Census Burea: QuickFacts Houston city, Texas, United States Census Bureau.

Al-Naiema, I.M., Yoon, S., Wang, Y.-Q., Zhang, Y.-X., Sheesley, R.J., Stone, E.A., 2018. Source apportionment of fine particulate matter organic carbon in Shenzhen, China by chemical mass balance and radiocarbon methods. Environmental pollution 240, 34-43.

Andreae, M., Gelencsér, A., 2006. Black carbon or brown carbon? The nature of light-absorbing carbonaceous aerosols. Atmos. Chem. Phys. 6, 3131-3148.

Barrett, T., Robinson, E., Usenko, S., Sheesley, R., 2015. Source contributions to wintertime elemental and organic carbon in the western arctic based on radiocarbon and tracer apportionment. Environ. Sci. Technol. 49, 11631-11639.

Baxter, J., Walton, A., 1970. A theoretical approach to the Suess effect. Proceedings of the Royal Society of London. A. Mathematical and Physical Sciences 318, 213-230.

Bean, J.K., Faxon, C.B., Leong, Y.J., Wallace, H.W., Cevik, B.K., Ortiz, S., Canagaratna, M.R., Usenko, S., Sheesley, R.J., Griffin, R.J., 2016. Composition and Sources of Particulate Matter Measured near Houston, TX: Anthropogenic-Biogenic Interactions. Atmosphere 7, 73.

Bernardoni, V., Calzolai, G., Chiari, M., Fedi, M., Lucarelli, F., Nava, S., Piazzalunga, A., Riccobono, F., Taccetti, F., Valli, G., 2013. Radiocarbon analysis on organic and elemental carbon in aerosol samples and source apportionment at an urban site in Northern Italy. J. Aerosol Sci. 56, 88-99.

Birch, M., Cary, R., 1996. Elemental carbon-based method for monitoring occupational exposures to particulate diesel exhaust. Aerosol Sci. Technol. 25, 221-241.

Brook, R.D., Rajagopalan, S., Pope, C.A., Brook, J.R., Bhatnagar, A., Diez-Roux, A.V., Holguin, F., Hong, Y., Luepker, R.V., Mittleman, M.A., 2010. Particulate matter air pollution and cardiovascular disease: an update to the scientific statement from the American Heart Association. Circulation 121, 2331-2378.

Chow, J.C., Watson, J.G., Crow, D., Lowenthal, D.H., Merrifield, T., 2001. Comparison of IMPROVE and NIOSH carbon measurements. Aerosol Science & Technology 34, 23-34.

Chow, J.C., Watson, J.G., Pritchett, L.C., Pierson, W.R., Frazier, C.A., Purcell, R.G., 1993. The DRI thermal/optical reflectance carbon analysis system: description, evaluation and applications in US air quality studies. Atmospheric Environment. Part A. General Topics 27, 1185-1201.

Chung, C.E., Ramanathan, V., Decremer, D., 2012. Observationally constrained estimates of carbonaceous aerosol radiative forcing. Proc. Natl. Acad. Sci. 109, 11624-11629.

Coulter, T.C., 2004. EPA-CMB8.2 Users Manual, in: Agency, U.S.E.P. (Ed.), Air Quality Modeling Group.

Dockery, D.W., Pope, C.A., 1994. Acute respiratory effects of particulate air pollution. Ann. Rev. Pubic Health 15, 107-132.

El Haddad, I., Marchand, N., Wortham, H., Piot, C., Besombes, J.-L., Cozic, J., Chauvel, C., Armengaud, A., Robin, D., Jaffrezo, J.-L., 2011. Primary sources of PM2. 5 organic aerosol in an industrial Mediterranean city, Marseille.

Fraser, R.S., Kaufman, Y.J., 1985. The relative importance of aerosol scattering and absorption in remote sensing. IEEE transactions on geoscience and remote sensing, 625-633.

Gao, M., Guttikunda, S.K., Carmichael, G.R., Wang, Y., Liu, Z., Stanier, C.O., Saide, P.E., Yu, M., 2015. Health impacts and economic losses assessment of the 2013 severe haze event in Beijing area. Science of the Total Environment 511, 553-561.

Gunsch, M.J., Schmidt, S.A., Gardner, D.J., Bondy, A.L., May, N.W., Bertman, S.B., Pratt, K.A., Ault, A.P., 2018. Particle growth in an isoprene-rich forest: Influences of urban, wildfire, and biogenic air masses. Atmos. Environ. 178, 255-264.

Gustafsson, Ö., Kruså, M., Zencak, Z., Sheesley, R.J., Granat, L., Engström, E., Praveen, P., Rao, P., Leck, C., Rodhe, H., 2009. Brown clouds over South Asia: biomass or fossil fuel combustion? Science 323, 495-498.

Hansen, A., Rosen, H., Novakov, T., 1983. Aethalometer-an instrument for the real-time measurement of optical absorption by aerosol particles. Lawrence Berkeley Lab., CA (USA).

Hansen, J., Sato, M., Ruedy, R., 1997. Radiative forcing and climate response. J. Geophys. Res. Atmos. 102, 6831-6864.

Heal, M.R., 2014. The application of carbon-14 analyses to the source apportionment of atmospheric carbonaceous particulate matter: a review. Analytical and bioanalytical chemistry 406, 81-98.

Hodzic, A., Kasibhatla, P., Jo, D., Cappa, C., Jimenez, J., Madronich, S., Park, R., 2015. Rethinking the global secondary organic aerosol (SOA) budget: stronger production, faster removal, shorter lifetime. Atmospheric Chemistry & Physics Discussions 15.

Jimenez, J.L., Canagaratna, M., Donahue, N., Prevot, A., Zhang, Q., Kroll, J.H., DeCarlo, P.F., Allan, J.D., Coe, H., Ng, N., 2009. Evolution of organic aerosols in the atmosphere. Science 326, 1525-1529.

Kan, H., Chen, B., 2004. Particulate air pollution in urban areas of Shanghai, China: health-based economic assessment. Science of the Total Environment 322, 71-79.

Kanakidou, M., Seinfeld, J., Pandis, S., Barnes, I., Dentener, F., Facchini, M., Dingenen, R.V., Ervens, B., Nenes, A., Nielsen, C., 2005. Organic aerosol and global climate modelling: a review. Atmos. Chem. Phys. 5, 1053-1123.

Kleindienst, T.E., Jaoui, M., Lewandowski, M., Offenberg, J.H., Lewis, C.W., Bhave, P.V., Edney, E.O., 2007. Estimates of the contributions of biogenic and anthropogenic hydrocarbons to secondary organic aerosol at a southeastern US location. Atmos. Environ. 41, 8288-8300.

Kroll, J.H., Seinfeld, J.H., 2008. Chemistry of secondary organic aerosol: Formation and evolution of low-volatility organics in the atmosphere. Atmos. Environ. 42, 3593-3624.

Laden, F., Neas, L.M., Dockery, D.W., Schwartz, J., 2000. Association of fine particulate matter from different sources with daily mortality in six US cities. Environ. Health Perspect. 108, 941.

Leong, Y., Sanchez, N., Wallace, H., Karakurt Cevik, B., Hernandez, C., Han, Y., Flynn, J., Massoli, P., Floerchinger, C., Fortner, E., 2017. Overview of surface measurements and spatial characterization of submicrometer particulate matter during the DISCOVER-AQ 2013 campaign in Houston, TX. J. Air Waste Manag. Assoc. 67, 854-872.

Levin, I., Naegler, T., Kromer, B., Diehl, M., Francey, R.J., GOMEZ-PELAEZ, A.J., Steele, L.P., Wagenbach, D., Weller, R., Worthy, D.E., 2010. Observations and modelling of the global distribution and long-term trend of atmospheric 14CO2. Tellus B 62, 26-46.

Lewis, C.W., Klouda, G.A., Ellenson, W.D., 2004. Radiocarbon measurement of the biogenic contribution to summertime PM-2.5 ambient aerosol in Nashville, TN. Atmos. Environ. 38, 6053-6061.

Lubertino, G., 2019. Transportation Air Quality Conformity Report for the Houston-Brazoria-Galveston Region: 2045 Regional Transportation Plan. Houston-Galveston Area Council.

McLarney, T., Sarles, R., 2005. Spare the air tonight study: 2005-2006 winter wood smoke season., True North Research, Inc.

Moise, T., Flores, J.M., Rudich, Y., 2015. Optical properties of secondary organic aerosols and their changes by chemical processes. Chemical reviews 115, 4400-4439.

Nolen, J.E., Billings, P.G., Alexander, L.M., Bender, L.K., Van Vleet, D., Jump, S., 2017. State of Air 2017. American Lung Association.

Novakov, T., Penner, J., 1993. Large contribution of organic aerosols to cloud-condensation-nuclei concentrations. Nature 365, 823.

Nowak, D.J., Bodine, A.R., Hoehn, R.E.I., Edgar, C.B., Riely, G., Hartel, D.R., Dooley, K.J., Stanton, S.M., Hatfield, M.A., Brandeis, T.J., Lister, T.W., 2017. Houston's Urban Forest, 2015. United States Department of Agriculture, U.S. Forest Service.

Pandis, S.N., Harley, R.A., Cass, G.R., Seinfeld, J.H., 1992. Secondary organic aerosol formation and transport. Atmospheric Environment. Part A. General Topics 26, 2269-2282.

Perrone, M., Piazzalunga, A., Prato, M., Carofalo, I., 2011. Composition of fine and coarse particles in a coastal site of the central Mediterranean: Carbonaceous species contributions. Atmos. Environ. 45, 7470-7477.

Pope III, C.A., Burnett, R.T., Thun, M.J., Calle, E.E., Krewski, D., Ito, K., Thurston, G.D., 2002. Lung cancer, cardiopulmonary mortality, and long-term exposure to fine particulate air pollution. Jama 287, 1132-1141.

Pye, H.O., Seinfeld, J.H., 2010. A global perspective on aerosol from low-volatility organic compounds. Atmos. Chem. Phys. 10, 4377-4401.

Reimer, P.J., Brown, T.A., Reimer, R.W., 2004. Discussion: reporting and calibration of post-bomb 14C data. Radiocarbon 46, 1299-1304.

Rogge, W.F., Mazurek, M.A., Hildemann, L.M., Cass, G.R., Simoneit, B.R., 1993. Quantification of urban organic aerosols at a molecular level: identification, abundance and seasonal variation. Atmospheric Environment. Part A. General Topics 27, 1309-1330.

Schauer, J.J., Rogge, W.F., Hildemann, L.M., Mazurek, M.A., Cass, G.R., Simoneit, B.R., 1996. Source apportionment of airborne particulate matter using organic compounds as tracers. Atmos. Environ. 30, 3837-3855.

Sheesley, R.J., Kirillova, E., Andersson, A., Krusa, M., Praveen, P.S., Budhavant, K., Safai, P.D., Rao, P.S.P., Gustafsson, O., 2012. Year-round radiocarbon-based source apportionment of carbonaceous aerosols at two background sites in South Asia. J. Geophys. Res. Atmos. 117.

Stuiver, M., Polach, H.A., 1977. Discussion; reporting of C-14 data. Radiocarbon 19, 355-363.

Szidat, S., Jenk, T., Gäggeler, H., Synal, H.-A., Hajdas, I., Bonani, G., Saurer, M., 2004. THEODORE, a two-step heating system for the EC/OC determination of radiocarbon (14C) in the environment. Nuclear Instruments and Methods in Physics Research Section B: Beam Interactions with Materials and Atoms 223, 829-836.

Tsigaridis, K., Daskalakis, N., Kanakidou, M., Adams, P., Artaxo, P., Bahadur, R., Balkanski, Y., Bauer, S., Bellouin, N., Benedetti, A., 2014. The AeroCom evaluation and intercomparison of organic aerosol in global models. Atmos. Chem. Phys. 14, 10845-10895.

Wallace, H.W., Sanchez, N.P., Flynn, J.H., Erickson, M.H., Lefer, B.L., Griffin, R.J., 2018. Source apportionment of particulate matter and trace gases near a major refinery near the Houston Ship Channel. Atmos. Environ. 173, 16-29.

Xu, L., Guo, H., Boyd, C.M., Klein, M., Bougiatioti, A., Cerully, K.M., Hite, J.R., Isaacman-VanWertz, G., Kreisberg, N.M., Knote, C., 2015. Effects of anthropogenic emissions on aerosol formation from isoprene and monoterpenes in the southeastern United States. Proc. Natl. Acad. Sci. 112, 37-42.

Yoon, S., Fairley, D., Barrett, T.E., Sheesley, R.J., 2018. Biomass and fossil fuel combustion contributions to elemental carbon across the San Francisco Bay Area. Atmos. Environ. 195, 229-242.

Zotter, P., El-Haddad, I., Zhang, Y., Hayes, P.L., Zhang, X., Lin, Y.H., Wacker, L., Schnelle-Kreis, J., Abbaszade, G., Zimmermann, R., 2014. Diurnal cycle of fossil and nonfossil carbon using radiocarbon analyses during CalNex. J. Geophys. Res. Atmos. 119, 6818-6835.

CHAPTER TWO

Biomass and Fossil Fuel Combustion Contributions to Elemental Carbon across the San Francisco Bay Area

This chapter published as: Yoon, S.; Fairley, D.; Barrett, T.E.; Sheesley, R.J. Biomass and Fossil Fuel Combustion Contributions to Elemental Carbon across the San Francisco Bay Area. *Atmospheric Environment* **2018**. *195*, 229-242

Abstract

Ambient black carbon (BC) has detrimental effects on both human health and near-term global warming. To mitigate these negative effects, there have been significant efforts to reduce emissions of BC from anthropogenic and biomass burning sources in California's Bay Area since the 1960s. Recent reductions in BC have mainly been from fossil fuel combustion sources such as diesel but additional reductions may be needed for contemporary carbon sources like biomass burning and meat cooking. In this study, PM_{10} (particulate matter with aerodynamic diameter of less than or equal to 10μm) samples were collected at seven sites across the San Francisco Bay Area from November 2011 to October 2012 to create winter and non-winter composites for each site. Radiocarbon (^{14}C) abundance and chemical mass balance (CMB) modeling were used for source apportionment of ambient elemental carbon (EC, a proxy for BC). The ^{14}C abundance in the EC fraction was used to quantify the relative contributions of fossil carbon and contemporary carbon sources. The average biomass burning contributions are 48 ± 8% and 40 ± 5% for winter and non-winter seasons, respectively, across the Bay Area. Ambient concentrations of EC are approximately two to three times higher during the winter compared to the non-winter season, except for Cupertino. A CMB model, using

bulk aerosol composition and select inorganic compounds, was used to understand the contributions of natural gas combustion, gasoline exhaust, and diesel exhaust to fossil carbon as well as the contribution of biomass burning and meat cooking to contemporary carbon. The different apportionment methods for EC (^{14}C and CMB analysis) agree within 16 ± 12% for fraction fossil and biomass burning for both winter and non-winter season. The contemporary contribution to EC is much higher than estimated by current emission inventories, suggesting that the inventories may overestimate the contribution from fossil fuels, particularly diesel exhaust. The results from this study are compared to literature values from other ^{14}C-EC or BC studies from across the world.

Introduction

Since the 1960s, significant progress has been made in the Bay Area in reducing PM concentrations. Due to progressive regulations, including exhaust filters on diesel vehicles at the Port of Oakland and "no burn" days for residential fires, fine PM (aerodynamic diameter less than 2.5µm; $PM_{2.5}$), in particular black carbon (BC) has been reduced from an annual average concentration of 4 µg m^{-3} to less than 1 µg m^{-3} since the late 60s (Fairley, 2012; Kirchstetter et al., 2008b; Kirchstetter et al., 2017). Studies have found that the reduction in BC has contributed to negative radiative forcing (i.e. cooling effect) with an overall of -1.4 Wm^{-2} radiative forcing over California (Bahadur et al., 2011; Chow et al., 2010).

However, even with a threefold reduction in BC concentrations, there is still a need to understand high wintertime PM and BC concentrations and to determine which regulations would be most effective at further reducing emissions across the region. To that end, a recent year-long study was undertaken to determine source contributions to

BC at seven sites across the Bay Area. Previous efforts to understand BC in the Bay Area have focused on characterization of composition and quantification of potential impacts of diesel vehicle emissions (Dallmann et al., 2011; Dallmann et al., 2013; Kirchstetter et al., 2008a; Kirchstetter et al., 1999). BC concentrations have been declining in the Bay Area despite an increase in diesel vehicles and fuel consumption, likely due to implementation of cleaner diesel technology (i.e. diesel particulate filters at the Port of Oakland and reductions in fuel sulfur content) and regulations prohibiting prolonged idling of commercial diesel vehicles (~5 min) (Dallmann et al., 2011; Kirchstetter et al., 2017). With the improvement in diesel technology, it becomes more important to understand the contributions of contemporary carbon sources to BC (residential wood burning, cooking, agricultural burning, and wildfires) as these are also subject to increasing governmental regulations including the Bay Area Air Quality Management District's Wood-Burning Device Rule (http://www.baaqmd.gov/~/media/files/planning-and-research/rules-and-regs/reg-06/rg0603.pdf?la=en). Approximately 38 ± 2% of households in the area contain at least one fireplace, pellet stove or wood stove (Fairley, 2014). Households also reported that burning was most likely during the winter months between November and February (McLarney and Sarles, 2005). In addition to understanding seasonal trends of emission sources, it is also of great interest to determine the spatial trends across this region especially for regulation purposes. The sampling sites are part of the Bay Area Air Quality Management District's (BAAQMD) air pollution monitoring network and the chosen sites encompass locations (e.g. urban, residential, rural sites) that are varying distances from the coast. This study will provide better

understanding in how effective regulations have been/could be across the diverse Bay Area.

Radiocarbon (^{14}C) analysis is used as a means of source apportionment to distinguish contribution of fossil-fuel sources, which are depleted in ^{14}C (half-life of ^{14}C is 5730 years), from biogenic sources which have a ^{14}C signature similar to atmospheric ^{14}C. Source apportionment studies have used ^{14}C measurements to apportion total organic carbonaceous (TOC) aerosols to distinguish between contemporary (i.e. biomass burning, meat cooking, grass pruning, detritus matter, pollen, etc.) and fossil fuel sources (i.e. diesel and gasoline exhaust, natural gas, etc.) (Barrett et al., 2015; Sheesley et al., 2012; Zotter et al., 2014). In recent years, ^{14}C analysis of elemental carbon (EC) and TOC samples have been demonstrated to be a highly accurate method for quantifying contributions of fossil fuel versus biomass burning-derived EC in various locations (Barrett et al., 2015; Mouteva et al., 2017; Slater et al., 2002; Szidat et al., 2006; Zhang et al., 2014). However, very few ^{14}C studies of BC have been reported for urban areas in the US (Briggs and Long, 2016; Mouteva et al., 2017). A BC and EC source apportionment review from 2016 concluded that more studies which include inter-comparison of multiple source apportionment techniques, including ^{14}C, CMB and emission inventories are needed (Briggs and Long, 2016). This need for validation of apportionment methods and results is addressed in the current study by comparing results from ^{14}C, CMB and two emissions inventories in the Bay Area following the methods listed below. This study uses EC as a proxy for BC: BC refers to measurement of light-absorbing carbon quantified by optical methods, whereas, EC refers to refractory carbon determined by physical and chemical analyses (Chow et al., 2010). ^{14}C measurements of EC and TOC

were made to enable source apportionment of fossil vs contemporary carbon sources at seven sites across the Bay Area. CMB analysis was used to increase specificity of aerosol source apportionment from fossil (diesel and gasoline vehicle emissions) and contemporary (residential biomass burning, cooking and wildfires) sources for EC. Emission inventories for California and the Bay Area were also compared to the receptor-based apportionment of EC.

Experimental

Sample Collection

In accordance with BAAQMD's routine sampling, 24-hour PM_{10} samples were collected on a 1-in-6-day schedule at the seven sampling sites: Bethel Island, San Pablo, Concord, San Rafael, Napa, San Francisco and Cupertino (Figure. 2.1). All samples were collected on 8 x 10" pre-combusted Whatman QM-A (Ann Arbor, MI, USA) quartz fiber filters (QFFs) using Anderson and TISCH high volume air samplers (Table S1). For this study, filter samples collected during November 2011 to October 2012 were selected for analysis. Additionally, trace-gas measurements including CO and NO_2 were monitored using a Model 48*i* gas filter correction CO analyzer and a Model 42*i* NO-NO_2-NO_x analyzer (Thermo Fisher Scientific, Waltham, MA, USA), respectively. These trace gas data are included in the CMB model.

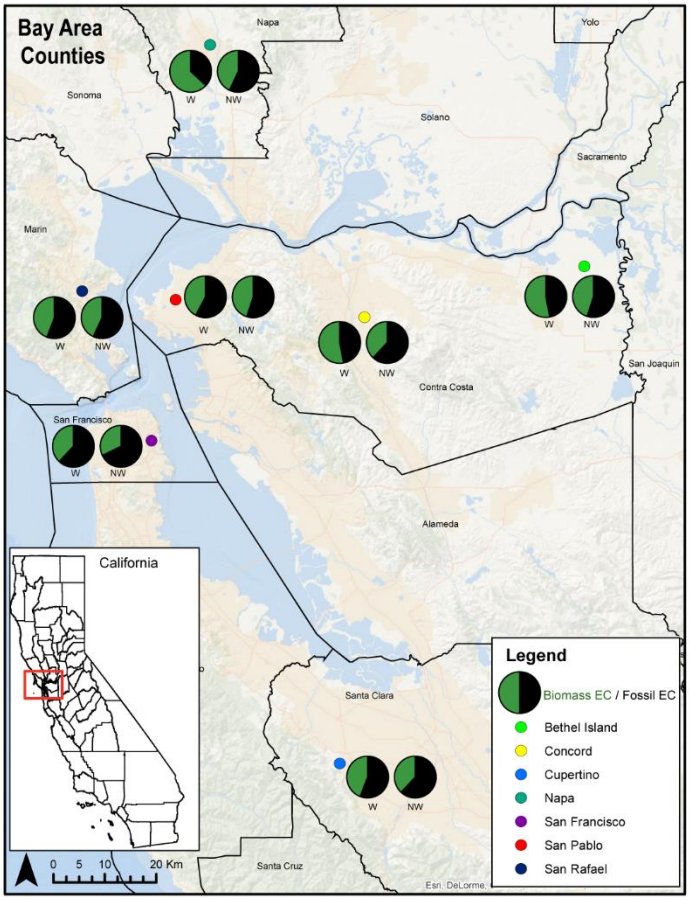

Figure 2.1. Map of the sampling sites in the San Francisco Bay Area map includes sampling sites, labels and counties, county-lines, and contribution of fossil fuel and biomass burning of the EC fraction for winter and non-winter seasons

Core Based Statistical Areas (CBSA) are geographic areas comprised of a county or counties which are socioeconomically tied to at least one urban center-based commute patterns (2012b). These seven sites are located in northern California and within three of the CBSAs: San Francisco-Oakland-Fremont, Santa Rosa-Petaluma, and Napa (Figure 2.1). The three CBSA regions combined, total to approximately 5 million residents (2012a; Malone, 2013). The sampling sites include urban, residential, rural, and highly industrialized areas. Location of the sites also vary in proximity to the coast.

- Bethel Island is rural site with a population of 2,137 (2012a), producing low levels of local emissions (Malone, 2013). The site is ideal to measure pollutant transport between California Central Valley and the San Francisco Bay Area. Easterly winds transport particles from the Central Valley which is one of the most productive agricultural regions in the California (Malone, 2013; Rinehart et al., 2006).
- Concord is the largest city in the Contra Costa County with a population of 122,067 (2012a). The city is located in the Diablo Valley. Local emission sources include major highways and two oil refineries at the north end of the valley (Claire, 2015). The sampling site is in a residential neighborhood (Malone, 2013).
- San Pablo has a population of 29,139 (2012a) and is heavily influenced by industry and high traffic volume including two major freeways. The sampling site is 1.2 miles downwind of the Chevron Refinery (Malone, 2013).
- San Rafael is the largest city in Marin county with a population of 57,713 (2012a). There is no industrial activity in the immediate area. However, the sampling site is close to a major transportation corridor (Malone, 2013).
- San Francisco is the second largest city in the Bay Area and largest among these sampling sites with a population of 805,235 (2012a). The densely populated city includes residents, year-round visitors and daytime commuters. The city also has some industry and has high traffic volume.
- Napa has historically had high levels of PM due to agricultural burning and fireplace use (Malone, 2013). It is also the largest city in Napa County with a population of 76,915 (2012a). The sampler at this site is situated a mile north of downtown Napa in a mixed residential and commercial neighborhood.

- Cupertino has two major highways passing through the city. This site was selected to determine the pollution impacts to residents from vehicle traffic and the Lehigh Cement Plant located one mile west of the site (Malone, 2013). The city has a population of 58,302 (2012a). The sampler was situated in Monta Vista Park (Malone, 2013).

Chemical Analysis of Tracers

Each PM_{10} filter was analyzed for OC, EC, potassium ion (K) and chloride ion (Cl). For EC and OC analysis, filters were punched and analyzed by a thermal optical reflectance (TOR) instrument using the IMPROVE protocol (Chow et al., 1993). For K and Cl analysis, the ions were extracted from QFFs using deionized water and analyzed using a Dionex Ion Chromatograph (IC) System 5000 (Thermo Fisher Scientific, Waltham, MA, USA). A substantial portion of the soluble K is from sea salt. In order to quantify the biomass burning portion, which is needed for the CMB analysis, the following equation is used to calculate non-sea salt K (nss K) (Fairley, 2012).

$$\text{nss K} = \text{K} - (0.011/0.55 * Cl) \quad (1)$$

Bulk carbon concentrations and inorganic ions were measured by the BAAQMD. All statistical analyses in this study use the Student t-test or the Mann Whitney, depending on whether the data set is symmetric or non-symmetric, respectively.

Description of EC Composites

Two seasonal composites were established based on the need to distinguish periods of heavy firewood and biomass burning practices which are generally during the months between November to February (McLarney and Sarles, 2005). Samples were

separated into two periods: “winter” (November-February) and “non-winter” (March-October) composites. To obtain an equal representation of samples collected during these two seasonally different composites, a protocol was used to select seven sampling dates for each site and composite in such a way that each day of the week and months were represented as evenly as possible. Portions of each of the filters from the selected days were combined into a winter and non-winter composite for the seven sites, creating 14 composites in total. Detailed sample contributions for the composites are included in the Supporting Information (Table A.2). These samples were composited for ^{14}C analysis of both EC and TOC. A description of TOC sample preparation is included in the next section.

The seasonal average ambient EC concentration calculation for EC based ^{14}C composites (^{14}C-EC) which used a mass-normalized contribution approach included equal EC mass representation from each filter sample. Each of the seven filter samples contributed approximately 15 µg of EC for a total of at least 100 µg of carbon mass – the mass needed for ^{14}C analysis. The protocol ensures that the composite equally represents the source contribution from each sample, which allows understanding the average contribution of sources regardless of daily concentration. However, in order to calculate the ambient concentration of contemporary and fossil EC, a different seasonal average ambient EC concentration needs to be calculated. The average seasonal EC concentration ($Avg\ EC_{ms}$) was calculated using the following equation:

$$Avg\ EC_{ms} = \sum_{f=1}^{g} a_{fs}\, b_f \quad (2)$$

where *m* is mass-based EC concentration, *s* is the seasonal composite, *f* is the filter sample, *a* is the relative contribution of EC mass, and *b* is the ambient EC concentration. The sum of the relative contribution of ambient EC concentrations from all filter samples, *g*, in *s* represents the average seasonal EC concentration. This representation of seasonal average ambient EC concentrations is slightly different (average difference of 14 ± 5%) from a true seasonal average ambient concentration which is used for the CMB-EC and ^{14}C-TOC measurements. The slight difference in the EC seasonal average ambient EC concentrations can be seen in Figure 2.6 (b,c,e, and f) when comparing apportionment of EC using ^{14}C to CMB analysis.

Preliminary OC-EC runs on all samples were completed to establish the split-time for the EC harvest by the IMPROVE method. The split-time is the time after which the laser reflectance of the filter is equal to the original reflectance filter while the instrument is operating under a He and O_2 atmosphere. This split-time marks the transition from combustion of OC, including pyrolyzed OC, from the filter to EC. This method operates under assumption that pyrolyzed OC (PyrC) volatilizes prior to native EC. Once the split-time was established, the run protocol was adjusted to stop at or near the split-time, which would allow removal of the filter with isolated EC. The protocols were adjusted to harvest 82% to 97% of the EC from each filter sample. Thus, the protocol is biased towards a more recalcitrant EC. There are uncertainties in this collection protocol related to PyrC, which are addressed below. Select samples were also tested for potential contribution of carbonate carbon (CC) to ambient concentration of EC. In the IMPROVE method, CC would be present in the EC4 fraction (Chow et al., 2001), so EC4 peaks in each thermogram were visually inspected and samples with the highest EC4 peaks were

chosen for acid-fumigation and carbon analysis. Of these select filters, average contribution of CC to TOC is at most 5 ± 5% based on seven filters across sites and seasons. The average difference in split-time is 7 ± 3 seconds earlier for the acid-fumigated filter, meaning that the EC isolation based on untreated split-times would be biased towards low EC recovery not towards inclusion of PryC. Because of the low contribution, and the bias towards low EC recovery in the ^{14}C-EC samples, there is likely minimal impact of CC on the results of this study.

For the EC harvest, up to three punches of a filter sample were loaded in the analyzer at one time until a target of 100 μg of EC per composite is collected in a baked glass petri dish. Recovery of EC was tested using the number of punches from the final harvest to guarantee efficient recovery. EC recovery of each of the triple punches were from 73 to 99% while the double punches were from 84% to 98%, with no multiple punch collection resulting in the inclusion of PryC or OC. Once the EC was harvested, the filters were acid-fumigated in a desiccator over 1N hydrochloric acid (HCl) for 12 hours and then dried at 60°C for 1 hour. The glass petri dishes containing each EC composite were sealed using Teflon tape, labeled, wrapped in baked aluminum foil, bagged in individual Ziploc bags and shipped on ice to National Ocean Sciences Accelerator Mass Spectrometry (NOSAMS) facility in Woods Hole Oceanographic Institution (Woods Hole, MA, USA) for ^{14}C analysis.

There are multiple potential sources of uncertainty in the EC ^{14}C method which have been discussed previously (Liu et al., 2017; Zenker et al., 2017). To understand the potential contribution of PyrC, which can be inadvertently included in the isolated EC, a sensitivity test was performed. There are published methods that correct for the potential

bias including a water extraction pretreatment prior to EC isolation. However, this method has documented up to 20% loss of EC due to the extraction (Dusek et al., 2014). For this study we used another protocol which conducts a post-analysis sensitivity test to report bias of PyrC if included in the ^{14}C of isolated EC (Andersson et al., 2015; Budhavant et al., 2015; Chen et al., 2013). Results from this test calculate a maximum underestimation of fossil contribution to EC by 8.5 and 9.9% for winter and non-winter samples, respectively. To incorporate potential carbon contamination from shipping and handling of the EC harvested samples, a separate sensitivity test was conducted. Several blank filters were prepared replicating a similar EC harvest sample (e.g. volatilized off OC by heating the sample, acid fumigation, drying, etc.), and shipped and handled using the same method as the EC harvested ambient samples. These travel blanks were then analyzed for carbon contamination using the carbon analyzer. The average contribution of contaminated carbon on the travel blanks is 0.09 ± 0.08 μg cm^{-2}. A maximum ^{14}C contribution from this contaminated carbon mass is calculated assuming the carbon to be pure fossil (-1000‰) or pure biomass burning (+107.5‰). Results from this test indicate a maximum percent difference of ^{14}C of the EC due to blank subtraction of 2.5 and 11.3% for winter and non-winter samples, respectively. The results from both sensitivity tests, potential contribution of PryC during EC harvest, and potential contribution of contaminated carbon during shipping and handling, were combined to calculate the uncertainty of ^{14}C of the ambient samples.

Description of TOC Composites

Sample preparation for ^{14}C analysis of the TOC composite samples was completed at the BAAQMD. As with the EC composite samples, the TOC samples were separated into two composites: "winter" (November-February) and "non-winter" (March-October). These composites were composed of the same filter samples as the EC composites (Table A.2).

The TOC composite samples and a PM_{10} filter blank were sent to University of Arizona Accelerator Mass Spectrometry Laboratory (Tucson, AZ, USA) where carbon isotope analysis was performed. The ^{14}C results of the TOC sample composites were blank corrected, using ^{14}C results from the filter blank, to account for potential contamination of carbon from shipping and handling of the samples.

Method for Radiocarbon Analysis

The sample composites were first oxidized to CO_2, purified and quantified by manometry. Samples were then reduced to graphite and subjected to accelerator mass spectrometry (AMS) to determine the fraction of modern carbon (F_M) which is the $^{14}C/^{12}C$ ratio of the sample to the "Modern" or a reference material: NBS Oxalic Acid I (in AD 1950) (Stuiver and Polach, 1977).

$$F_M = \frac{(^{14}C/^{12}C)_{sample}}{(^{14}C/^{12}C)_{AD1950}} \quad (3)$$

Source Apportionment Modeling

Radiocarbon-based apportionment. For apportionment, the F_M value is used to calculate the $\Delta^{14}C_{sample}$ for the EC and TOC samples.

$$\Delta^{14}C_{sample} = 1000 * \left(F_M * exp\left((1/8267) - (1950 - 2012)\right) - 1\right) \quad (4)$$

The isotope signature can be apportioned between fossil fuel and biomass burning by using a mixing model ratio for $\Delta^{14}C_{sample}$ with end members specific to these sources:

$$\Delta^{14}C_{sample} = (\Delta^{14}C_{contemporary})\ (\ f_M) + (\Delta^{14}C_{fossil})\ (1\text{-}f_M) \quad (5)$$

The $\Delta^{14}C_{fossil}$ component of $\Delta^{14}C_{sample}$ has a value of -1000‰ while $\Delta^{14}C_{biomass\ burning}$ can be between +28.1‰ (Zotter et al., 2014) and +102.5‰. The +102.5‰ corresponds to the end member value of EC from wood smoke which was derived from averaging sections of an 80-year-old pinewood from the Bay Area. This was based on an auxiliary study in collaboration with BAAQMD. The calculated end member value from this auxiliary study (+102.5‰) is similar to a published wood smoke end member value (+107.5‰) which was derived from a tree growth model by averaging 10 to 85 year old wood fractions (Mohn et al., 2008). The ^{14}C value of +28.1‰ corresponds to biomass burning of annual sources including combustion of grass, pruning, and agricultural waste, as well as meat cooking (Zotter et al., 2014). A bottom-up approach using the BAAQMD's 2011 Emissions Inventory (EI) for Criteria Air Pollutants was employed to calculate a $\Delta^{14}C_{biomass\ burning}$ end member value specific to its region and season (Fanai et al., 2014).

$$\Delta^{14}C_{biomass\ burning} = (f_{wood\ smoke})\ (+102.5‰) + (f_{annual\ biomass\ burning})\ (+28.1‰) \quad (6)$$

The Bay Area-tailored $\Delta^{14}C_{biomass\ burning}$ end member for winter and non-winter periods were calculated to be +98.5‰ and +71.2‰ respectively. This customized end member is also applied for the ^{14}C analysis of the TOC samples.

Chemical Mass Balance modeling. To further apportion sources of fossil fuel and biomass burning, CMB analysis using a Monte Carlo source apportionment technique was employed to determine contribution of major sources collected on sampled PM_{10} filters. The CMB is a receptor-based model that uses known speciated source profiles to identify sources and source contribution to carbonaceous aerosol. The model uses the following set of linear equations to estimate the c_{ik} which is the concentration of elemental carbon, i, at receptor site k:

$$c_{ik} = \sum_{j=1}^{m} f_{ij} s_{jk} \quad (7)$$

which equals the sum of m source types where s_{jk} is the contribution to the ambient elemental mass concentration from source j at receptor site k, f_{ij} is the relative concentration of chemical component i in the emissions from source j. In this analysis, the standard deviation of the measured and model estimated masses is determined by using a Monte Carlo approach. This technique repeatedly samples from the profile distribution (approximately 100,000 times).

The CMB analysis relied on measurements of OC, EC, ^{14}C-EC, ^{14}C-OC and nss K from the filters, and 24h average NO_x and CO measurements. The ^{14}C-OC values were determined using ^{14}C-TOC and ^{14}C-EC values (SI). Profiles from five source categories were used: gasoline, diesel, natural gas, biomass burning, and cooking (Fairley, 2012; Fanai et al., 2014). These five sources account for over 90% of directly emitted carbonaceous $PM_{2.5}$ and nearly 100% of EC, based on the BAAQMD's EI. These sources are also commonly used in other urban source apportionment studies (Fraser et al., 2003; Mohr et al., 2009; Rogge et al., 1991; Schauer et al., 1996; Zheng et al., 2002). Except for

wood smoke/biomass burning, the same profiles were used for the winter and non-winter composite analysis. During the winter season biomass burning is predominately from wood smoke while the non-winter season had similar contributions from wood smoke and annual biomass burning. For the winter season, a source profile of wood smoke was used while a combined wood smoke and annual biomass burning profile was used for the non-winter season. However, for the CMB analysis we will report apportioned wood smoke and/or biomass burning as "wood smoke". The term "biomass burning", when discussing the CMB analysis, will refer to combined "wood smoke" and "cooking" sources.

Results and Discussion

Bulk Carbon Concentrations and OC to EC Ratios

The ambient concentrations of OC and EC composites during the winter ranged from 1.29 to 8.67µg m^{-3} and 0.23 to 2.77µg m^{-3}, respectively, while non-winter samples ranged from 1.21 to 3.70µg m^{-3} and 0.35 to 0.45 µg m^{-3}, respectively (Table 2.1). For both seasons, Napa consistently had the highest concentrations of OC and EC while Cupertino and San Pablo had the smallest in the winter and non-winter season, respectively. It was initially thought that Bethel Island would be a background site, but inland sources (i.e. Central Valley) kept carbonaceous aerosol concentrations relatively high. Ambient concentrations of OC and EC were significantly enhanced ($p < 0.05$) in the winter versus non-winter samples for Bethel Island, San Rafael, Napa and San Francisco. San Pablo had a significantly enhanced ambient OC concentration ($p < 0.05$) during the winter season, however there was no significant difference ($p = 0.05$) in the EC

concentration during the two seasons. Concord had no significant difference ($p = 0.07$) of ambient OC concentration between the two seasons, but the EC concentration was more enhanced ($p < 0.05$) during the winter season. For Cupertino, there was no significant difference between the two seasons for either OC ($p = 0.29$) or EC ($p = 0.19$). The seasonal trend observed from some of the sampling sites (i.e. higher carbonaceous aerosol concentration during the winter versus non-winter season) has historically been observed in the Bay Area (Kirchstetter et al., 2017) and can be partially explained by meteorological factors (i.e. wind speed, mixing heights, etc.). Glen et al. observed dispersion of pollutants to be 2 to 3 times stronger in the summer (May-August) than the winter in the Bay Area (Glen et al., 1996). In addition to meteorological influences, residential wood burning significantly impacts wintertime air quality in this region (McLarney and Sarles, 2005).

Table 2.1. Average (mean standard deviation) ambient EC and TOC concentrations for each composite sample. Isotope analysis including $\Delta^{14}C$ and $\delta^{13}C$ (‰), contribution biomass burning (%BB) or contemporary (%Cont) for EC harvest and TOC samples, respectively, are included in the table.

		Ambient Concentration		EC			TOC		
Locations	**Composite**	**EC (µg m^{-3})[a]**	**TC (µg m^{-3})**	**$\Delta^{14}C$ (‰)**	**$\delta^{13}C$ (‰)**	**%BB**	**$\Delta^{14}C$ (‰)**	**$\delta^{13}C$ (‰)**	**%Cont**
Bethel Island	Winter	0.79 ± 0.09	6.10 ± 3.00	-415.7	-25.74 ± 0.22	53 ± 6	-257.4	-26.01 ± 0.02	68 ± 6
	Non-Winter	0.32 ± 0.06	2.99 ± 1.05	-516.6	-27.14 ± 0.13	45 ± 10	-333.8	-26.89 ±0.02	62 ± 7
Concord	Winter	0.73 ± 0.08	4.93 ± 5.05	-414.4	-26.12 ± 0.25	53 ± 7	-264.4	-26.08 ± 0.01	67 ± 6
	Non-Winter	0.36 ± 0.07	3.06 ± 1.11	-591.1	-26.91 ± 0.15	38 ± 11	-378.7	-26.99 ± 0.03	58 ± 6
San Pablo	Winter	0.72 ± 0.08	4.97 ± 1.90	-537.3	-26.00 ± 0.20	42 ± 7	-381.8	-26.13 ± 0.01	56 ± 4
	Non-Winter	0.37 ± 0.07	2.52 ± 0.92	-522.2	-24.96 ± 0.13	45 ± 14	-496.5	-26.73 ± 0.05	47 ± 3
San Rafael	Winter	0.79 ± 0.09	5.36 ± 2.69	-518.5	-25.61 ± 0.25	44 ± 8	-339.3	-26.33 ± 0.01	60 ± 5
	Non-Winter	0.36 ± 0.07	3.04 ± 0.62	-534.1	-25.65 ± 0.12	44 ± 8	-317.6	-26.91 ± 0.06	64 ± 8
San Francisco	Winter	0.94 ± 0.09	5.75 ± 2.63	-577.1	-24.47 ± 0.21	39 ± 7	-426.6	-26.32 ± 0.01	52 ± 3
	Non-Winter	0.37 ± 0.07	2.82 ± 1.13	-661.5	-25.74 ± 0.13	32 ± 13	-445.3	-26.70 ± 0.01	52 ± 4
Napa	Winter	1.34 ± 0.11	8.95 ± 2.91	-308.0	-25.13 ± 0.15	63 ± 9	-137.3	-25.98 ± 0.01	79 ± 7
	Non-Winter	0.40 ± 0.07	3.59 ± 1.28	-544.5	-25.90 ± 0.14	43 ± 8	-364.9	-26.49 ± 0.02	59 ± 5
Cupertino	Winter	0.50 ± 0.07	4.08 ± 1.79	-515.0	-25.21 ± 0.21	44 ± 5	-405.2	-26.38 ± 0.01	54 ± 4
	Non-Winter	0.38 ± 0.07	3.06 ± 1.01	-597.2	-26.20 ± 0.14	38 ± 10	-413.4	-26.60 ± 0.01	55 ± 4

[a] *mass-normalized composite*

EC (or BC) is a highly stable, combustion byproduct that is directly emitted into the atmosphere from combustion sources (Strader et al., 1999; Turpin and Huntzicker, 1995). Particulate OC can be directly emitted (primary OC), but can also be produced in the atmosphere via chemical reactions of precursor volatile organic compounds (secondary OC). Primary OC is also less stable in the atmosphere with respect to chemical reactions, compared to EC. Using the ratio of OC to EC provides a qualitative measure of the impact of these secondary compounds, which are referred to as secondary organic aerosols (SOA) (Turpin and Huntzicker, 1995). An increase in the OC to EC ratio may indicate an increase in SOA contribution, while a high correlation between OC and EC may indicate that primary combustion emissions dominate the aerosol.

During the winter, OC more strongly correlates to EC ($r^2 = 0.85$) (Figure 2.2A) compared to the non-winter season ($r^2 = 0.56$) (Figure 2.2B), however, this may be due to greater range of concentrations in the winter season producing higher correlation. The average OC: EC ratios are 4.5 and 6.2 during the winter and non-winter season, respectively. All sampling sites, except San Pablo ($p = 0.59$) and Cupertino ($p = 0.25$) registered significantly higher OC: EC ratios during the non-winter versus winter season ($p < 0.05$) (Figure 2.3). The largest average OC: EC ratio was at Bethel Island (7.33 ± 1.12) during the non-winter period. The smallest average OC/EC was at San Francisco (3.83 ± 0.96) in the winter. For the Bay Area samples, the higher OC/EC ratio during the non-winter season is supporting evidence that the winter OC and EC are likely from combustion sources, while non-winter OC is mostly more influenced by SOA production (Turpin et al., 1991).

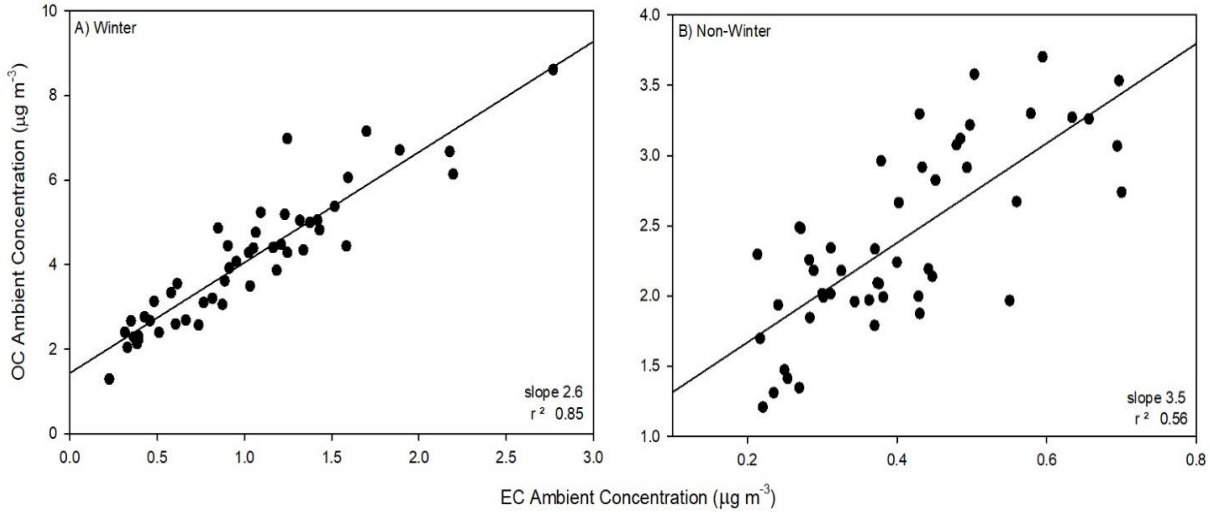

Figure 2.2. Correlation of ambient OC and EC concentrations for (A) winter and (B) non-winter samples.

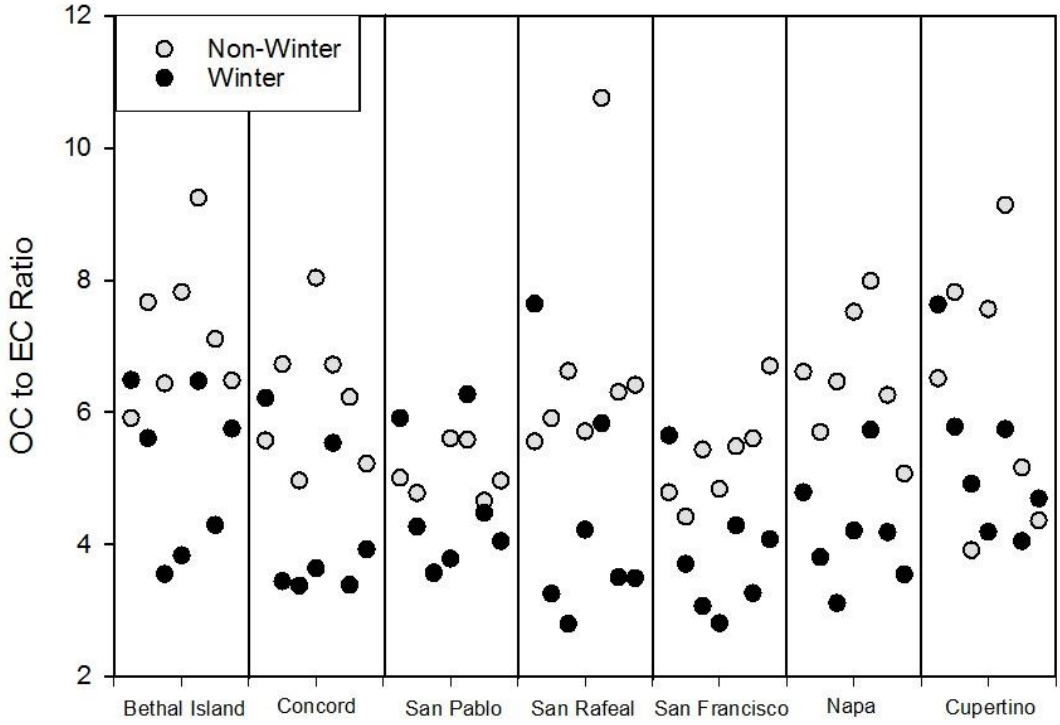

Figure 2.3. Comparison of OC to EC ratio for winter and non-winter samples specific to each sampling site.

Since SOA is a subset of carbonaceous aerosols formed via reactions of volatile and intermediate volatility precursors with atmospheric oxidants like ozone, hydroxyl radical, or nitrate radicals (Kleindienst et al., 2007), correlations of OC to ozone were used to further investigate whether increased OC/EC ratio is due to SOA. Production of ozone is largely dependent on meteorology (i.e. warmer temperature, stagnant air masses and clear skies), with mixing ratios higher during summer months. A stronger correlation is observed between OC and 8-hr max ozone concentration during the summer season (r^2 = 0.46: slope = 12.9) (Figure 2.4) compared to the winter season (r^2 = 0.17). The higher OC/EC ratios collected during the non-winter season (March to October) and correlation between ozone and OC during the summer (subset of non-winter samples) season (May to August) point to higher impacts of SOA in the non-winter season. However, average OC/EC ratios in the Bay Area during the non-winter season were less than half the average ratio observed during summer months in Nashville, TN (12.11 ± 5.50), an area with high biogenic SOA impacts (Lewis et al., 2004).

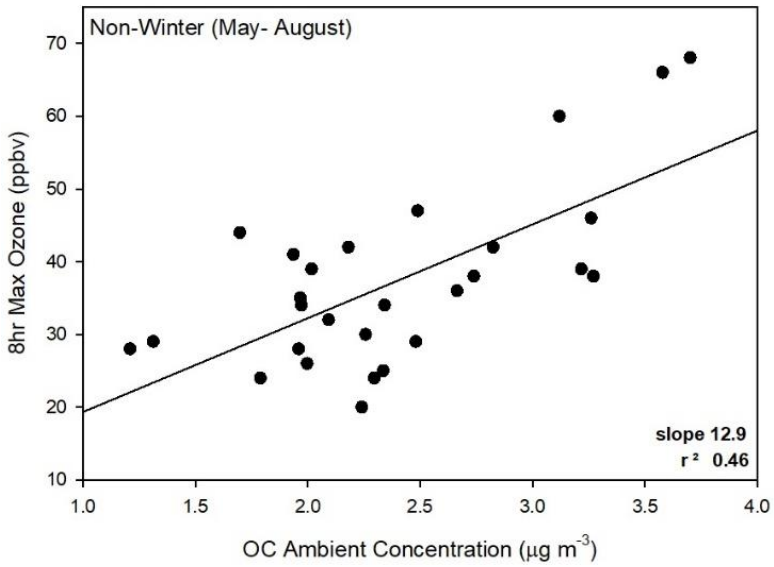

Figure 2.4. Correlation of 8hr ozone max to ambient OC concentrations on days sampled during months May through August.

Source Apportionment Studies

Radiocarbon analysis of TOC. Contemporary contributions to TOC include combustion (e.g. biomass burning and meat cooking), biogenic (e.g. vegetative detritus), and secondary sources. During the winter season, TOC composites had significantly larger ($p < 0.05$) contribution of contemporary ($62 \pm 9\%$) compared to fossil fuel sources ($38 \pm 9\%$) (Figure 2.5A and 5D). Average ambient concentrations from contemporary and fossil fuel sources during the winter season were 3.67 ± 1.59 μg m^{-3} and 2.06 ± 0.35μg m^{-3} of TOC, respectively. Napa had both the largest contribution ($79 \pm 7\%$) and ambient concentration (7.03 ± 0.65 μg m^{-3}) from contemporary sources. San Francisco had the largest contribution ($48 \pm 3\%$) and ambient concentration (2.75 ± 0.20 μg m^{-3}) from fossil fuel sources during the winter season.

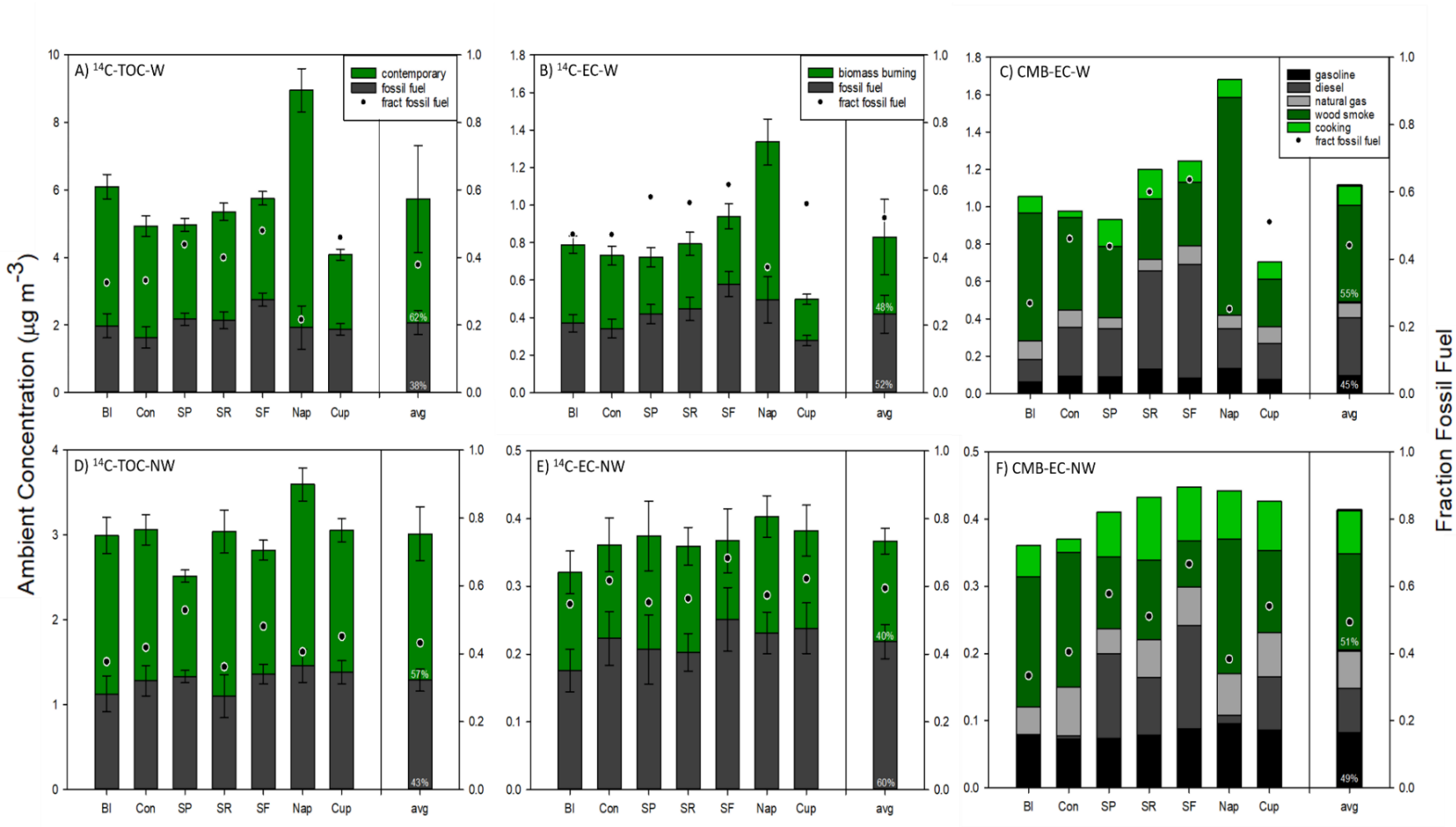

Figure 2.5. Ambient concentration of fossil fuel and contemporary sources using radiocarbon-based source apportionment of (A) winter TOC samples, (D) non winter TOC samples (B) winter EC samples. Ambient concentration of fossil fuel (e.g. gasoline, diesel, and natural gas), wood smoke, and cooking sources for (C) winter and (F) non-winter EC samples using chemical mass balance-based apportionment. Fraction fossil fuel included in each graph

The non-winter TOC samples also had a statistically larger ($p < 0.05$) contribution of contemporary ($57 \pm 6\%$) compared to fossil fuel ($43 \pm 6\%$) sources. Fossil fuel and contemporary contribution sources are closer to equal parts during the non-winter season, although the two seasons are not significantly different ($p = 0.12$). Average ambient TOC concentrations for contemporary and fossil fuel sources were 1.72 ± 0.32 and 1.29 ± 0.13 $\mu g\ m^{-3}$, respectively. Though Bethel Island had the largest contribution from contemporary sources ($62 \pm 7\%$), ambient concentrations from contemporary sources were largest in Napa ($2.14 \pm 0.19 \mu g\ m^{-3}$). San Pablo had largest contribution from fossil fuel sources ($53 \pm 3\%$), however Napa had the largest ambient concentration (1.46 ± 0.20 $\mu g\ m^{-3}$) of TOC from fossil fuel sources.

For both winter and non-winter TOC composites, contemporary sources are the dominant contributor of carbonaceous aerosols. Napa has significantly more contemporary carbon compared to other sampling sites, especially during the winter season. The Napa sampling site is in the center of Napa Valley where agricultural burning and fireplace usage during fall and winter are more frequent. During the winter season, as expected, the urban San Francisco site was the most impacted by fossil fuel sources (Figure 2.5a). San Francisco also had the same fossil fuel contribution (48%) in both season composites. The San Francisco winter composite had the largest fossil fuel contribution while the non-winter composite has second largest fossil fuel contribution after San Pablo ($53 \pm 3\%$) which is considered an outlier. The average contribution from contemporary sources of TOC aerosols in the Bay Area ($59 \pm 8\%$) was comparable to other major Californian cities including Pasadena, where average summer contribution of contemporary sources is $51 \pm 15\%$ (Zotter et al., 2014). However,

ambient concentrations from contemporary sources were generally greater in Pasadena (2-4μg m^{-3}) (Zotter et al., 2014) compared to the Bay Area (~2μg m^{-3}).

Radiocarbon Analysis of EC

As EC is from combustion processes, the contemporary contribution of EC includes sources from biomass burning and meat cooking. These sources will be referred to as "biomass burning" for the ^{14}C-EC analysis. During the winter season, average contributions from biomass burning and fossil fuel sources were 48 ± 9% and 52 ± 9%, respectively. Unlike the TOC composite samples, there was no statistically significant difference ($p = 0.42$) between fraction of biomass burning and fossil fuel sources in the EC samples during the winter season across the sites. However, there was a significant difference ($p < 0.05$) between EC apportioned to biomass burning and fossil fuel sources during the non-winter season, where average biomass burning contributions (41 ± 5%) were significantly smaller compared to fossil fuel contributions (59 ± 6%). During the winter, average ambient EC concentrations from biomass burning and fossil fuel sources were 0.41 ± 0.20 and 0.42 ± 0.10 μg m^{-3}, respectively. Average ambient concentrations during the non-winter season for biomass burning and fossil fuel sources were 0.15 ± 0.02 and 0.22 ± 0.03 μg m^{-3}, respectively. For the winter season, Napa had the largest contribution and ambient concentration of EC from biomass burning during the winter: 63 ± 9% and 0.84 ± 0.12μg m^{-3}, respectively. San Francisco had the largest contribution and ambient concentration of EC from fossil fuel: 62 ± 7 % and 0.58 ± 0.07μg m^{-3}, respectively. For the non-winter season, Bethel Island had the largest contribution of EC from biomass burning: 45 ± 10%, while the largest ambient EC concentration from biomass burning was from Napa: 0.17 ± 0.03μg m^{-3}. Bethel Island likely received

transport of biomass burning pollutants from Central Valley where there is heavy agricultural activity. Consistent with the winter, San Francisco had the largest contribution and ambient concentration of EC from fossil fuel during non-winter season: 68 ± 13% and 0.25 ± 0.05μg m^{-3}, respectively.

Major sources of EC in this region have historically been from on- and off-road diesel exhaust (Bond et al., 2004; Kirchstetter et al., 2017). A major source of future EC may be from wildfires, as studies have found increasing trends and projections of large-scale fires in California (Barbero et al., 2015; Riley et al., 2013; Westerling et al., 2006). However, a study by Schauer and Cass (2000) of California carbonaceous aerosol samples collected over 15 years prior to this study, found that even with the inclusion of a major wildfire events, biomass burning contributed only 20% of EC (Schauer and Cass, 2000). From our results, with the large decrease in emissions of EC from diesel, there is evidence that biomass burning, and potentially meat cooking, are becoming more prominent contributors to EC or BC concentrations. These trends are also observed in the TOC samples, aside from the outlier (i.e. non-winter San Pablo composite). Contributions from the winter season show an overall equal contribution of biomass burning and fossil fuel combustion sources for EC amongst the seven sampling sites (Figure 2.5B and 5E). Although non-winter samples have statistically higher contributions from fossil fuel sources, average biomass burning (40 ± 5%) contributions from all sites were still much larger than the estimated 20% from the Schauer and Cass (2000) study.

Based on the State of California's Cal Fire website (http://cdfdata.fire.ca.gov/incidents/incidents_seasondeclarations?year=2012), summer and winter wildfire seasons in northern California begin approximately in May and

November, respectively. During the period of this study, however, there were few recorded large fires in the region (2012). Thus, the enhanced concentrations from biomass burning in this study derive from residential wood burning and possibly some agricultural burning. The EC contribution from biomass burning during the winter season is significantly ($p = 0.03$) greater compared to the non-winter season. There is also a strong correlation between the biomass burning (EC composite) and contemporary (TOC composite) sources during the winter ($r^2 = 0.96$) and non-winter ($r^2 = 0.89$, excluding the San Pablo outlier) season (Figure 2.6). The strong correlations during the two seasons are an indication that the biomass burning contribution from the EC fraction and the contemporary OC are from the same source or combination of common sources. However, as the non-winter OC/EC ratios are greater, these aerosols are likely more impacted by secondary OC sources.

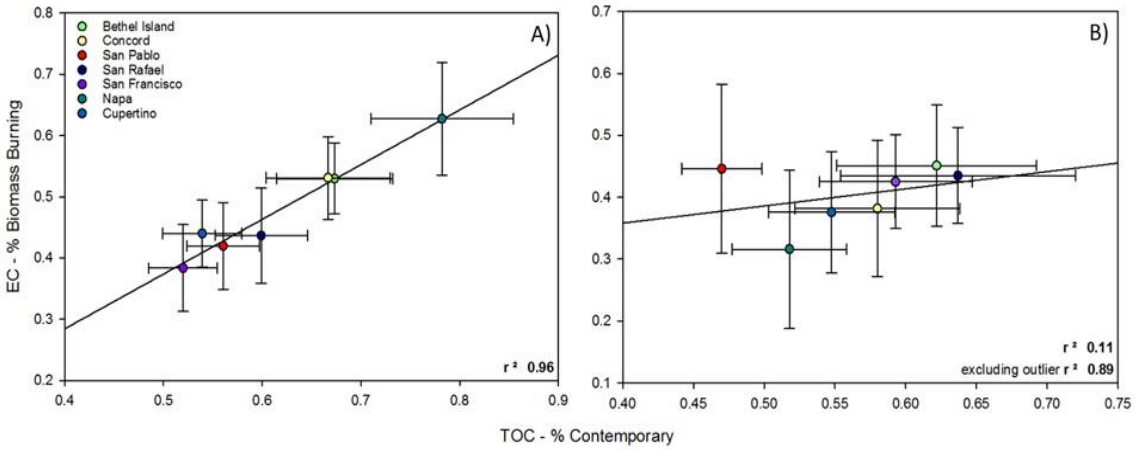

Figure 2.6. Comparison of contribution of biomass burning from EC harvested composite samples to contribution of contemporary sources from TOC composite samples for (A) winter and (B) non-winter seasons.

Chemical Mass Balance Apportionment of EC

The apportionment of EC is different between the CMB and ^{14}C analysis (Figure 2.5B-C, 5E-F). The CMB analysis uses volume-normalized contributions (same method as the TOC ^{14}C) to calculate average EC mass for each sample site. The ^{14}C analysis calculates average EC by equal mass representation. Due to the difference in average EC calculation method per site, an average of 14 ± 6% higher EC ambient concentration is present in the CMB apportionment. For the CMB analysis, EC was apportioned to three fossil fuel sources (i.e. gasoline exhaust, diesel exhaust, and natural gas) and two biomass burning sources (i.e. wood smoke and cooking) (Figure 2.5C, 5F). The relative contributions of EC from the CMB and ^{14}C source apportionment analysis can be easily compared.

During the winter season, the average estimated contributions from fossil fuel and biomass burning sources were 45 ± 15% and 55 ± 15%, respectively, for CMB. Contributions of natural gas (8 ± 3%) and gasoline (9 ± 2%) were relatively consistent across the sites. The largest contribution of fossil EC is diesel exhaust with an average contribution of 28 ± 14%. San Francisco had the highest ambient concentration of diesel exhaust at 0.61 ± 0.12 μg m^{-3}. Wood smoke dominates the biomass burning fraction of EC with an average of 45 ± 17% contribution to winter EC concentrations. Napa had the highest ambient concentrations of biomass burning at 1.16 ± 0.23 μg m^{-3} and the highest contribution 69 ± 9%.

During the non-winter season, average contributions from fossil fuel and contemporary sources are 49 ± 12 % were 51 ± 12%, respectively, for the CMB. The largest contribution of fossil EC in the non-winter season was from gasoline exhaust with

an average of 20 ± 2% amongst the sites. Contribution of gasoline exhaust was also consistent across the sites like in the winter season. Diesel exhaust was quite variable throughout the region, with San Francisco having the largest contribution and ambient concentration with 34% and 0.15μg m^{-3}, respectively, whereas for Bethel Island, the CMB analysis apportioned no contribution of carbonaceous aerosols to diesel exhaust. As with the winter season, biomass burning also dominated the contemporary combustion fraction of EC during the non-winter season. Average contribution and concentration of biomass burning was 36 ± 15% and 0.14 ± 0.05μg m^{-3}. The largest contribution and ambient concentration of biomass burning was from Napa with 45% and 0.20 μg m^{-3}.

Ambient concentrations of all sources were significantly ($p < 0.05$) enhanced in the winter versus non-winter season, aside from the gasoline exhaust ($p = 0.26$). Ambient concentrations of gasoline exhaust remained consistent throughout the seasons proving that this is not a seasonally influenced source like residential wood smoke (i.e. biomass burning). The relative contribution of gasoline exhaust was enhanced during the non-winter season ($p < 0.05$), however, this was likely due to decrease of overall aerosol concentrations during this season.

Comparison of Source Apportionment Methods

The different apportionment methods, ^{14}C and CMB analysis for EC, agree within 16 ± 12% for contribution of fraction fossil and biomass burning for both winter and non-winter season. Samples from Bethel Island and Napa consistently had larger differences between the two analysis methods for both seasons. Both sites had significant contributions from contemporary sources. Interestingly, CMB analysis consistently over-predicted the contemporary contribution by an average of 9 ± 9%. The CMB analysis

uses non-sea salt potassium ion (nss K) as the only tracer for biomass burning. Though nss K is a stable compound and resistant to chemical degradation, the ion is not a unique tracer for biomass burning and adds uncertainty in the apportionment.

Comparison to Emissions Inventory Data

California Air Resources Board's Black Carbon Emission Inventory (CARB-EI) reports statewide speciation of EC from its different sources (2016) . The CARB-EI estimates that on-road motor vehicle exhaust contributes 20% of total EC emissions (18% from diesel and 2% from gasoline) while off-road mobile sources (e.g. aircraft, off-road equipment, commercial harbor craft, and trains) contribute 36% of total EC (Figure 2.7). The combined total of off-road mobile and on-road gasoline and diesel sources contribute 56% of total EC emissions which closely aligns to the ^{14}C-EC analysis: average fossil fuel contribution of EC is 56 ± 8%. However, if EC from industrial sources (i.e. petroleum production, wood and paper, mineral processes) is included as fossil fuel, then the CARB-EI estimates 70% contribution of EC from all mobile plus industrial sources, which is significantly higher than the ^{14}C-EC average.

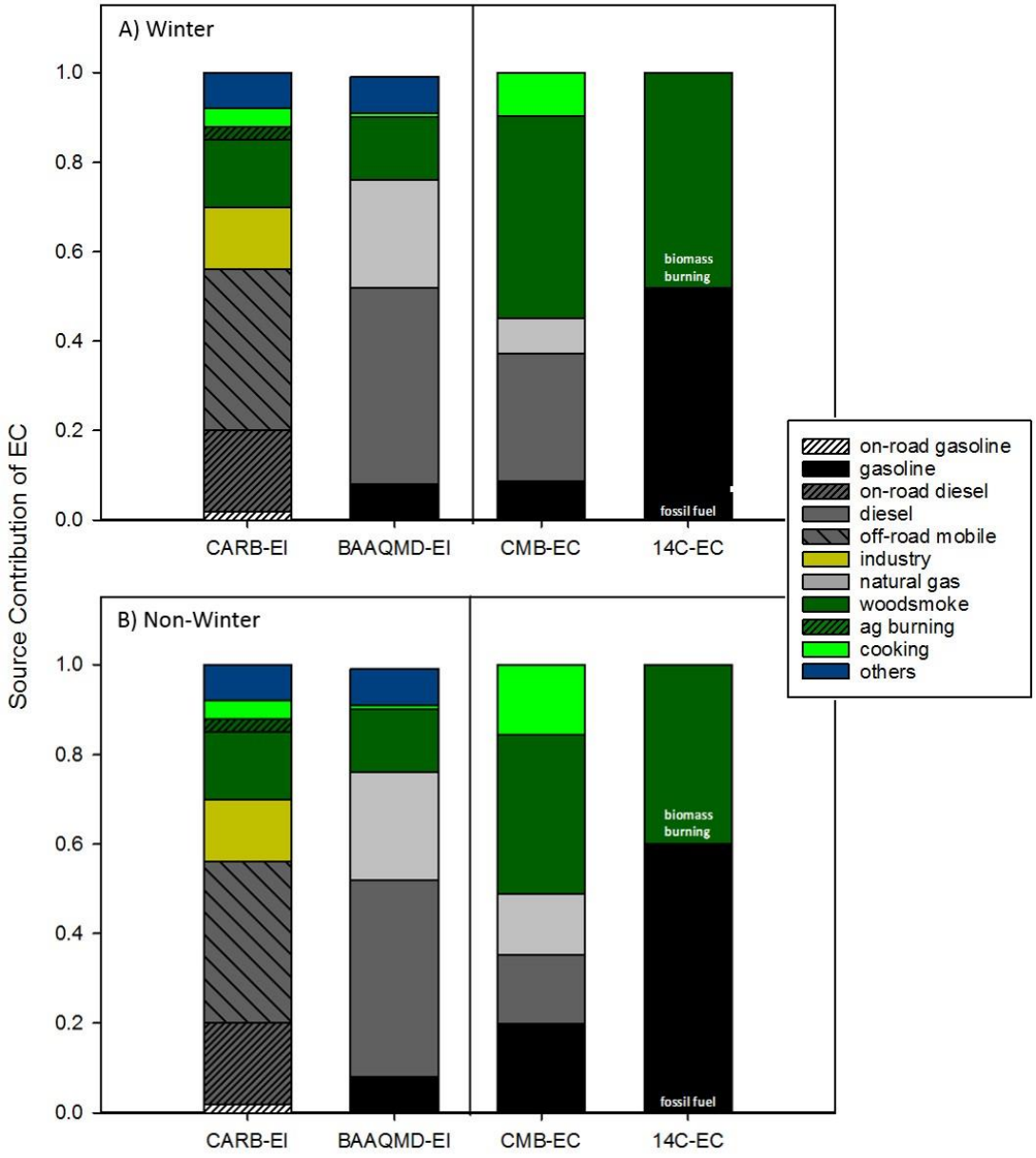

Figure 2.7. Comparison of estimated source contribution of EC based on CARB's BC Emission Inventory (CARB-EI), BAAQMD's $PM_{2.5}$ Emission Inventory (BAAQMD-EI), and CMB and 14C EC analysis for (A) winter and (B) non-winter samples.

The CARB-EI is an average estimate of the contribution of EC from across the state of California. The BAAQMD has published the Bay Area Emissions Inventory for $PM_{2.5}$ (BAAQMD-EI) (Claire, 2015) providing detailed speciation for $PM_{2.5}$ specific to

the sampling region. The contribution of EC by fuel type was calculated for this paper using the BAAQMD-EI and EPA's factors for estimating the fraction of $PM_{2.5}$ to BC (Figure 2.7), however, this may be uncertain with regards to BC source ratios and number of source types. This calculation estimates that fossil fuel sources contribute 76% of total EC emissions: 44% from diesel, 8% from gasoline and 24% from natural gas. The CMB-EC analysis estimates lower fossil fuel contributions from diesel (22 ± 15%) and natural gas (11 ± 4%). However, the contribution of EC from gasoline exhaust is larger in the CMB analysis (14 ± 6%) compared to the BAAQMD-EI (2%). This may be due to underestimation of high emitters within the gasoline exhaust category in the emissions inventory (Lough et al., 2007).

The BAAQMD-EI estimates contemporary sources to contribute 15% of EC emissions including 14% from wood smoke and 1% from cooking. The CARB-EI estimates that contemporary sources contribute 22% of EC emissions, including 15% from residential wood smoke, 4% from meat cooking, and 3% from agricultural burning (Figure 2.7). The ^{14}C-EC analysis estimates a contribution from contemporary sources (44 ± 8%) larger than either EIs. The CMB-EC analysis estimates larger contributions from wood smoke (41 ± 16%) and cooking sources (13 ± 5%) compared to the EIs (Figure 2.7). The CMB and ^{14}C apportionment analysis for EC has a considerably larger contribution of EC from contemporary, wood smoke and cooking emissions compared to the EI. In summary, the EIs consistently predict lower contributions from biomass burning as compared to receptor-based techniques (^{14}C and CMB). However, differences in the EI and observation-based apportionment can be partially due to differences in methodology of bottom-up (i.e. EI models) and top-down (receptor-based) approaches.

Comparison of Radiocarbon-based EC Results to Other Studies

To assess how source contributions to EC in the Bay Area of California compares to other locations, a review of the current literature for global ^{14}C studies of BC and EC was completed. Table 2.2 includes ^{14}C apportionment of EC or BC, by method and season, from across the globe. The region with the most ^{14}C EC and BC studies is Asia, followed by Europe, the Artic, and finally, the contiguous United States (U.S.) (Table 2.2). At the time of this publication, there has been only one other study in the contiguous U.S., by Mouteva et al. in Utah, (2017). There are no reported studies in the Southern Hemisphere. Figure 2.8 and Figure A.1 (Appendix A) plot the ^{14}C apportioned EC or BC data on a global map for the winter and non-winter (and annual) seasons, respectively. Regional trends in the contribution of biomass burning to EC or BC can be visualized using these global maps (Figure 2.8 and Figure A.1). In Asia, studies can be grouped between East (i.e. China, South Korea, and Japan) and South (i.e. India, Maldives, and Himalaya-Tibet) Asia. Generally, there is a larger contribution of fossil fuel combustion to EC and BC in East Asia, while South Asia has a larger contribution of biomass burning. There is significant variability across the many European studies and the two contiguous U.S. studies.

Table 2.2. Compilation of literature values of contribution of biomass burning (%BB) of EC or BC carbonaceous fraction. Sampling location, sampling period and method of EC or BC isolation also included. Arctic and near-Artic studies are listed in a separate section at the end of the table.

Location	City	Manuscript	%BB - W	%BB - NW	%BB - annual	Sampling Period	EC/BC Isolation
Asia							
China	Beijing [a]	Andersson et al. 2015	26 [j]			Winter 2013	NIOSH [o]
		Zhang et al. 2015a	18 - 28 [j]			Winter 2013	Swiss_4S
		Zhang et al. 2015b *	24	20	21 ± 6	2010 to 2011	Swiss_4S
		Chen et al. 2013	17 ± 4			Winter 2009 – 2010	NIOSH [o]
	Shanghai [a]	Andersson et al. 2015	32 [j]			Winter 2013	NIOSH [o]
		Zhang et al. 2015a	21 – 23 [j]			Winter 2013	Swiss_4S
		Chen et al. 2013 *	17 ± 4			Winter 2009 – 2010	NIOSH [o]
	Guangzhou [a]	Andersson et al. 2015	32 [j]			Winter 2013	NIOSH [o]
		Zhang et al. 2015a	19 – 43 [j]			Winter 2013	Swiss 4S
		Liu et al. 2014 *	29 ± 10 [j]			Winter 2012 – 2013	Theodore [p]
	Xiamen [a]	Chen et al. 2013 *	13 ± 3			Winter 2009 – 2010	NIOSH [o]
	Xi'an [a]	Zhang et al. 2015a *	22 [j]			Winter 2013	Swiss_4S
	Xinxiang [a]	Liu et al. 2017 *	20 ± 01	14 ± 01 [k]	19 ± 3	2013 – 2014	multi-methods [p]
	Ningbo [c]	Liu et al. 2013 *	12	40 [k]	22	2009 – 2010	Theodore [p]
	Hainan Island [c]	Zhang et al. 2014 *			62 ± 11	2005 – 2006	Swiss_4S
	Shinglin Bay [c]	Chen et al. 2013 *	22 ± 3			Winter 2009 – 2010	NIOSH [o]
South Korea	Jeju Island [c]	Zhang et al. 2016 *	31 ± 12	21 ± 10	24 ± 11	2013 – 2014	Swiss_4S
		Chen et al. 2013		25 ± 6 [l]		Spring 2011	NIOSH [o]
Japan	Tokyo [a]	Uchida et al. 2010	24 - 28	39 - 42 [k]		2002 – 2004	CTO-375
	Okinawa [c]	Handa et al. 2010		69 [l, j, r]		Spring 2008	CTO-375
India	Sinhagad [c]	Budhavant et al. 2015 *	56 ± 3	48 ± 8		2008 – 2009	NIOSH [o]
		Sheesley et al. 2012			59 ± 5	2008 – 2009	CTO-375
		Gustafsson et al. 2009	54			Winter 2006	NIOSH [o]
Maldives	Hanimaadhoo [c]	Bosch et al. 2014	59 ± 4			Winter 2012	NIOSH [o]
		Budhavant et al. 2015 *	53 ± 5	53 ± 11		2008 – 2009	NIOSH [o]
		Sheesley et al. 2012			73 ± 6	2008 – 2009	CTO-375
		Gustafsson et al. 2009	41			Winter 2006	NIOSH [o]
Himalaya-Tibet	Mustang Valley [d]	Li et al. 2016 *			42 – 70	2013 – 2014	NIOSH [o]
	Langtang Valley [e]	Li et al. 2016 *			8 – 63	2013 – 2014	NIOSH [o]
Europe							
Spain	Barcelona [a]	Minguillon et al. 2011	13 ± 1	9 ± 1 [k]		2009	Theodore [p]
	Montseny [b]	Minguillon et al. 2011	34 ± 3	21 ± 4 [k]		2009	Theodore [p]
United Kingdom	Birmingham [b]	Heal et al. 2011			7	2007 – 2008	Theodore [p]

Netherlands	Rotterdam [a, f]	Keuken et al. 2013		17 [k]		Summer 2011	Theodore [p]
Switzerland	Zurich [a]	Zhang et al. 2013	36 ± 6			Winter 2008	Swiss_4S
		Szidat et al. 2006 *	25 ± 5	6 ± 2 [k]		2002 – 2003	Theodore [p]
	Bern [a]	Zhang et al. 2013 *		9 [k]		Summer 2009	Swiss_4S
	North of Alps [g]	Zotter et al. 2014 *	42 ± 13 [j]			Winter 2007 – 2012	Swiss_4S
	Roveredo [b]	Sandradewi et al. 2008	51			Winter 2005	Theodore
		Szidat et al. 2007	38 – 71	27 – 73 [l]		2005	Theodore [p]
		Zhang et al. 2013 *	63			Winter 2005	Theodore [p]
	Moleno [b]	Szidat et al. 2007	4 – 18			Winter 2005	Theodore [p]
		Zhang et al. 2013 *		8 [k]		Summer 2005	Theodore [p]
	South of Alps [h]	Zotter et al. 2014 *	49 ± 15 [j]			Winter 2007 – 2012	Swiss_4S
Italy	Milan [a]	Bernardoni et al. 2013 *	16			Winters 2009 – 2011	Theodore [p]
Sweden	Stockholm [a]	Andersson et al. 2011 *	43 ± 23	35 ± 18 [m]		2006 – 2007	CTO-375
		Zencak et al. 2007	70 - 79			Winter 2005	CTO-375
	Råö [b]	Szidat et al. 2009	30 – 36			Winter 2005	Theodore [p]
	Aspvreten [b]	Andersson et al. 2011 *	38 ± 2	45 ± 10 [m]		2006 – 2007	CTO-375
		Zencak et al. 2007	88 – 99			Winter 2005	CTO-375
	Göteborg [a]	Szidat et al. 2009	7 – 13	3 – 16 [k]		2005 – 2006	Theodore [p]
Lithuania	Preila [c]	Ulevicius et al. 2016 *		67 ± 3 [l, n]		Spring 2014	Swiss_4S
United States							
California	Bethel Island [b]	This study	53 ± 6	45 ± 10	49 ± 6	2011 – 2012	IMPROVE [o]
	Concord [a]	This study	53 ± 7	38 ± 11	46 ± 11	2011 – 2012	IMPROVE [o]
	San Pablo [a]	This study	42 ± 7	45 ± 14	44 ± 2	2011 – 2012	IMPROVE [o]
	San Rafael [a]	This study	44 ± 8	44 ± 8	44 ± 1	2011 – 2012	IMPROVE [o]
	San Francisco [a]	This study	39 ± 7	32 ± 13	36 ± 5	2011 – 2012	IMPROVE [o]
	Napa [a]	This study	63 ± 9	43 ± 8	53 ± 14	2011 – 2012	IMPROVE [o]
	Cupertino [a]	This study	44 ± 5	38 ± 10	41 ± 4	2011 – 2012	IMPROVE [o]
	avg of Bay Area, CA	This study *	48 ± 8	41 ± 5	45 ± 6	2011 – 2012	IMPROVE [o]
Utah	Salt Lake City [a, i]	Mouteva et al. 2017 *	12	8 [k]	11	2012 – 2013	Swiss_4S
Artic/sub-Artic							
Alaska, US	Barrow [c]	Barrett et al. 2015 *	31 ± 9	52 ± 6 [l]		Winter 2012 – 2013	NIOSH [o]
	Interior Alaska [r]	Mouteva et al. 2015		-10 – (+106) ‰ [s, n]		Summer 2013	Swiss_4S
	Interior Alaska [r]	Mouteva et al. 2015		-354 – (-57) ‰ [s]		Summer 2013	Swiss_4S
Norway	Svalbard [c]	Winiger et al. 2015 *	52 ± 15 [j]			Winter 2009	NIOSH [o]
Russia	Tiksi [c]	Winiger et al. 2017 *	19 ± 3	73 ± 5 [k]	31 ± 19	2012 – 2014	NIOSH [o]
Sweden	Abisko [c]	Winiger et al. 2016 *	17	68 [k]	42 ± 15	2011 – 2013	NIOSH [o]

[a] urban site. [b] rural site. [c] remote site. [d] average of four sampling sites: Zhongba, Jomsom, Pokhara, and Lumbini. [e] average of five sampling sites: Kathmandu, Dhunche, Nyalam, Lhasa, and Namco. [f] average of three sites in Rotterdam: edge of residential area north, south of city, and on a center city street. [g] average of eleven sites north of the Alps. [h] average of five sites south of the Alps. [i] average of three sites in Salt Lake City: urban site, industrial site, suburban site. [j] high pollution event/smog event. [k] summer season. [l] spring season or late winter. [m] autumn season. [n] biomass burning event. [o] using the split-time from this run method to volatilize the OC and isolate EC. [p] modified Theodore method which can include a water extraction and varying modifications to the temperature and run time. [q] He-200, He-EUSSAR_2, and He/O2-300. [r] average reported as percent modern carbon study [s] includes measurements from two sampling sites (Fairbanks and Delta Junction) and reports findings as $\Delta^{14}C$ value (per mil) *measurement from study included in Figure 8 and Figure S1

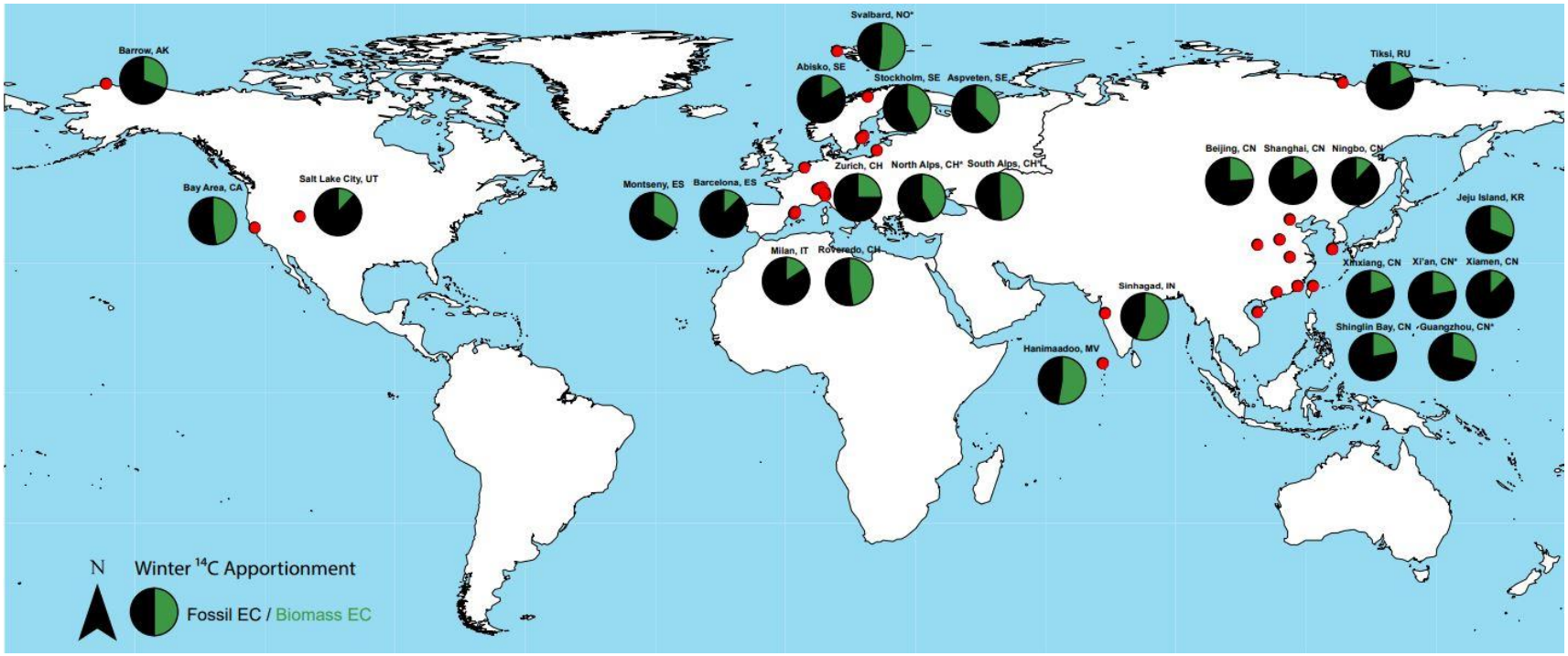

Figure 2.8. Global map of biomass burning and fossil fuel contribution of winter EC/BC values from radiocarbon-based source apportionment studies. The studies included in the figure are from literature values which have reported average winter values. *samples collected during high pollution/haze or biomass burning events.

Looking in more detail at Table 2.2, the average winter season contribution of biomass burning is 48 ± 8% for the Bay Area sites, with relatively little variability amongst the study sites. The European-based EC apportionment studies report highly varying contribution (4 – 99%) from biomass burning sources overall for winter. However, the average winter season in the Bay Area is most comparable to winter measurements in Switzerland (%BB of 25 – 63%; excluding Moleno where contribution of EC was dominated by fossil fuel sources at a %BB of 4-18%). Overall winter measurements in East Asia (%BB: 12 – 43%) had a lower EC and BC contribution from biomass burning compared to the Bay Area and the European sites. The consistently high contribution of fossil fuel combustion derived-EC in China is likely due to prominent usage of coal combustion (Cao et al., 2011; Huang et al., 2014). Relative to East Asia, South Asia had higher contribution from biomass burning (41 – 59%), which is more comparable to measurements in the Bay Area. Biomass burning, especially during the winter, is likely influenced by residential, biofuel and agricultural burning in South Asia (Bond et al., 2004; Stone et al., 2010). In the Bay Area, the average contribution of biomass burning is lower in the non-winter season (41 ± 5%). This pattern is also seen in the European studies (excluding rural site Aspvreten, Sweden). The Asian studies do not have a consistent pattern for winter versus non-winter measurements.

There are only two reported studies to compare for the contiguous U.S., which reflect very different emission scenarios. Although both studies represent urban metropolitan areas, the Bay Area results reported here have a much higher contribution from biomass burning than Salt Lake City, Utah (Mouteva et al., 2017). This may partially reflect differences in urban air quality strategies for the two regions. The Bay

Area has been reducing fossil sources, including diesel exhaust, through environmental policy while Salt Lake City is currently working on effective strategies to reduce the recent increases in wintertime $PM_{2.5}$.

Conclusion

This study provides a detailed description of the sources and seasonal trends for carbonaceous aerosols in the San Francisco Bay Area, including inter-comparison across two receptor-based EC apportionments techniques, two emissions inventories, and a comparison to global studies of ^{14}C -based EC apportionment. The two receptor-based techniques ($\Delta^{14}C$ and CMB) were very similar on average, although individual sites had larger differences. Of the seven cities included in this study, San Francisco and Napa were the most different in terms of source contributions. Napa had the highest EC mass concentration (winter and non-winter: 1.34 and 0.40 μg m^{-3}, respectively) for both seasons, and a significantly higher contribution from biomass burning than the other sites in winter (^{14}C and CMB: 63 and 75%, respectively). In Napa, enhancement of aerosols in the winter is influenced by both meteorology and change of emission sources (i.e. increased residential wood burning). EC in San Francisco is mainly from fossil fuel combustion for both seasons, (^{14}C and CMB: both 65%). For the remaining four sites (Concord, San Pablo, San Rafael, and Cupertino) EC concentrations and source contributions are similar for the non-winter, but Cupertino has a much lower EC concentration in the winter. For San Francisco and these four sites, unlike Napa, the similar fractions of contemporary and biomass burning contributions during the two seasons suggest that seasonal variation in concentrations is largely driven by meteorology.

Although the receptor-based source apportionment techniques had similar results for the split between biomass burning and fossil fuel combustion, there was a larger difference between the receptor-based versus the emissions inventories. Average biomass burning contribution from both emissions inventories is 19% which under predicts receptor-based results by 27% and 35% for ^{14}C and CMB, respectively. Contribution of diesel sources in both emissions inventories (including off-road mobile from CARB-EI) has an estimated average contribution of 49% which over predicts receptor-based CMB results by 27%. These results suggest that current EIs have not yet sufficiently accounted for the reductions in EC from diesel emissions that have resulted from improvements in diesel engines and cleaner fuels. Another potential reason may be inherent differences in bottom-up and top-down approaches: EIs account for a comprehensive set of emissions in a specified area and time while receptor-based ambient aerosol measurements will represent all aerosol, whether emitted within the EI region or transported from another region. However, transport of biomass burning EC into the Bay Area from outside of California (therefore outside of the EIs), maybe partially responsible for the observed higher biomass burning contribution to EC. Even so, based on this study the Bay Area will require emission reductions specific to the samples. Additional biomass burning regulations would most improve air quality in Napa, while more stringent motor vehicle regulations would have the largest impact in San Francisco.

Though it has been established that EC (or BC) concentrations have been decreasing across the US in the last several decades (Kirchstetter et al., 2017), results of the current study and the accumulated global studies indicate that in developed countries with intense air pollution regulations, biomass burning may be increasingly important for

ambient EC concentrations. With the variation reported for the U.S. and Europe, continued characterization of EC, including source apportionment by ^{14}C, is needed in the U.S. to evaluate the efficacy of pollution control strategies and to continue to reduce PM pollution in urban, rural and remote regions.

Acknowledgments

Funding: This work was supported by the Bay Area Air Quality Management District [contract numbers 2013.075 and 2015.160].

References

2012a. 2012 Wildfire Activity Statistics, California Department of Forestry and Fire Protection (CAL FIRE), pp. 20-21.

2012b. California: 2010 Population and Housing Unit Counts, U.S. Census Bureau.

2012c. Texas: 2010. Population and Housing Unit Counts, 2010 Census of Population and Housing. U.S. Census Bureau.

2016. CARB Black Carbon Emission Inventory Technical Support Document, California Air Resources Board (CARB).

Andersson, A., Deng, J., Du, K., Zheng, M., Yan, C., Sköld, M., Gustafsson, O.r., 2015. Regionally-varying combustion sources of the January 2013 severe haze events over eastern China. Environ. Sci. Technol. 49, 2038-2043.

Bahadur, R., Feng, Y., Russell, L.M., Ramanathan, V., 2011. Impact of California's air pollution laws on black carbon and their implications for direct radiative forcing. Atmos. Environ. 45, 1162-1167.

Barbero, R., Abatzoglou, J., Larkin, N., Kolden, C., Stocks, B., 2015. Climate change presents increased potential for very large fires in the contiguous United States. International Journal of Wildland Fire 24, 892-899.

Barrett, T., Robinson, E., Usenko, S., Sheesley, R., 2015. Source contributions to wintertime elemental and organic carbon in the western arctic based on radiocarbon and tracer apportionment. Environ. Sci. Technol. 49, 11631-11639.

Bond, T.C., Streets, D.G., Yarber, K.F., Nelson, S.M., Woo, J.H., Klimont, Z., 2004. A technology-based global inventory of black and organic carbon emissions from combustion. J. Geophys. Res. Atmos. 109.

Briggs, N.L., Long, C.M., 2016. Critical review of black carbon and elemental carbon source apportionment in Europe and the United States. Atmos. Environ. 144, 409-427.

Budhavant, K., Andersson, A., Bosch, C., Kruså, M., Kirillova, E., Sheesley, R., Safai, P., Rao, P., Gustafsson, Ö., 2015. Radiocarbon-based source apportionment of elemental carbon aerosols at two South Asian receptor observatories over a full annual cycle. Environ. Res. Lett. 10, 064004.

Cao, J.-j., Chow, J.C., Tao, J., Lee, S.-c., Watson, J.G., Ho, K.-f., Wang, G.-h., Zhu, C.-s., Han, Y.-m., 2011. Stable carbon isotopes in aerosols from Chinese cities: Influence of fossil fuels. Atmos. Environ. 45, 1359-1363.

Chen, B., Andersson, A., Lee, M., Kirillova, E.N., Xiao, Q., Kruså, M., Shi, M., Hu, K., Lu, Z., Streets, D.G., 2013. Source forensics of black carbon aerosols from China. Environ. Sci. Technol. 47, 9102-9108.

Chow, J.C., Watson, J.G., Crow, D., Lowenthal, D.H., Merrifield, T., 2001. Comparison of IMPROVE and NIOSH carbon measurements. Aerosol Science & Technology 34, 23-34.

Chow, J.C., Watson, J.G., Lowenthal, D.H., Chen, L.-W.A., Motallebi, N., 2010. Black and organic carbon emission inventories: review and application to California. J. Air Waste Manag. Assoc. 60, 497-507.

Chow, J.C., Watson, J.G., Pritchett, L.C., Pierson, W.R., Frazier, C.A., Purcell, R.G., 1993. The DRI thermal/optical reflectance carbon analysis system: description, evaluation and applications in US air quality studies. Atmospheric Environment. Part A. General Topics 27, 1185-1201.

Claire, S.J., Dinh, T. M., Fanai, A. K., Nguyen, M. H., Schultz, S. A., 2015. Bay Area Emissions Inventory Summary Report: Greenhouse Gases. Base Year 2011. Bay Area Air Quality Management District.

Dallmann, T.R., Harley, R.A., Kirchstetter, T.W., 2011. Effects of Diesel Particle Filter Retrofits and Accelerated Fleet Turnover on Drayage Truck Emissions at the Port of Oakland. Environ. Sci. Technol. 45, 10773-10779.

Dallmann, T.R., Kirchstetter, T.W., DeMartini, S.J., Harley, R.A., 2013. Quantifying On-Road Emissions from Gasoline-Powered Motor Vehicles: Accounting for the Presence of Medium- and Heavy-Duty Diesel Trucks. Environ. Sci. Technol. 47, 13873-13881.

Dusek, U., Monaco, M., Prokopiou, M., Gongriep, F., Hitzenberger, R., Meijer, H., Röckmann, T., 2014. Evaluation of a 2-step thermal method for separating organic and elemental carbon for radiocarbon analysis. Atmospheric Measurement Techniques Discussions 7, 131-169.

Fairley, D., 2012. Sources of Bay Area Fine Particles: 2010 Update and Trends.

Fairley, D., 2014. Wood-burning devices in the San Francisco Bay Area-Update. Bay Area Air Qualtiy Management Office Memorandum.

Fanai, A.K., Claire, S.J., Dinh, T.M., Nguyen, T.H., Schultz, S.A., 2014. Bay Area Emissions Inventory Summary Report: Criteria Air Pollutants. Base Year 2011. Bay Area Air Quality Management District.

Fraser, M., Yue, Z., Buzcu, B., 2003. Source apportionment of fine particulate matter in Houston, TX, using organic molecular markers. Atmos. Environ. 37, 2117-2123.

Glen, W.G., Zelenka, M.P., Graham, R.C., 1996. Relating meteorological variables and trends in motor vehicle emissions to monthly urban carbon monoxide concentrations. Atmospheric Environment 30, 4225-4232.

Huang, R.-J., Zhang, Y., Bozzetti, C., Ho, K.-F., Cao, J.-J., Han, Y., Daellenbach, K.R., Slowik, J.G., Platt, S.M., Canonaco, F., 2014. High secondary aerosol contribution to particulate pollution during haze events in China. Nature 514, 218.

Kirchstetter, T.W., Aguiar, J., Tonse, S., Fairley, D., Novakov, T., 2008a. Black carbon concentrations and diesel vehicle emission factors derived from coefficient of haze measurements in California: 1967–2003. Atmos. Environ. 42, 480-491.

Kirchstetter, T.W., Agular, J., Tonse, S., Fairley, D., Novakov, T., 2008b. Black carbon concentrations and diesel vehicle emission factors derived from coefficient of haze measurements in California: 1967-2003. Atmos. Environ. 42, 480-491.

Kirchstetter, T.W., Harley, R.A., Kreisberg, N.M., Stolzenburg, M.R., Hering, S.V., 1999. On-road measurement of fine particle and nitrogen oxide emissions from light-and heavy-duty motor vehicles. Atmos. Environ. 33, 2955-2968.

Kirchstetter, T.W., Preble, C.V., Hadley, O.L., Bond, T.C., Apte, J.S., 2017. Large reductions in urban black carbon concentrations in the United States between 1965 and 2000. Atmos. Environ. 151, 17-23.

Kleindienst, T.E., Jaoui, M., Lewandowski, M., Offenberg, J.H., Lewis, C.W., Bhave, P.V., Edney, E.O., 2007. Estimates of the contributions of biogenic and anthropogenic hydrocarbons to secondary organic aerosol at a southeastern US location. Atmos. Environ. 41, 8288-8300.

Lewis, C.W., Klouda, G.A., Ellenson, W.D., 2004. Radiocarbon measurement of the biogenic contribution to summertime PM-2.5 ambient aerosol in Nashville, TN. Atmos. Environ. 38, 6053-6061.

Liu, J., Li, J., Ding, P., Zhang, Y., Liu, D., Shen, C., Zhang, G., 2017. Optimizing isolation protocol of organic carbon and elemental carbon for 14C analysis using fine particulate samples. Atmos. Environ. 154, 9-19.

Lough, G.C., Christensen, C.G., Schauer, J.J., Tortorelli, J., Mani, E., Lawson, D.R., Clark, N.N., Gabele, P.A., 2007. Development of molecular marker source profiles for emissions from on-road gasoline and diesel vehicle fleets. J. Air Waste Manag. Assoc. 57, 1190-1199.

Malone, K.B., M. and Nguyen, D., 2013. 2012 Air Monitoring Network Plan.

McLarney, T., Sarles, R., 2005. Spare the air tonight study: 2005-2006 winter wood smoke season., True North Research, Inc.

Mohn, J., Szidat, S.n., Fellner, J., Rechberger, H., Quartier, R., Buchmann, B., Emmenegger, L., 2008. Determination of biogenic and fossil CO 2 emitted by waste incineration based on 14 CO 2 and mass balances. Bioresource Technology 99, 6471-6479.

Mohr, C., Huffman, J.A., Cubison, M.J., Aiken, A.C., Docherty, K.S., Kimmel, J.R., Ulbrich, I.M., Hannigan, M., Jimenez, J.L., 2009. Characterization of primary organic aerosol emissions from meat cooking, trash burning, and motor vehicles with high-resolution aerosol mass spectrometry and comparison with ambient and chamber observations. Environ. Sci. Technol. 43, 2443-2449.

Mouteva, G.O., Randerson, J.T., Fahrni, S.M., Bush, S.E., Ehleringer, J.R., Xu, X., Santos, G.M., Kuprov, R., Schichtel, B.A., Czimczik, C.I., 2017. Using radiocarbon to constrain black and organic carbon aerosol sources in Salt Lake City. J. Geophys. Res. Atmos. 122, 9843-9857.

Riley, K.L., Abatzoglou, J.T., Grenfell, I.C., Klene, A.E., Heinsch, F.A., 2013. The relationship of large fire occurrence with drought and fire danger indices in the western USA, 1984–2008: the role of temporal scale. International Journal of Wildland Fire 22, 894-909.

Rinehart, L.R., Fujita, E.M., Chow, J.C., Magliano, K., Zielinska, B., 2006. Spatial distribution of PM2. 5 associated organic compounds in central California. Atmos. Environ. 40, 290-303.

Rogge, W.F., Hildemann, L.M., Mazurek, M.A., Cass, G.R., Simoneit, B.R., 1991. Sources of fine organic aerosol. 1. Charbroilers and meat cooking operations. Environ. Sci. Technol. 25, 1112-1125.

Schauer, J.J., Cass, G.R., 2000. Source apportionment of wintertime gas-phase and particle-phase air pollutants using organic compounds as tracers. Environ. Sci. Technol. 34, 1821-1832.

Schauer, J.J., Rogge, W.F., Hildemann, L.M., Mazurek, M.A., Cass, G.R., Simoneit, B.R., 1996. Source apportionment of airborne particulate matter using organic compounds as tracers. Atmos. Environ. 30, 3837-3855.

Sheesley, R.J., Kirillova, E., Andersson, A., Krusa, M., Praveen, P.S., Budhavant, K., Safai, P.D., Rao, P.S.P., Gustafsson, O., 2012. Year-round radiocarbon-based source apportionment of carbonaceous aerosols at two background sites in South Asia. J. Geophys. Res. Atmos. 117.

Slater, J., Currie, L.A., Dibb, J.E., Benner, B., 2002. Distinguishing the relative contribution of fossil fuel and biomass combustion aerosols deposited at Summit, Greenland through isotopic and molecular characterization of insoluble carbon. Atmos. Environ. 36, 4463-4477.

Stone, E.A., Schauer, J.J., Pradhan, B.B., Dangol, P.M., Habib, G., Venkataraman, C., Ramanathan, V., 2010. Characterization of emissions from South Asian biofuels and application to source apportionment of carbonaceous aerosol in the Himalayas. Journal of Geophysical Research: Atmospheres 115.

Strader, R., Lurmann, F., Pandis, S.N., 1999. Evaluation of secondary organic aerosol formation in winter. Atmos. Environ. 33, 4849-4863.

Stuiver, M., Polach, H.A., 1977. Discussion; reporting of C-14 data. Radiocarbon 19, 355-363.

Szidat, S., Jenk, T.M., Synal, H.A., Kalberer, M., Wacker, L., Hajdas, I., Kasper-Giebl, A., Baltensperger, U., 2006. Contributions of fossil fuel, biomass-burning, and biogenic emissions to carbonaceous aerosols in Zurich as traced by 14C. J. Geophys. Res. 111.

Turpin, B.J., Huntzicker, J.J., 1995. Identification of secondary organic aerosol episodes and quantitation of primary and secondary organic aerosol concentrations during SCAQS. Atmos. Environ. 29, 3527-3544.

Turpin, B.J., Huntzicker, J.J., Larson, S.M., Cass, G.R., 1991. Los Angeles summer midday particulate carbon: primary and secondary aerosol. Environ. Sci. Technol. 25, 1788-1793.

Westerling, A.L., Hidalgo, H.G., Cayan, D.R., Swetnam, T.W., 2006. Warming and earlier spring increase western US forest wildfire activity. Science 313, 940-943.

Zenker, K., Vonwiller, M., Szidat, S., Calzolai, G., Giannoni, M., Bernardoni, V., Jedynska, A.D., Henzing, B., Meijer, H.A., Dusek, U., 2017. Evaluation and Inter-Comparison of Oxygen-Based OC-EC Separation Methods for Radiocarbon Analysis of Ambient Aerosol Particle Samples. Atmosphere 8, 226.

Zhang, Y.-L., Li, J., Zhang, G., Zotter, P., Huang, R.-J., Tang, J.-H., Wacker, L., Prévôt, A.S., Szidat, S.n., 2014. Radiocarbon-based source apportionment of carbonaceous aerosols at a regional background site on Hainan Island, South China. Environ. Sci. Technol. 48, 2651-2659.

Zheng, M., Cass, G.R., Schauer, J.J., Edgerton, E.S., 2002. Source apportionment of PM2. 5 in the southeastern United States using solvent-extractable organic compounds as tracers. Environ. Sci. Technol. 36, 2361-2371.

Zotter, P., El-Haddad, I., Zhang, Y., Hayes, P.L., Zhang, X., Lin, Y.H., Wacker, L., Schnelle-Kreis, J., Abbaszade, G., Zimmermann, R., 2014. Diurnal cycle of fossil and nonfossil carbon using radiocarbon analyses during CalNex. J. Geophys. Res. Atmos. 119, 6818-6835.

CHAPTER THREE

Fine and Coarse Carbonaceous Aerosol in Houston, TX during DISCOVER-AQ

This chapter published as: Yoon, S.; Usenko, S.; Sheesley, R.J. Fine and Coarse Carbonaceous Aerosol in Houston, TX during DISCOVER-AQ. *Atmosphere* **2020**. *11(5)*, 482

Abstract

To investigate major sources and trends of particulate pollution in Houston, total suspended particulate (TSP) and fine particulate matter ($PM_{2.5}$) samples were collected and analyzed. Characterization of organic (OC) and elemental (EC) carbon combined with realtime black carbon (BC) concentration provided insight into the temporal trends of $PM_{2.5}$ and coarse PM (subtraction of $PM_{2.5}$ from TSP) during the Deriving Information on Surface Conditions from Column and VERtically Resolved Observations Relevant to Air Quality (DISCOVER-AQ) Campaign Houston 2013. Ambient OC, EC, and BC concentrations were highest in the morning, likely due to motor vehicle exhaust emissions associated with the morning rush hour. The morning periods also had the lowest OC to EC ratios, indicative of primary combustion sources. Houston also had significant coarse EC at the downtown site, with an average (± standard deviation) $PM_{2.5}$ to TSP ratio of 0.52 ± 0.18 and an average coarse EC concentration of 0.44 ± 0.24 $\mu g \cdot C \cdot m^{-3}$. The coarse EC concentrations were likely associated with less efficient industrial combustion processes from industry near downtown Houston. During the last week (20–28 September, 2013), increases in OC and EC concentrations were predominantly in the fine fraction. Both $PM_{2.5}$ and TSP samples from the last week were

further analyzed using radiocarbon analysis. Houston's carbonaceous aerosol was determined to be largely from contemporary sources for both size fractions; however, $PM_{2.5}$ had less impact from fossil sources. There was an increasing trend in fossil carbon during a period with the highest carbonaceous aerosol concentrations (September 24 night and 25 day) that was observed in both the $PM_{2.5}$ and TSP. Overall, this study provided insight into the sources and trends of both fine and coarse PM in a large urban U.S. city impacted by a combination of urban, industrial, and biogenic emissions sources.

Introduction

It is important to improve characterization of carbonaceous aerosols because they impact both human health and global climate. Carbonaceous aerosols can impact climate change directly via absorption and scattering of radiation (Chung et al., 2012), as well as indirectly due to the aerosols' ability to act as cloud condensation nuclei (Novakov and Penner, 1993; Spracklen et al., 2011). The complex interactions between carbonaceous aerosols and climate change are still being studied (Kanakidou et al., 2005; Tsigaridis et al., 2014). Similarly, the human health impacts of atmospheric aerosols are being investigated in urban settings. Prolonged exposure to respirable PM (PM_{10}; particulates with an aerodynamic diameter of 10 μm and smaller), and more significantly fine PM ($PM_{2.5}$; particulates with an aerodynamic diameter of 2.5 μm and smaller), has been found to cause respiratory and cardiopulmonary diseases and overall increased mortality (Brook et al., 2010; Dockery and Pope, 1994; Laden et al., 2000). In the short term, epidemiological studies have observed an increase in nonaccidental, respiratory-related hospital emergency visits on days with enhanced PM (Chen et al., 2013; Delfino et al.,

1998). Thus, improving understanding of the sources and trends in urban aerosol will enable better mitigation strategies for both climate and human health.

Houston, TX, is the fourth most populous city in the U.S., with 2.3 million residents (2019b), and has an abundance of anthropogenic and natural emissions. The city's air quality is impacted by urban emissions (e.g., motor vehicle exhaust (MVE), cooking, residential wood burning, etc.) and industrial emissions associated with activities in and around the Houston Ship Channel (HSC) (e.g., heavy-duty diesel exhaust, ship emissions, petrochemical and refinery processes, etc.) (Schulze et al., 2018; Sullivan et al., 2013b; Wallace et al., 2018; Zhang et al., 2017). Houston, like many southeastern U.S. cities, is also heavily impacted by biogenic emissions from vegetation within the city and forested regions surrounding the city (e.g., Piney Woods) (Figure 3.1) (Bean et al., 2016; Leong et al., 2017; Park et al., 2011). The objective of this study was to chemically characterize Houston's carbonaceous aerosol in the fine and coarse PM ($PM_{TSP-2.5}$; subtraction of carbon concentration of $PM_{2.5}$ from TSP) fractions to better understand the major sources and trends of PM in the city. For this study, filter samples and measurements were taken during the NASA-sponsored Deriving Information on Surface Conditions from Column and VERtically Resolved Observations Relevant to Air Quality (DISCOVER-AQ) campaign in September 2013 (NASA, 2019). The purpose of the DISCOVER-AQ campaign was to use ground and airborne measurements to improve the efficiency of satellites in diagnosing ground-level air quality. This study focused on ground-based measurements and sampling at two sites: a primary urban site located near the downtown area, representative of the urban Houston region, while the auxiliary site located southeast of the city was near Trinity Bay and the HSC (Figure 3.1) (Schulze et

al., 2018; Wallace et al., 2018). Organic and elemental carbon (OC and EC, respectively) concentrations and radiocarbon (^{14}C) analysis of the total organic carbon (TOC: OC + EC) were used to characterize the carbonaceous aerosols. From these measurements, week 4 of the campaign (21–28 September), was designated as the week of interest due to the increased TOC concentration in both the $PM_{2.5}$ and TSP. Previous studies also observed increased $PM_{2.5}$ mass and a peak ozone event across the Houston metropolitan area during week 4 (Baier et al., 2015; Mazzuca et al., 2016; Yoon et al., under review). In addition to these off-line analyses, real-time measurement of black carbon (BC) was made during this sampling period to evaluate hourly BC trends and compare to filter-based EC measurements. Though BC and EC are both used to describe the refractory fraction of carbonaceous aerosols, BC is defined by the aerosol's optical attenuation (Hansen et al., 1983), while EC is measured based on a thermal-optical approach (Chow et al., 2001). More recent aerosol studies in Houston have focused on fine and submicron PM size fractions; however, this study provides an in-depth characterization of both fine and coarse carbonaceous aerosols in Houston in order to identify sources, trends, and relationships between these PM size fractions.

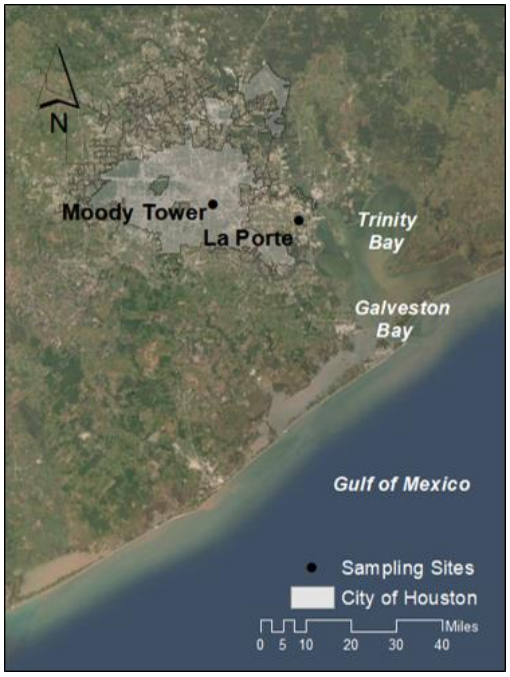

Figure 3.1. Map of the Moody Tower (MT) and La Porte (LP) sampling sites. Map includes outline of the city of Houston.

Methods and Materials

Sampling

PM filter-sample collection and BC measurement took place from 4 to 28 September and 1 to 30 September 2013, respectively. This sampling campaign was part of the larger DISCOVER-AQ campaign in Houston. The primary sampling site was on top of Moody Tower (MT; 29.7197, −95.3432), a high-rise residence hall (~70 m) located on the University of Houston's campus. This site is approximately 4.4 km southeast of downtown Houston and northwest of the HSC (Figure 3.1). The auxiliary sampling site, La Porte (LP; 29.6721, −95.0647), was located within a small municipal airport approximately 5.6 km west of Trinity Bay and close to the HSC (Figure 3.1). The LP site provides spatial comparison to the primary urban site (MT), providing insight into whether trends observed

at the urban core were present in other parts of the metropolitan area. The LP site is close to Trinity Bay and closer to the Gulf of Mexico, serving as potential upwind site for marine onshore winds to MT (Figure 3.1). This LP site is also in close proximity to the highly industrialized region of Houston (i.e., HSC).

During the campaign, $PM_{2.5}$ samples were collected at MT, while TSP samples were collected at MT and LP. A Tisch sampler with a $PM_{2.5}$ inlet (200 $L \cdot min^{-1}$, Tisch Environmental Inc. Cleves, OH, USA) and a URG medium-volume sampler with a $PM_{2.5}$ cyclone (82 $L \cdot m^{-1}$, URG Corporation, Chapel Hill, NC, USA) were used for $PM_{2.5}$ sample collection at MT. Two Tisch high-volume samplers (1170 and 1130 $L \cdot m^{-1}$) were alternated for TSP sample collection at MT. A Tisch high-volume sampler (1000 $L \cdot m^{-1}$) was also used for TSP sample collection at LP. The $PM_{2.5}$ filter-sample collections at MT included morning (06:30 to 10:00), afternoon (10:00 to 20:00), day (06:30 to 20:00), and 24-h (06:30 to 06:00) samples (Table 2.1). The TSP filter-sample collections at MT included day and night (20:00 to 06:30) samples. The TSP filter-sample collection at LP included 24-h samples (Table 2.1). Both filter samples and blanks were collected on 90 mm and 102 mm quartz fiber filters for $PM_{2.5}$ samples, respectively, while 20 × 25 cm quartz fiber filters were used for the TSP samples. All quartz fiber filters were pre-cleaned (i.e., baked at 500 °C for 12 h), wrapped in pre-cleaned aluminum foil packages, sealed in Ziploc bags, and stored in on-sight freezers until they were brought back to Baylor University for permanent storage. A more detailed sampling description of the MT samples has been published previously (Clark et al., 2015).

Table 3.1. Description of filter samples for reported filter-based analysis. MT = Moody Tower; LP = La Porte; PM = particulate matter; TSP = total suspended particulate; MV = medium volume; HV = high volume; OC = organic carbon; EC = elemental carbon.

Site	Size Fraction	Sampler Type	Samples	Sample Duration	Analysis
MT	$PM_{2.5}$	Tisch	4–28 September	morning, afternoon, day	OC EC
			21–28 September	day	^{14}C
		MV URG	6–28 September	24-h	OC EC
			23–25 September	24-h	^{14}C
LP	TSP	HV Tisch	4–28 September	morning, afternoon, day, night, 24-h	OC EC
			23–25 September	day and night	^{14}C
		HV Tisch	21–26 September	24-h	OC EC, ^{14}C

The BC measurement was made at MT using a seven-channel AE42 Aethalometer (Magee Scientific, Berkeley, CA, USA). The instrument had a $PM_{2.5}$ impactor at the inlet with a flowrate of 4 $L \cdot m^{-1}$. The time interval for data logging of the aethalometer was set to 5 m and was averaged for hourly BC data. For comparison to filter-based bulk carbon measurements, the hourly BC concentrations were averaged in agreement to the duration of each filter sample.

Sample and Measurement Analysis

Bulk carbon analysis. All filter-based samples were analyzed for bulk OC and EC concentrations (Table S1) with a thermal-optical-transmittance carbon analyzer (Sunset Laboratory Inc., Tigard, OR, USA) utilizing the National Institute for Occupational Safety and Health 5040 protocol (Barrett and Sheesley, 2014; Birch and Cary, 1996; Schauer, 2003). For quality assurance purposes, sucrose spikes were run daily, and triplicate analysis was completed for every tenth sample run with a relative standard deviation of 4.6 and 1.9% for OC and EC, respectively. Each sample was blank-corrected using an average of several field blanks. $PM_{2.5}$ blank filters (n = 7) averaged (± standard deviation; SD) 0.83 ± 0.65 $\mu g \cdot C \cdot cm^{-2}$, which was an average of 14 ± 9% of the sample OC. TSP blank filters (n = 4) averaged 0.24 ± 0.06 $\mu g \cdot C \cdot cm^{-2}$, which was an

average of 2 ± 1% of the sample OC. There were no EC contributions in either $PM_{2.5}$ and TSP filter blanks.

TSP samples were also analyzed for calcium carbonate (CC) contribution utilizing removal by acid fumigation (Cachier et al., 1989; Tian et al., 2019) and then reanalysis of the OC and EC. In brief, a 1.5 cm^2 punch of each TSP filter sample was placed in a pre-cleaned glass petri dish and exposed to 1 N hydrochloric acid (Fisher Chemical, Hampton, NH, USA) in a desiccator for 12 h, where CC would be released. These samples were then dried at 60 °C for 1 h and analyzed for CC-free OC and EC on the carbon analyzer. Average percent contributions (±SD) of CC to OC and EC concentrations were −8 ± 7% and 13 ± 22%, respectively. This low CC contribution in the TSP was not considered significant as it was within the OC and EC uncertainty (79 and 88% of CC concentration were within the uncertainty for OC and EC, respectively). Therefore, there was no indication of a positive bias in EC due to CC contribution for these Houston samples. This is in contrast to samples collected in Beijing, where CC contributed from 22–88% of coarse EC (Tian et al., 2019). The CC contribution in Houston was more comparable to contributions at urban-industrial sites in the southeastern U.S. cities (less than 10%) (Edgerton et al., 2009). Since there was minimal CC contribution and its concentration was largely within the measure of uncertainty for the OC and EC concentration, no further discussion of CC will be included.

BC Corrections

The AE42 measures the light attenuation of light-absorbing aerosols deposited onto a filter at seven different wavelengths: 370, 470, 520, 590, 660, 880, and 950 nm. The 880 nm wavelength was used as the BC equivalent (Snyder and Schauer, 2007).

However, the aethalometer is biased to multiple light scattering (C) and shadowing effects (R(ATN)). Corrections were made for these biases for the absorption coefficient at 880 nm based on Schmid et al.'s (2006) calculation:

$$\sigma_{aeth} = \frac{\sigma_{ATN}}{C\ R(ATN)}. \quad (1)$$

The calculation for these corrections is further detailed in the Supplementary Materials (S1).

Radiocarbon Analysis of TOC

Filter samples, including day and 24-h $PM_{2.5}$ samples from MT, day and night TSP samples from MT, and 24-h TSP samples from LP (Table 1, Table S2), were analyzed for ^{14}C by accelerator mass spectrometry (AMS) at the National Ocean Sciences AMS facility (Woods Hole, MA, USA). All filter preparation was completed at Baylor University. For the ^{14}C measurement, a filter area equivalent to ~60 µg of TOC per sample was allocated for the analysis. The collected filter aliquots were stored in pre-cleaned glass Petri dishes. These samples and blank filters were acid fumigated using the same 1 N hydrochloric acid method for the CC protocol. The samples were then shipped to the National Ocean Sciences AMS facility where samples are compressed to graphite and analyzed for ^{14}C abundance using their AMS.

The AMS measures the ratio of ^{14}C to ^{12}C for the samples, field blanks, and a modern reference standard, which is 0.95 times the specific activity of oxalic acid, the standard reference material (Stuiver and Polach, 1977). The National Ocean Sciences AMS report their data as fraction modern (F_m), which is described in equation 2.

$$F_m = \frac{(^{14}C/^{12}C)_{sample} - (^{14}C/^{12}C)_{blank}}{(^{14}C/^{12}C)_{AD1950} - (^{14}C/^{12}C)_{blank}}. \quad (2)$$

As in equation 3, the $\Delta^{14}C$ value can be calculated from the F_m value, where the λ is the inverse of the ^{14}C half-life (i.e., 5730 years). The $\Delta^{14}C$ is corrected for Y_c, and the year the sample was collected.

$$\Delta^{14}C = \left[F_m * e^{\lambda(1950-Y_c)} - 1\right] * 1000. \quad (3)$$

^{14}C Source Apportionment of TOC

The $\Delta^{14}C$ value of each sample can be used to apportion the TOC to fossil (f_{fossil}) and contemporary carbon (f_{cont}) using equation 4. For this calculation, a contemporary end member ($\Delta^{14}C_{cont}$) of +67.5‰ (average of +107.5‰ and +28‰ representing wood burning and annual growth, respectively (Zotter et al., 2014)) and a fossil end member ($\Delta^{14}C_{fossil}$) of −1000‰ (Gustafsson et al., 2009) was used.

$$\Delta^{14}C_{sample} = \left(\Delta^{14}C_{cont}\right)\left(f_{cont}\right) + \left(\Delta^{14}C_{fossil}\right)(1 - f_{cont}). \quad (4)$$

Uncertainty for each measurement was calculated based on the instrumental standard error, the relative difference of the F_m blank correction, and the SD between results using contemporary end member separately (+107.5‰ and +28‰) for the $\Delta^{14}C$ calculation.

Results and Discussion

Bulk Carbon Measurements

Carbonaceous aerosols trends of $PM_{2.5}$ at MT. Based on the bulk carbon measurement (Table S1), two distinct periods of increased TOC concentrations were observed: 8–15 September (week 2; W2) and 21–28 September (week 4; W4), respectively (Figure 3.2a,b). Both weeks began with several days of increasing TOC until

reaching a peak concentration followed by a few days of declining TOC concentration (Figure 3.2a,b). The ambient OC concentration for both weeks was statistically larger compared to the rest of the sampling period (*t*-test; $p > 0.05$). The temporal trends observed in the MT TOC were also observed in $PM_{2.5}$ mass concentrations measured across the Houston metropolitan area (Bean et al., 2016; Leong et al., 2017; Yoon et al., under review). The description of these two weeks will be further detailed in a future study (under review).

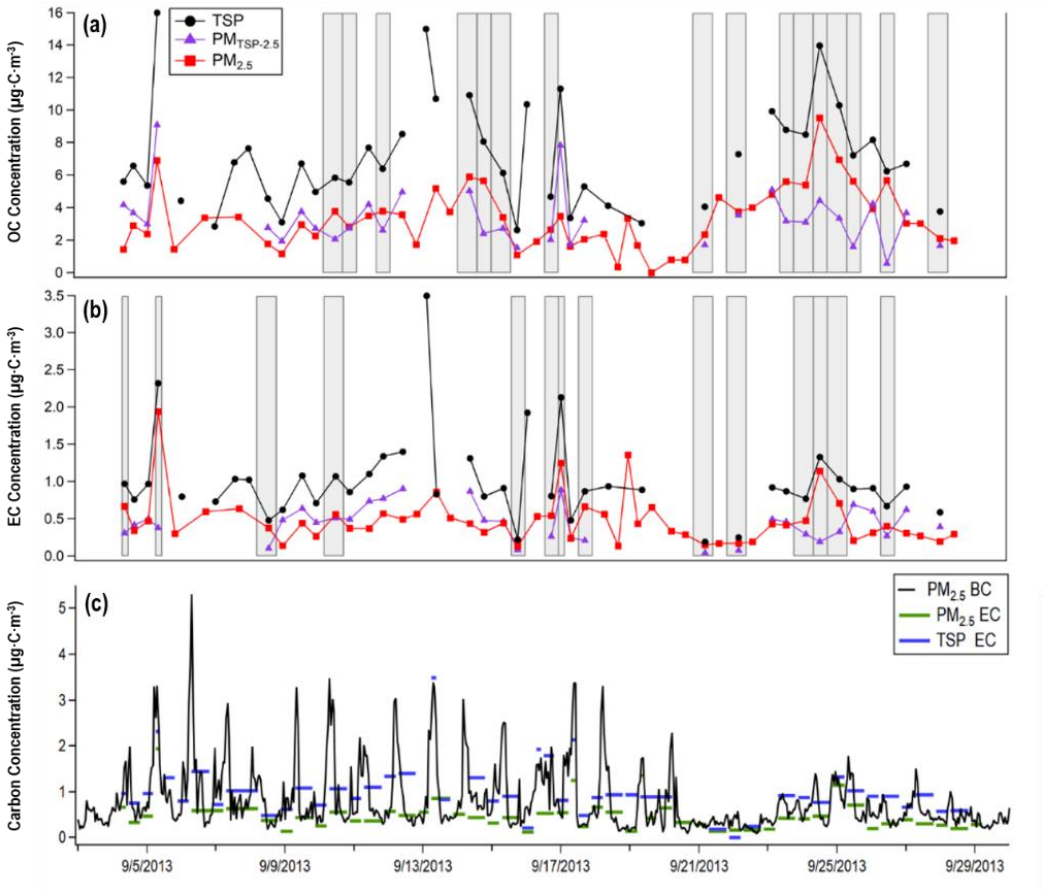

Figure 3.2. Carbonaceous aerosol concentrations at MT during the full sampling campaign. Figure includes filter-based (a) OC and (b) EC concentration of TSP, $PM_{2.5}$, and the calculated coarse PM. For (a),(b) The lines between each marker indicate continuous filter collection, while the gray boxes highlight samples where carbon concentrations were higher in the fine than the coarse PM. (c) Hourly-averaged black carbon (BC) and filter-based $PM_{2.5}$ and TSP EC concentration. The filter-based samples include morning, afternoon, day, and night samples.

The average $PM_{2.5}$ OC and EC concentrations during the campaign (morning, afternoon, day, and night) are reported in Tables 2 and 3. The highest average OC and EC concentrations (±SD) were from the morning (n = 4) with an average of 3.8 ± 2.3 and 1.3 ± 0.5 µg C m^{-3}, respectively, while afternoon (n = 3) periods had the lowest average concentrations of OC and EC at 2.06 ± 0.72 and 0.34 ± 0.10 µg·C·m^{-3}, respectively. There was no significant difference between morning and daytime OC concentrations (Mann-Whitney test; $p > 0.05$), while the EC concentration during the morning was significantly higher than the daytime (Mann-Whitney test; $p < 0.05$). The morning sampling periods (06:00–10:00) were shorter and intended to capture the morning rush hour where emission of carbonaceous aerosol was likely increased due to the influx of MVE emission combined with the lower boundary layer; this will be discussed further in Section 3.1.2 with the hourly BC results. The OC and EC concentrations during the day and nighttime were not significantly different (t-test; $p > 0.05$).

Table 3.2. The average and maximum concentration of OC for the different (morning, afternoon, day, and night) PM2.5 and TSP samples at Moody Tower. The number of samples for each sample type and the sample day for maximum OC concentrations are also included.

PM Type	Sample Type	Sample No.	Average OC (±SD) (μg·C·m^{-3})	Max. OC sample	Max. OC Conc (μg·C·m^{-3})
$PM_{2.5}$	morning	4	3.79 ± 2.27	5 September	6.90 ± 0.71
	afternoon	3	2.06 ± 0.72	4 September	2.89 ± 0.27
	day	19	3.55 ± 1.56	25 September	6.94 ± 0.44
	night[1]	22	3.21 ± 2.25	24 September	9.51 ± 0.89
TSP	morning	5	11.64 ± 4.13	5 September	15.98 ± 1.14
	afternoon	3	6.87 ± 3.67	13 September	10.69 ± 0.78
	day	16	7.24 ± 2.12	14 September	10.92 ± 0.60
	night	16	6.07 ± 2.78	24 September	13.95 ± 0.83

[1]includes calculated night carbon concentration from PM_{TSP} (24-h) and $PM_{2.5}$ (morning and afternoon or day) samples.

Table 3.3. The average and maximum concentration of EC for the different (morning, afternoon, day, and night) PM2.5 and TSP samples at Moody Tower. The number of samples for each sample type and the sample day for maximum EC concentrations are also included.

PM Type	Sample Type	Sample No.	Average EC (±SD) (μg·C·m^{-3})	Max. EC sample	Max. EC Conc (μg·C·m^{-3})
$PM_{2.5}$	morning	4	1.30 ± 0.52	September 5	1.94 ± 0.40
	afternoon	3	0.34 ± 0.10	September 19	0.43 ± 0.14
	day	19	0.43 ± 0.18	September 13	0.86 ± 0.12
	night[1]	22	0.40 ± 0.24	September 24	1.14 ± 0.21
TSP	morning	5	2.17 ± 0.90	September 13	3.49 ± 0.46
	afternoon	3	0.69 ± 0.18	September 13	0.83 ± 0.28
	day	16	0.87 ± 0.34	September 12	1.40 ± 0.16
	night	16	0.84 ± 0.26	September 11	1.34 ± 0.20

[1]includes calculated night carbon concentration from PM_{TSP} (24-h) and $PM_{2.5}$ (morning and afternoon or day) samples.

The $PM_{2.5}$ OC to EC ratio (OC/EC) was utilized as a qualitative indicator of potential secondary organic aerosol (SOA) contribution (Benetello et al., 2017; Chow et

al., 1994; Turpin and Huntzicker, 1995). As EC is a tracer for primary emissions, a higher OC/EC is indicative of enhanced secondary processes. Biomass burning (BB) sources can also contribute to increased OC/EC (Benetello et al., 2017; Ram and Sarin, 2011); however, the emission ratio of OC and EC from BB can be highly variable (Hong et al., 2017; Zhang et al., 2013). Urban studies have utilized OC/EC for identifying BB contribution generally during the winters as SOA contribution is more prominent during the summer periods (Benetello et al., 2017; Viana et al., 2007). For this study, high OC/EC may indicate increased SOA contribution, but BB cannot be ruled out by this method. Average OC/EC during the full campaign period was 8.7 ± 5.8. The average OC/EC (±SD) of $PM_{2.5}$ for the morning, afternoon, day, and night periods were 2.7 ± 0.6, 6.4 ± 2.3, 9.3 ± 4.7, and 9.8 ± 7.6, respectively. The high nighttime OC/EC is in line with Leong et al. (2017) and Bean et al.'s (2016) studies, where increased aerosols concentration due to nighttime SOA formation was observed. Unlike nighttime, the morning period (06:00–10:00) was impacted by more primary emissions reflected by increased EC concentration, a lower OC/EC, followed by a near factor of two increase in OC/EC in the afternoon (10:00–20:00) when photochemically driven SOA formation would be more prevalent.

The average OC/EC (±SD) during W2 and W4 was 8.1 ± 3.4 and 14.6 ± 6.4, respectively. The OC/EC was significantly higher during W4 compared to W2 (*t*-test; $p < 0.05$). The W4, which included an ozone event, was influenced by high atmospheric processing. Previously published studies identified an increase in processed aerosols and highly oxygenated organic aerosols across the metropolitan area during W4 (Bean et al., 2016; Leong et al., 2017). Southeastern U.S. cities are well known to be impacted by

SOA contributions associated with high biogenic emissions in this region (Zeng and Wang, 2011). Even so, overall OC/EC from this study was higher than reported for other south and southeastern U.S. cities, including Dallas, TX (summer average: 5.56) (Barrett and Sheesley, 2014), Atlanta, GA (3.05), and Centreville, AL (6.31) (Blanchard et al., 2008). They were also much higher than annual and seasonal averages in Los Angeles, CA (annual average: 2.03) (Kim et al., 2000), and New York City, NY (summer average: 4.0) (Rattigan et al., 2010), respectively.

BC and EC Comparison.

The average BC concentration (±SD) during the full sampling period was 0.80 ± 0.69 μg·C·m^{-3}. Based on hourly-averaged BC measurements for the entire campaign (Table B.3), the highest BC concentrations were between 04:00 to 10:00, peaking at 07:00 (Figure B.1). This captures Houston's morning rush hour (Czader et al., 2015). The early start may also be associated with industrial activity near the HSC, including trains and other combustion sources. The morning peak in BC concentration was also present in EC results, where the morning samples had the highest EC concentration (Figure 3.2b,c). The BC concentration was significantly higher during W2 (average: 0.93 ± 0.21 μg·C·m^{-3}) compared to W4 (0.55 ± 0.22 μg·C·m^{-3}) (*t*-test; $p < 0.05$). Defined morning peaks of BC can be observed during W2 but were not present in W4 (Figure 3.2c). Windrose plots of the BC concentrations in W2 and W4 reveal differences in wind direction between the two weeks (Figure 3). The high BC concentrations, which occurred in the mornings during W2, all come from the East, towards the HSC. This pattern was not observed in the fine EC, where there was no significant difference between W2 (average: 0.43 ± 0.18 μg·C·m^{-3}) and W4 (average: 0.36 ± 0.25 μg·C·m^{-3}) (*t*-test; $p >$

0.05). Despite this, the BC was well correlated to the fine and coarse EC with a linear regression r^2 value of 0.72 and 0.74, respectively, and a slope of 1.17 with the fine EC. It is not clear why the BC deviates from fine EC with respect to higher concentrations in W2; however, the daily filter change occurred at 06:00–06:30 every morning. This small gap in the filter data record during the peak BC hours may have resulted in a low bias for W2 EC.

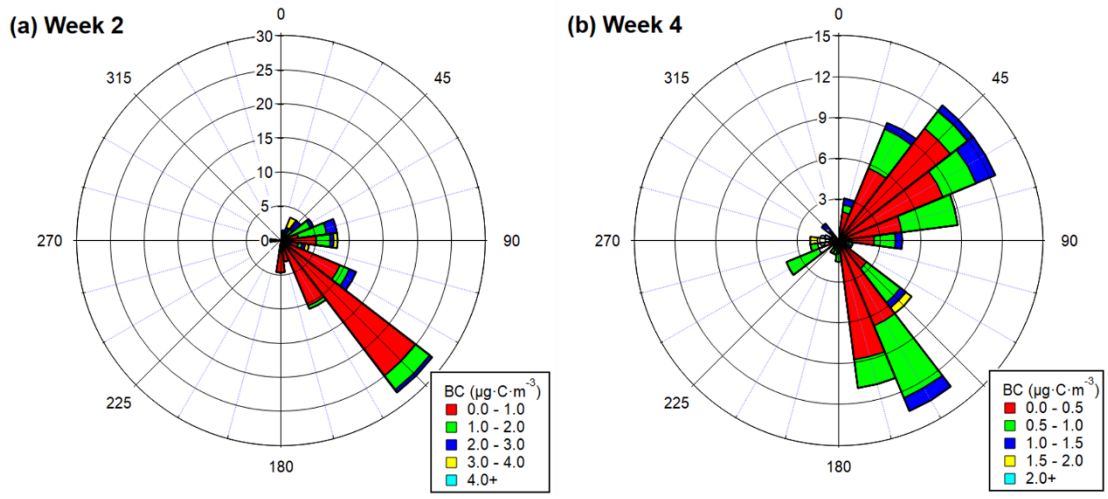

Figure 3.3. Windrose plots for BC concentration during (a) week 2 and (b) week 4 at MT. The radius axis indicates the percent contribution of wind direction sector relative to total week. The BC concentration is indicated by color, with different scales for Week 2 and Week 4.

The observed daily trend of BC was comparable to measurements made in the spring (April to May) of 2009 during the Study of Houston Atmospheric Radical Precursors (SHARP) field campaign. BC concentrations during SHARP were also high in the early morning with a peak concentration at 07:00 (Levy et al., 2013). Average BC and EC concentrations (±SD) during SHARP were 0.31 ± 0.22 and 0.38 ± 0.19 $\mu g \cdot C \cdot m^{-3}$, respectively, which is lower than the BC and EC concentrations (±SD) measured for this study in 2013 (average: 0.80 ± 0.69 and 0.48 ± 0.34 $\mu g \cdot C \cdot m^{-3}$, respectively). SHARP

measurements were made during late spring, while this study was during late summer/fall. EC measurement in both Houston and Dallas have reported higher EC concentrations during the fall and winter periods relative to spring and summer (Barrett and Sheesley, 2014), so this may just represent a seasonal difference between SHARP and DISCOVER-AQ.

Carbonaceous Aerosol Trends of TSP

The average TSP OC and EC concentrations (±SD) for the morning, afternoon, day, and night samples are reported in Table 3.2. The TSP TOC concentrations during the day and night were not significantly different (*t*-test; $p > 0.05$); however, OC and EC concentrations during the morning were significantly higher than the night (Mann-Whitney test: $p < 0.05$). This is the same trend observed in the $PM_{2.5}$ EC and BC. The TSP OC and EC concentrations were not statistically different between the two weeks of interest (W2 and W4) for either daytime (*t*-test; $p > 0.05$) or nighttime (Mann-Whitney test; $p > 0.05$). During the campaign period, the largest TSP OC concentration (±SD) was on the morning of September 5 (16 ± 1.1 μg·C·m^{-3}), while the largest EC concentration was on the morning of September 13 (3.5 ± 0.46 μg·C·m^{-3}, Table 3.2). The highest non-morning TSP OC concentration (±SD) was during the night of September 24, with a concentration of 13.95 ± 0.83 μg·C·m^{-3} (Table 3.2).

The average OC/EC for TSP during the full campaign was 8.2 ± 4.6. The average OC/EC (±SD) for the morning, afternoon, day, and night TSP were 5.5 ± 0.94, 9.5 ± 3.1, 10.1 ± 6.4, and 7.3 ± 2.4, respectively. Unlike the $PM_{2.5}$, average OC/EC was higher during the day than at night, indicating a larger contribution of non-combustion aerosols during the day. Like the $PM_{2.5}$, the day–night difference was not significant (*t*-test; $p >$

0.05). Sources of coarse OC include resuspension of soil, as well as primary biological aerosol particles (e.g., lignan polymers), which were found to be a relatively important source of coarse aerosol in Houston (Shakya et al., 2011). The average OC/EC (± SD) for W2 and W4 were 7.5 ± 2.6 and 12 ± 6.6, respectively. Like the $PM_{2.5}$, the average OC/EC during W4 was significantly higher than the average OC/EC measured during the W2 (*t*-test; $p < 0.05$). The carbonaceous aerosol in the W4 was likely impacted by increased secondary processing in the $PM_{2.5}$, while the TSP also was influenced by a change in atmospheric processing and/or sources in the later week.

Comparison of Carbonaceous Aerosols Between $PM_{2.5}$ and TSP

Direct comparison between $PM_{2.5}$ and TSP was possible for 33 samples (three morning, two afternoon, 15 day, and 13 night samples; Figure 3.2a,b). Although there were few morning and afternoon samples, these were included in the comparison. The OC and EC concentrations for $PM_{2.5}$ and TSP were strongly correlated ($r^2 = 0.70$ and 0.72, respectively). The $PM_{2.5}$ to TSP ratio ($PM_{2.5}$/TSP) for TOC, OC, and EC concentrations were each 0.52 with SDs of 0.12, 0.14, and 0.18, respectively. Average $PM_{2.5}$/TSP (±SD) for OC was slightly higher at night, 0.57 ± 0.16, compared to the day, 0.52 ± 0.09. Within the daytime, the $PM_{2.5}$/TSP for OC was higher in the afternoon, 0.46 ± 0.03, compared to the mornings, 0.33 ± 0.09. The $PM_{2.5}$/TSP for OC was also significantly higher during W2 and W4 (0.55 ± 0.13) compared to the other sampling days (0.41 ± 0.10) (*t*-test; $p < 0.05$). During these periods of enhanced TOC concentrations (W2 and W4), the enhancement in the OC was driven by an increase in fine PM relative to the coarse PM (Figure 3.2a). In Figure 3.2a,b, the gray boxes highlight periods when the carbon concentration of the fine PM was greater than the coarse PM. In

general, the W2 and W4 periods both had relatively higher OC/EC ($PM_{2.5}$) and $PM_{2.5}$/TSP. The results of these qualitative tests support that $PM_{2.5}$ OC during these periods was enhanced due to secondary processes. SOA formation is via oxidation of gas-phase precursors (e.g., volatile organic compounds (VOC)) and/or condensation of semi-volatile organic compounds. Previous studies, at varying study sites (i.e., urban, marine, and forests), have generally found these photochemically-produced aerosols in the fine and ultrafine aerosol fractions (Kavouras and Stephanou, 2002; Shiraiwa et al., 2013).

EC is formed from the incomplete combustion of either fossil fuel or BB sources and is typically distributed in the fine to ultrafine particulate fraction (Offenberg and Baker, 2000), but this was not the case for this study. Average $PM_{2.5}$/TSP (± SD) of EC was largest in the morning (0.70 ± 0.13) relative to afternoon (0.47 ± 0.03), day (0.50 ± 0.17) and night (0.50 ± 0.19) periods. The measured morning periods had higher concentrations of fine than coarse EC (Figure 3.2b). This was likely due to enhanced contribution of fine EC from MVE or activity associated with the HSC. However, the overall average $PM_{2.5}$/TSP ratio for EC was 0.52 ± 0.18, which indicates a significant contribution of EC from the coarse fraction. Concentrations of the coarse EC ranged from 0.04–0.90 $\mu g \cdot C \cdot m^{-3}$ with an average of 0.44 ± 0.24 $\mu g \cdot C \cdot m^{-3}$. Coarse EC has been measured in high concentrations in Karachi, Pakistan (2.9 $\mu g \cdot C \cdot m^{-3}$); Lahore, India (~6.3 $\mu g \cdot C \cdot m^{-3}$); and Beijing, China (2.0 $\mu g \cdot C \cdot m^{-3}$) (Shahid et al., 2016). Studies have attributed coarse EC to open field or other uncontrolled BB and/or use of less efficient/older technology for industrial combustion processes, including coke ovens, steelmaking, and transportation (Edgerton et al., 2009; Lee et al., 2008; Shahid et al., 2016). Average coarse EC concentration from this study (0.44± 0.24 $\mu g \cdot C \cdot m^{-3}$) was larger than coarse EC ($PM_{10-2.5}$)

measured in other U.S. cities, including Atlanta, GA (urban site; 0.21 ± 0.13 μg·C·m^{-3}), and Centerville, AL (rural site; 0.27 ± 0.16 μg·C·m^{-3}). However, Houston's coarse EC was significantly less than North Birmingham, AL (urban/industrial site) with an average of 2.70 ± 3.52 μg·C·m^{-3} (Edgerton et al., 2009). The large concentration of coarse EC in North Birmingham was attributed to local industrial processes, including coke ovens and steel making (Edgerton et al., 2009). The coarse EC in Houston may also be due to the different industrial activities that are close in proximity to the MT site, including a petroleum coke facility along with other industrial operations in the HSC, located approximately 10 km southeast of MT.

^{14}C-based Apportionment of $PM_{2.5}$ and TSP

Fossil and contemporary carbon for TSP versus $PM_{2.5}$. To better understand the contribution of different sources to the TOC, ^{14}C-based source apportionment was performed on $PM_{2.5}$ and TSP TOC for day and night samples during W4 (Table S2). Overall, the contribution of contemporary carbon was larger than fossil carbon for both size fractions at MT and LP. Aside from the daytime $PM_{2.5}$ on September 27 at MT where contemporary contribution (± SD) was 48 ± 3%, all contemporary contribution of TOC ($PM_{2.5}$ and TSP) was above 50% (Figure 3.4). For MT $PM_{2.5}$, the average daytime contemporary carbon contribution and concentration (± SD) during W4 was 61 ± 10% and 2.7 ± 1.1 μg·C·m^{-3}, respectively, while the nighttime (23–25 September) was 65 ± 5% and 4.7 ± 1.2 μg·C·m^{-3}, respectively. In general, daytime carbonaceous aerosols were more impacted by fossil fuel sources, while nighttime aerosols were more impacted by contemporary sources (Figure 3.4), which could include biogenic SOA or BB. A more

detailed examination of the daytime ^{14}C is included in a future manuscript (Yoon et al., under review). For MT TSP (day and night samples from 23–25 September), the average contemporary carbon contribution and concentration were 58 ± 5% and 6.2 ± 1.3 $\mu g \cdot C \cdot m^{-3}$, respectively. Like the diurnal trends observed in the $PM_{2.5}$, average contemporary carbon contribution and concentration was greater during the night (61 ± 4% and 6.7 ± 1.8 $\mu g \cdot C \cdot m^{-3}$, respectively) than the day (55 ± 5% and 5.75 ± 0.25 $\mu g \cdot C \cdot m^{-3}$, respectively). When considering source differences between fine and coarse aerosol, the average ± SD $PM_{2.5}$/TSP for contemporary carbon was 0.69 ± 0.09, while the fossil carbon was 0.56 ± 0.08. Considered as a percent contribution, the coarse PM had larger contribution from fossil carbon, ranging from 46 to 53%, compared to fine PM, ranging from 30 to 45% for 23–25 September (Figure 3.4). It is not clear if the source of this coarse fossil TOC was associated with industrial activities or is linked to soil/crustal PM.

Within W4, September 24 day to September 25 day has a different trend. The OC and EC concentrations in the fine were greater than coarse PM (Figure 3.2a,b), and the contemporary carbon contribution decreased. The carbonaceous aerosol during this period was likely driven by secondary processing of fossil carbon emissions specifically impacting the fine particulate fraction.

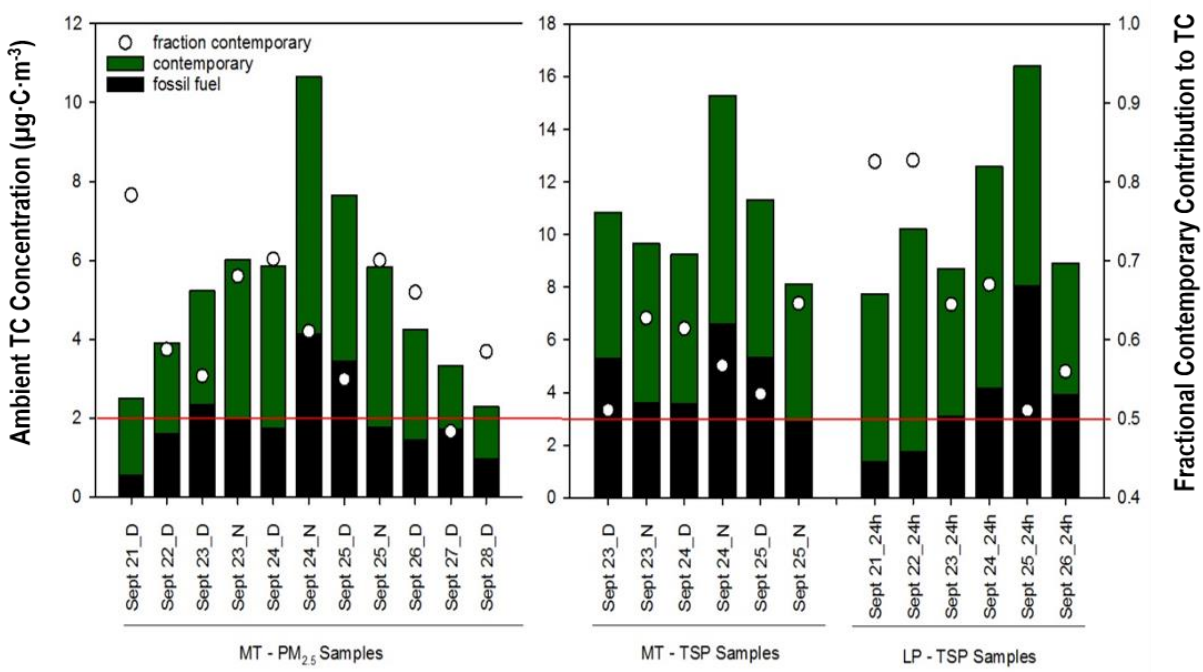

Figure 3.4**.** Radiocarbon-based apportionment of ambient total organic carbon concentration (left-axis) and fractional contemporary contribution (right-axis) of $PM_{2.5}$ day (D) and calculated night (N) samples and TSP D and N samples at MT. Apportioned TSP 24-h filter samples from LP are also included. Red line is a marker for the 0.5 contemporary carbon contribution of total organic carbon (TOC).

Source apportionment results from the auxiliary site, LP, reported a larger contribution of contemporary carbon contribution relative to the urban core site at MT. The average ± SD contemporary contribution and concentration of TSP at LP was 67 ± 13% and 7.1 µg·C·m^{-3}, respectively. The average ± SD fossil contribution and concentration for LP was 33 ± 13% and 3.7 ± 2.4 µg·C·m^{-3}, respectively. Though the LP site is closer to the HSC, the contemporary carbon contribution was higher than in MT (day and night) (Figure 3.4). However, the general trends observed during the W4 at MT for both $PM_{2.5}$ and TSP were also observed in the LP TSP (Figure 3.4). The largest contribution and concentration (± SD) of fossil carbon at LP was on September 25 with 49 ± 3 % and 8.0 µg·C·m^{-3} (Figure 3.4). Both fossil carbon contribution and concentration were higher at LP than at MT (day and night) on 25 September. Previous

studies have attributed the high pollution event on 25 September to the bay breeze, where a re-circulation of air mass via continental offshore winds transports it out to the Gulf and then back to Houston city (crossing over the HSC), where the resultant wind speeds across the Houston metropolitan area were low, producing stagnant conditions (Baier et al., 2015; Caicedo et al., 2019). Point source emissions from Houston's HSC was another important factor for the high pollution event on 25 September (Caicedo et al., 2019; Dunker et al., 2019). The larger contribution and concentration of fossil carbon observed at LP than at MT on 25 September could be due to LP's closer proximity to this industrial region of Houston.

Conclusion

In this study, a detailed characterization of the carbonaceous aerosols for $PM_{2.5}$ and TSP provided a better understanding of PM sources and trends in Houston. This study (1) identified important diurnal and temporal trends and (2) distinguished major sources and aerosol size fractions contributing to poor air quality days (i.e., increased PM and/or ozone levels) in Houston. Initial bulk carbon analysis identified the highest OC and EC concentrations during mornings for both $PM_{2.5}$ and TSP. Real-time BC measurements confirmed these morning peaks (i.e., 04:00–10:00). The enhanced OC, EC, and BC concentrations during the morning period were likely due to a combination of increased emissions and favorable meteorological conditions (i.e., low boundary layer). For these mornings, as expected, EC was more enhanced in the fine than the coarse PM, likely due to the incomplete combustion from MVE. The large contribution of coarse EC was also observed during this project, likely from less efficient industrial processes near the Houston MT site.

Overall, the OC/EC was relatively high, especially in the $PM_{2.5}$ fraction. The OC/EC was high during both W4 and W2. During both weeks, the OC concentration in the fine was larger than the coarse fraction, particularly during W4. The enhanced concentration of carbonaceous aerosol during W4 was driven by OC and EC in the fine fraction. The high OC/EC during this period supports enhanced contribution from secondary processes and/or biomass burning.

Further analysis of W4 was accomplished using ^{14}C analysis to distinguish the contribution and concentration of contemporary and fossil carbon. Overall, Houston aerosol was largely from contemporary sources in both $PM_{2.5}$ and TSP. However, the coarse TOC had more impact from fossil sources than the fine TOC, with an average ± SD of 51 ± 3% for coarse and 38 ± 7% for fine aerosol. The LP TSP, relative to MT TSP, had larger variability in contemporary and fossil carbon concentrations. Depending on meteorology and wind patterns, the LP site can be impacted by either strong, clean onshore winds or by industrial emissions. For days with poor air quality, 24 to 25 September, the carbonaceous aerosols were impacted by an increase in fossil carbon contribution at both MT and LP sites but driven by fine PM. This study has identified differences in coarse and fine sources of EC in Houston. Further study is needed to identify the sources of coarse EC and monitor potential seasonal trends.

Acknowledgments

The authors would like to acknowledge the U.S. Environmental Protection Agency, especially Rachelle Duvall and Russell Long, for providing a Tisch $PM_{2.5}$ sampler used at MT and for sample collection at LP. The authors would also like to thank James Schauer of the University of Wisconsin–Madison for providing two Tisch high

volume TSP samplers used at MT and LP. In addition, the authors would like to thank Raj B. Nadkarni and Jim Thomas at Texas Commission on Environmental Quality for site access and support.

References

2019. United States Census Burea: QuickFacts Houston city, Texas, United States Census Bureau.

Baier, B.C., Brune, W.H., Lefer, B.L., Miller, D.O., Martins, D.K., 2015. Direct ozone production rate measurements and their use in assessing ozone source and receptor regions for Houston in 2013. Atmos. Environ. 114, 83-91.

Barrett, T.E., Sheesley, R.J., 2014. Urban impacts on regional carbonaceous aerosols: Case study in central Texas. J. Air Waste Manag. Assoc. 64, 917-926.

Bean, J.K., Faxon, C.B., Leong, Y.J., Wallace, H.W., Cevik, B.K., Ortiz, S., Canagaratna, M.R., Usenko, S., Sheesley, R.J., Griffin, R.J., 2016. Composition and Sources of Particulate Matter Measured near Houston, TX: Anthropogenic-Biogenic Interactions. Atmosphere 7, 73.

Benetello, F., Squizzato, S., Hofer, A., Masiol, M., Khan, M.B., Piazzalunga, A., Fermo, P., Formenton, G.M., Rampazzo, G., Pavoni, B., 2017. Estimation of local and external contributions of biomass burning to PM 2.5 in an industrial zone included in a large urban settlement. Environ. Sci. Pollut. Res. 24, 2100-2115.

Birch, M., Cary, R., 1996. Elemental carbon-based method for monitoring occupational exposures to particulate diesel exhaust. Aerosol Sci. Technol. 25, 221-241.

Blanchard, C.L., Hidy, G.M., Tanenbaum, S., Edgerton, E., Hartsell, B., Jansen, J., 2008. Carbon in southeastern US aerosol particles: Empirical estimates of secondary organic aerosol formation. Atmos. Environ. 42, 6710-6720.

Brook, R.D., Rajagopalan, S., Pope, C.A., Brook, J.R., Bhatnagar, A., Diez-Roux, A.V., Holguin, F., Hong, Y., Luepker, R.V., Mittleman, M.A., 2010. Particulate matter air pollution and cardiovascular disease: an update to the scientific statement from the American Heart Association. Circulation 121, 2331-2378.

Cachier, H., Bremond, M.-P., Buat-Menard, P., 1989. Determination of atmospheric soot carbon with a simple thermal method. Tellus B. 41, 379-390.

Caicedo, V., Rappenglueck, B., Cuchiara, G., Flynn, J., Ferrare, R., Scarino, A., Berkoff, T., Senff, C., Langford, A., Lefer, B., 2019. Bay Breeze and Sea Breeze Circulation Impacts on the Planetary Boundary Layer and Air Quality From an Observed and Modeled DISCOVER-AQ Texas Case Study. J. Geophys. Res. Atmos. 124, 7359-7378.

Chen, R., Zhao, Z., Kan, H., 2013. Heavy smog and hospital visits in Beijing, China. Am. J. Respir. Crit. Care Med. 188, 1170-1171.

Chow, J.C., Watson, J.G., Crow, D., Lowenthal, D.H., Merrifield, T., 2001. Comparison of IMPROVE and NIOSH carbon measurements. Aerosol Science & Technology 34, 23-34.

Chow, J.C., Watson, J.G., Fujita, E.M., Lu, Z., Lawson, D.R., Ashbaugh, L.L., 1994. Temporal and spatial variations of PM2. 5 and PM10 aerosol in the Southern California air quality study. Atmos. Environ. 28, 2061-2080.

Chung, C.E., Ramanathan, V., Decremer, D., 2012. Observationally constrained estimates of carbonaceous aerosol radiative forcing. Proc. Natl. Acad. Sci. 109, 11624-11629.

Clark, A.E., Yoon, S., Sheesley, R.J., Usenko, S., 2015. Pressurized liquid extraction technique for the analysis of pesticides, PCBs, PBDEs, OPEs, PAHs, alkanes, hopanes, and steranes in atmospheric particulate matter. Chemosphere 137, 33-44.

Czader, B.H., Choi, Y., Li, X., Alvarez, S., Lefer, B., 2015. Impact of updated traffic emissions on HONO mixing ratios simulated for urban site in Houston, Texas. Atmos. Chem. Phys. 15, 1253-1263.

Delfino, R.J., Murphy-Moulton, A.M., Becklake, M.R., 1998. Emergency room visits for respiratory illnesses among the elderly in Montreal: association with low level ozone exposure. Environ. Res. 76, 67-77.

Dockery, D.W., Pope, C.A., 1994. Acute respiratory effects of particulate air pollution. Ann. Rev. Pubic Health 15, 107-132.

Dunker, A.M., Koo, B., Yarwood, G., 2019. Source apportionment of organic aerosol and ozone and the effects of emission reductions. Atmos. Environ. 198, 89-101.

Edgerton, E.S., Casuccio, G.S., Saylor, R.D., Lersch, T.L., Hartsell, B.E., Jansen, J.J., Hansen, D.A., 2009. Measurements of OC and EC in coarse particulate matter in the southeastern United States. J. Air Waste Manag. Assoc. 59, 78-90.

Gustafsson, Ö., Kruså, M., Zencak, Z., Sheesley, R.J., Granat, L., Engström, E., Praveen, P., Rao, P., Leck, C., Rodhe, H., 2009. Brown clouds over South Asia: biomass or fossil fuel combustion? Science 323, 495-498.

Hansen, A., Rosen, H., Novakov, T., 1983. Aethalometer-an instrument for the real-time measurement of optical absorption by aerosol particles. Lawrence Berkeley Lab., CA (USA).

Hong, L., Liu, G., Zhou, L., Li, J., Xu, H., Wu, D., 2017. Emission of organic carbon, elemental carbon and water-soluble ions from crop straw burning under flaming and smoldering conditions. Particuology 31, 181-190.

Kanakidou, M., Seinfeld, J., Pandis, S., Barnes, I., Dentener, F., Facchini, M., Dingenen, R.V., Ervens, B., Nenes, A., Nielsen, C., 2005. Organic aerosol and global climate modelling: a review. Atmos. Chem. Phys. 5, 1053-1123.

Kavouras, I.G., Stephanou, E.G., 2002. Particle size distribution of organic primary and secondary aerosol constituents in urban, background marine, and forest atmosphere. J. Geophys. Res. Atmos. 107, AAC 7-1-AAC 7-12.

Kim, B.M., Teffera, S., Zeldin, M.D., 2000. Characterization of PM25 and PM10 in the South Coast air basin of Southern California: part 1—spatial variations. J. Air Waste Manag. Assoc. 50, 2034-2044.

Laden, F., Neas, L.M., Dockery, D.W., Schwartz, J., 2000. Association of fine particulate matter from different sources with daily mortality in six US cities. Environ. Health Perspect. 108, 941.

Lee, T., Yu, X.-Y., Ayres, B., Kreidenweis, S.M., Malm, W.C., Collett Jr, J.L., 2008. Observations of fine and coarse particle nitrate at several rural locations in the United States. Atmos. Environ. 42, 2720-2732.

Leong, Y., Sanchez, N., Wallace, H., Karakurt Cevik, B., Hernandez, C., Han, Y., Flynn, J., Massoli, P., Floerchinger, C., Fortner, E., 2017. Overview of surface measurements and spatial characterization of submicrometer particulate matter during the DISCOVER-AQ 2013 campaign in Houston, TX. J. Air Waste Manag. Assoc. 67, 854-872.

Levy, M.E., Zhang, R., Khalizov, A.F., Zheng, J., Collins, D.R., Glen, C.R., Wang, Y., Yu, X.Y., Luke, W., Jayne, J.T., 2013. Measurements of submicron aerosols in Houston, Texas during the 2009 SHARP field campaign. J. Geophys. Res. Atmos. 118, 10,518-510,534.

Mazzuca, G.M., Ren, X., Loughner, C.P., Estes, M., Crawford, J.H., Pickering, K.E., Weinheimer, A.J., Dickerson, R.R., 2016. Ozone production and its sensitivity to NOx and VOCs: Results from the DISCOVER-AQ field experiment, Houston 2013. Atmos. Chem. Phys. 16, 14463–14474.

NASA, 2019. DISCOVER-AQ, National Aeronautics and Space Administration.

Novakov, T., Penner, J., 1993. Large contribution of organic aerosols to cloud-condensation-nuclei concentrations. Nature 365, 823.

Offenberg, J.H., Baker, J.E., 2000. Aerosol size distributions of elemental and organic carbon in urban and over-water atmospheres. Atmos. Environ. 34, 1509-1517.

Park, C., Schade, G.W., Boedeker, I., 2011. Characteristics of the flux of isoprene and its oxidation products in an urban area. J. Geophys. Res. Atmos. 116, D21303.

Ram, K., Sarin, M., 2011. Day–night variability of EC, OC, WSOC and inorganic ions in urban environment of Indo-Gangetic Plain: implications to secondary aerosol formation. Atmos. Environ. 45, 460-468.

Rattigan, O.V., Felton, H.D., Bae, M.-S., Schwab, J.J., Demerjian, K.L., 2010. Multi-year hourly PM2. 5 carbon measurements in New York: Diurnal, day of week and seasonal patterns. Atmos. Environ. 44, 2043-2053.

Schauer, J.J., 2003. Evaluation of elemental carbon as a marker for diesel particulate matter. J. Expo. Sci. Environ. Epidemiol. 13, 443.

Schmid, O., Artaxo, P., Arnott, W., Chand, D., Gatti, L.V., Frank, G., Hoffer, A., Schnaiter, M., Andreae, M., 2006. Spectral light absorption by ambient aerosols influenced by biomass burning in the Amazon Basin. I: Comparison and field calibration of absorption measurement techniques. Atmos. Chem. Phys. 6, 3443-3462.

Schulze, B.C., Wallace, H.W., Bui, A.T., Flynn, J.H., Erickson, M.H., Alvarez, S., Dai, Q., Usenko, S., Sheesley, R.J., Griffin, R.J., 2018. The impacts of regional shipping emissions on the chemical characteristics of coastal submicron aerosols near Houston, TX. Atmos. Chem. Phys. 18, 14217-14241.

Shahid, I., Kistler, M., Mukhtar, A., Ghauri, B.M., Ramirez-Santa Cruz, C., Bauer, H., Puxbaum, H., 2016. Chemical characterization and mass closure of PM10 and PM2. 5 at an urban site in Karachi–Pakistan. Atmos. Environ. 128, 114-123.

Shakya, K.M., Louchouarn, P., Griffin, R.J., 2011. Lignin-derived phenols in Houston aerosols: Implications for natural background sources. Environ. Sci. Technol. 45, 8268-8275.

Shiraiwa, M., Yee, L.D., Schilling, K.A., Loza, C.L., Craven, J.S., Zuend, A., Ziemann, P.J., Seinfeld, J.H., 2013. Size distribution dynamics reveal particle-phase chemistry in organic aerosol formation. Proc. Natl. Acad. Sci. 110, 11746-11750.

Snyder, D.C., Schauer, J.J., 2007. An inter-comparison of two black carbon aerosol instruments and a semi-continuous elemental carbon instrument in the urban environment. Aerosol Sci. Technol. 41, 463-474.

Spracklen, D., Carslaw, K., Pöschl, U., Rap, A., Forster, P., 2011. Global cloud condensation nuclei influenced by carbonaceous combustion aerosol. Atmos. Chem. Phys. 11, 9067-9087.

Stuiver, M., Polach, H.A., 1977. Discussion; reporting of C-14 data. Radiocarbon 19, 355-363.

Sullivan, D.W., Price, J.H., Lambeth, B., Sheedy, K.A., Savanich, K., Tropp, R.J., 2013. Field study and source attribution for PM2. 5 and PM10 with resulting reduction in concentrations in the neighborhood north of the Houston Ship Channel based on voluntary efforts. J. Air Waste Manag. Assoc. 63, 1070-1082.

Tian, S., Pan, Y., Liu, Z., Wen, T., Wang, Y., 2019. Reshaping the size distribution of aerosol elemental carbon by removal of coarse mode carbonates. Atmos. Environ. 214, 116852.

Tsigaridis, K., Daskalakis, N., Kanakidou, M., Adams, P., Artaxo, P., Bahadur, R., Balkanski, Y., Bauer, S., Bellouin, N., Benedetti, A., 2014. The AeroCom evaluation and intercomparison of organic aerosol in global models. Atmos. Chem. Phys. 14, 10845-10895.

Turpin, B.J., Huntzicker, J.J., 1995. Identification of secondary organic aerosol episodes and quantitation of primary and secondary organic aerosol concentrations during SCAQS. Atmos. Environ. 29, 3527-3544.

Viana, M., Maenhaut, W., Ten Brink, H., Chi, X., Weijers, E., Querol, X., Alastuey, A., Mikuška, P., Večeřa, Z., 2007. Comparative analysis of organic and elemental carbon concentrations in carbonaceous aerosols in three European cities. Atmos. Environ. 41, 5972-5983.

Wallace, H.W., Sanchez, N.P., Flynn, J.H., Erickson, M.H., Lefer, B.L., Griffin, R.J., 2018. Source apportionment of particulate matter and trace gases near a major refinery near the Houston Ship Channel. Atmos. Environ. 173, 16-29.

Yoon, S., Ortiz, S., Clark, A.E., Barrett, T.E., Usenko, S., Duvall, R.M., Hildebrandt Ruiz, L., Bean, J.K., Faxon, C.B., Flynn, J., leong, Y.J., Griffin, R., Sheesley, R.J., under review. Apportioned primary and secondary organic aerosol during pollution events of DISCOVER-AQ Houston, Atmos. Environ.

Zeng, T., Wang, Y., 2011. Nationwide summer peaks of OC/EC ratios in the contiguous United States. Atmos. Environ. 45, 578-586.

Zhang, X., Craft, E., Zhang, K., 2017. Characterizing spatial variability of air pollution from vehicle traffic around the Houston Ship Channel area. Atmos. Environ. 161, 167-175.

Zhang, Y., Zotter, P., Perron, N., Prévôt, A., Wacker, L., Szidat, S., 2013. Fossil and non-fossil sources of different carbonaceous fractions in fine and coarse particles by radiocarbon measurement. Radiocarbon 55, 1510-1520.

Zotter, P., El-Haddad, I., Zhang, Y., Hayes, P.L., Zhang, X., Lin, Y.H., Wacker, L., Schnelle-Kreis, J., Abbaszade, G., Zimmermann, R., 2014. Diurnal cycle of fossil and nonfossil carbon using radiocarbon analyses during CalNex. J. Geophys. Res. Atmos. 119, 6818-6835.

CHAPTER FOUR

Apportioned Primary and Secondary Organic Aerosol during Pollution Events of DISCOVER-AQ Houston

This chapter under review at *Atmospheric Environment* as: Yoon, S.; Ortiz, S. M.; Clark, A. E.; Barrett, T. E.; Usenko, S.; Duvall, R. M.; Hildebrandt-Ruiz, L.; Bean, J. K.; Faxon, C. B.; Flynn, J. H. III; Lefer, B. L.; Leong, Y.J.; Griffin, R.J.; Sheesley, R.J. Apportioned Primary and Secondary Organic Aerosol during Pollution Events of DISCOVER-AQ Houston.

Abstract

Understanding the drivers for high ozone (O_3) and atmospheric particulate matter (PM) concentrations is a pressing issue in urban air quality, as this understanding informs decisions for control and mitigation of these key pollutants. The Houston, TX metropolitan area is an ideal location for studying the intersection between O_3 and atmospheric secondary organic carbon (SOC) production due to the diversity of source types (urban, industrial, and biogenic) and the on- and off-shore cycling of air masses over Galveston Bay, TX. Detailed characterization of filter-based samples collected during Deriving Information on Surface Conditions from Column and VERtically Resolved Observations Relevant to Air Quality (DISCOVER-AQ) Houston field experiment in September 2013 were used to investigate sources and composition of organic carbon (OC) and potential relationships between daily maximum 8 h average O_3 and PM. The current study employed a novel combination of chemical mass balance modeling defining primary (i.e. POC) versus secondary (i.e. SOC) organic carbon and radiocarbon (^{14}C) for apportionment of contemporary and fossil carbon. The apportioned sources include contemporary POC (biomass burning [BB], vegetative detritus), fossil

POC (motor vehicle exhaust), biogenic SOC and fossil SOC. The filter-based results were then compared with real-time measurements by aerosol mass spectrometry. With these methods, a consistent urban background of contemporary carbon and motor vehicle exhaust was observed in the Houston metropolitan area. Real-time and filter-based characterization both showed that carbonaceous aerosols in Houston was highly impacted by SOC or oxidized OC, with much higher contributions from biogenic than fossil sources. However, fossil SOC concentration and fractional contribution had a stronger correlation with daily maximum 8 h average O_3, peaking during high PM and O_3 events. The results indicate that point source emissions processed by on- and off-shore wind cycles likely contribute to peak events for both PM and O_3 in the greater Houston metropolitan area.

Introduction

The Houston metropolitan area has added nearly 1 million residents in the last decade (U.S. Census Bureau, 2019a). Due to this rapid growth and expansion, traffic remains a major challenge for the city with an estimated 278 million km driven per day by the metropolitan area residents (Lubertino, 2019). Aside from urban emissions associated with residents (motor vehicles, cooking, etc.), the Houston metropolitan area also has strong influences from industrial and biogenic emissions (Bean et al., 2016; Dunker et al., 2019; Wallace et al., 2018). The Houston Ship Channel (HSC) is lined with dense zones of industrial facilities, including a petrochemical complex that is the largest in the U.S and second largest in the world (Port Houston Overview, 2019a). The Port of Houston, one of the busiest U.S. seaports (AAPA, 2019), contributes ship and heavy-duty diesel (HDD) emissions to the city's atmosphere (Schulze et al., 2018; Wallace et al.,

2018). The Houston metropolitan area, much like other southeastern U.S. cities, is also highly vegetated with large forested regions north of the metropolitan area (Figure 4.1); approximately 18.4% of land in the city of Houston is covered by tree canopy (Nowak et al., 2017).

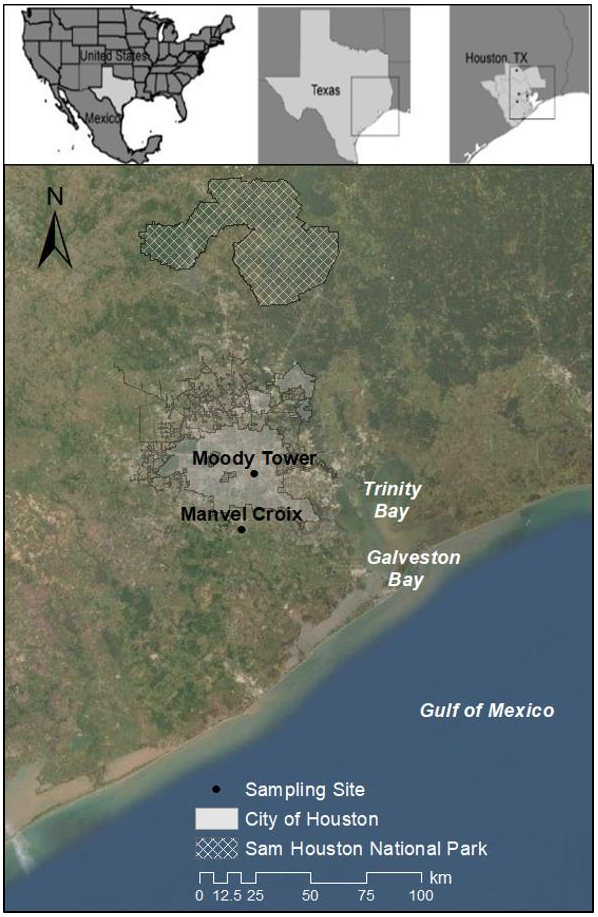

Figure 4.1. Ground-based sampling sites: Moody Tower and Manvel Croix.

Air quality in Houston is a result of population growth, large-scale industrial areas, and vegetation. Historically, the Houston metropolitan area has been in nonattainment for O_3, based on the National Ambient Air Quality Standards from the U.S. Environmental Protection Agency (EPA, 2019). While PM concentrations have not exceeded these national standards, a TCEQ monitoring site located between Houston's

urban core and the HSC has measured PM levels close to national standards: annual average fine PM ($PM_{2.5}$; PM with an aerodynamic diameter less than 2.5 μm) concentration ranging from 11 to 16 μg m^{-3} from 2005 to 2014 (H-GAC, 2015; Allen and Fraser, 2006; Sullivan et al., 2013a). To better understand the sources and atmospheric chemistry driving O_3 and PM in Houston, there have been several large-scale field campaigns starting with The Texas Air Quality Study (TexAQS) in 2000 which identified the importance of highly reactive volatile organic compounds (VOC) to O_3 production and PM (Allen et al., 2018; Kleinman et al., 2002; Ryerson et al., 2003). Following these studies, the State Implementation Plan (Allen et al., 2018) enacted strategies aimed at reducing NO_x and highly reactive VOCs, where then the follow-up campaign, TexAQS II, in 2005 – 2006, observed significant reduction in highly reactive VOCs and slower O_3 production rates (Parrish et al., 2009; Zhou et al., 2014). A companion study of TexAQS, the Gulf Coast Aerosol Research and Characterization was a longer-term (2000 – 2001) field experiment with the objective of identifying spatial and diurnal trends and key processes of $PM_{2.5}$ formation in southeastern Texas. The major findings from this campaign relevant to the current study include 1) the importance of secondary organic aerosol (SOA) to $PM_{2.5}$; 2) the need for more study of the impact of point sources on $PM_{2.5}$; and 3) an assessment that there was a lack of spatial variability in the PM concentration (Allen and Fraser, 2006). The objective of the Study of Houston Atmospheric Radical Precursors in 2009 was to better understand the influence of radical precursors, formaldehyde, and nitrous acid to O_3 production in Houston's urban and industrial areas (Olaguer et al., 2014). These campaigns were vital steps in reducing emissions and improving air quality in the Houston metropolitan area. However, due to

continuous population growth, improvements in control technologies, and the changing landscape of the metropolitan area, extrapolating from previous air quality field studies and/or from studies specific to only the most urban/industrial parts of the city is problematic when wanting to most effectively combat current air quality issues and reduce exposure to air pollution for all Houston metropolitan area residents.

The Deriving Information on Surface Conditions from Column and VERtically Resolved Observations Relevant to Air Quality (DISCOVER-AQ) field campaign is the most recent multi-site, high-intensity field experiment in Houston. This field campaign, conducted in 2013, was part of a broader NASA project with the goal to better interpret and improve measurement of ground-level pollutant concentrations via satellite data (NASA, 2019). This manuscript contributes to the spatial assessment of ground-level pollutants during DISCOVER-AQ, with a focus on organic aerosol (OA) sources and their relationship with daily O_3 concentrations at representative sites in the urban core and suburb of the metropolitan area.

Published results from the DISCOVER-AQ field experiment have demonstrated the increasing contribution of OA and SOA to PM concentrations at sites across Houston. During the DISCOVER-AQ, mobile and stationary measurements indicated significant contribution of oxygenated OA (OOA) to PM across the Houston metropolitan area during this period (Bean et al., 2016; Leong et al., 2017). However, Leong et al. (2017) observed more primary sources and sulfate emissions in urban/industrial regions (Leong et al., 2017). The current manuscript describes OA and OC measurements during a peak O_3 event at a downtown and suburb site, which allows for analysis of the evolving

interaction between O_3 and PM in the metropolitan area during a peak event and additional characterization of the sources driving SOA production.

A peak O_3 event on Sept. 25 – 26, 2013 during DISCOVER-AQ provided an opportunity to study the conditions and emissions associated with this pollution regime in Houston (Baier et al., 2015). The production of O_3, especially in Houston, is known to be impacted by sea breeze re-circulation patterns (Tucker et al., 2010; Wang et al., 2016), which was present during a peak O_3 event during DISCOVER-AQ. For O_3 production, dependence on precursor compounds including NO_x (NO and NO_2) and VOC, specific regimes were determined for Houston during DISCOVER-AQ. From a previous DISCOVER-AQ study, O_3 production in most parts of the metropolitan area was found to be VOC-dependent in the morning and NO_x-dependent in the afternoon (Mazzuca et al., 2016). However, in the urban/industrial zones, O_3 production was VOC-dependent throughout the day (Mazzuca et al., 2016). On Sept. 25, high O_3 production within the Houston urban core occurred, followed by advection to outlying areas due to transport and bay-breeze recirculation (Baier et al., 2015). Mazzuca et al. (2016) determined that the enhanced O_3 concentration during this peak O_3 event was likely due to higher concentrations of precursor compounds and/or meteorological conditions (e.g. lower boundary layer, stagnant conditions, bay breezes) rather than a faster production rate as the O_3 production efficiency, a measure of O_3 production to rate of NO_x oxidation, was similar to the rest of the week. These findings stress the importance of understanding emission sources and atmospheric processing across the metropolitan area. The current study is investigating how these sources and conditions impacted aerosol composition and concentration.

Finally, Dunker et al. (2019) investigated emission impacts on O_3 and OA during DISCOVER-AQ using the Comprehensive Air Quality Model with Extensions (CAMx). Dunker et al. (2019) provided more specific apportionment of OA and O_3 at several sites, identifying point sources to be a major contribution (29 and 21% fraction contribution, respectively) to both pollutants. The results from the current manuscript can also validate whether modelled changes in sources of OA match field measurements of OA components.

The objective of the current study was to quantify contributions of major sources and evaluate the trends and spatial distribution of daytime total organic carbon (TOC; OC + EC) and O_3 in the Houston metropolitan area. During the DISCOVER-AQ campaign in September 2013, filter-based daytime samples were collected at two sites. Detailed chemical composition including molecular and isotopic analysis was performed on these filter samples to characterize carbonaceous aerosols at a downtown and suburb site. A molecular marker-based chemical mass balance (CMB) model was utilized in combination with ^{14}C analysis to characterize TOC and OC, respectively. Comparison with co-located high-resolution time-of-flight aerosol mass spectrometer (HR-ToF-AMS) at the suburb site further confirmed contribution of oxidized aerosol contribution. Particular focus was given to identifying major sources and drivers for PM formation during periods of peak PM and O_3. Day samples were chosen for detailed analysis, as daytime periods are most affected by O_3 and photochemical processes. In all, this analysis improves our understanding of sources and transport of PM across the metropolitan area and its connection to peak O_3 events.

Materials and Methods

Sampling Sites

$PM_{2.5}$ samples were taken in conjunction with NASA's DISCOVER-AQ campaign at Moody Tower (MT; 29.7197, -95.3432) and Manvel Croix (MC; 29.5205, -95.3925) representing a downtown and suburb region, respectively, in the Houston metropolitan area (Figure 4.1). MT is 4.6 km south of downtown Houston and located on top of a high-rise building at approximately 70 m above ground level (AGL). This site has been a focus for many air quality and meteorological studies for the Houston area (Czader et al., 2015; Lefer et al., 2010; Wong et al., 2012) as the site is representative of Houston's urban atmosphere. MC is in a suburb 22.5 km south of MT located in a park near a residential area (Figure 4.1).

Sampling

Filter-based sampling. $PM_{2.5}$ samples were collected on 90- and 102-mm-diameter quartz fiber filters (Pall Corporation, Port Washington, NY, USA) using medium-volume (90 L min^{-1}; URG Corporation, Chapel Hill, North Carolina, USA) and high-volume (Tisch Environmental, Cleves, OH, USA) samplers, respectively. For the high-volume samplers, the flow rate was 200 L min^{-1} and 225 L min^{-1} at MT and MC, respectively. All samplers were calibrated prior to field deployment; differences in flow rate were due to small differences in sampler design. The quartz fiber filters used for samples and field blanks were pre-cleaned by baking at 550 °C for 12 h in individual aluminum foil packets. Filters were stored in -10 °C freezers pre- and post-sampling. A total of 14 field blanks were obtained from the three samplers: seven blanks from the

high-volume at MT, three blanks from the medium-volume at MT, and four blanks from the high-volume at MC. Filter blanks were handled in the same manner as the ambient samples including filter preparation, travel (e.g. transport to Houston and to the sites), and storage (e.g. long-term laboratory and short-term onsite). For collection of the field blanks, the pre-cleaned filters were placed into sample holders and then into the samplers without turning them on.

Filter samples were collected from Sept. 4 – 28, 2013. A flexible sampling schedule was used for filter collection which included morning (06:30 – 10:00), afternoon (10:00 – 20:00), day (06:30 – 20:00), night (20:00 to 6:30), and 24 h (06:00 – 05:30) samples. This flexible schedule was implemented to allow intensive sampling periods within the month and to separate sources and chemistry that are time-of-day dependent. All samples were analyzed for bulk carbon (i.e. OC and EC) while select samples collected during Sept. 8 – 15 (week 2) and Sept. 21 – 28 (week 4) were further analyzed for chemical and carbon isotope measurements. These select samples included day samples from MT and MC, and a few 24-h MT samples (Sept. 8, 11, 12, and 14).

Real-time Measurements in Mobile Air Quality Laboratory (MAQL)

Mass spectral data of non-refractory submicron PM (PM_1) was collected using a HR-ToF-AMS (Aerodyne Research, Inc., Billerica, MA, USA). The instrument was housed in the University of Houston's MAQL. Non-refractory PM_1 was sampled from a dried (< 40% relative humidity) aerosol inlet, which was raised approximately 5.5 m AGL when the MAQL was stationary. Measurements made during stationary sampling at MC during week 4 was included in the current study. Further details of CO and PM_1 sampling in the MAQL, measurements methods, and detection limits and uncertainties

have previously been published elsewhere (Leong et al., 2017). The PMF protocol applied to the HR-ToF-AMS data is outlined in the Supplementary Data (S1).

Additional Measurements at TCEQ Monitoring Sites

The current study utilized measurements of daily maximum 8-h average O_3 and daily average $PM_{2.5}$ concentrations from Texas Commission on Environmental Quality (TCEQ) Continuous Air Monitoring Stations across the Houston-Galveston-Brazoria (HGB) regions including Park Place (C416), Galveston (C1034), Seabrook (C45), Deer Park (C35), Houston East (C1), Clinton (C403), UH Moody Tower (C695), Manvel Croix (C84) and Conroe (C78). Daily maximum 8-h average O_3 concentrations, which will be referred simply as "O_3 concentration", (Sept. 1 – 29, 2013) were retrieved from the Texas Air Monitoring Information System web interface (TCEQ, 2018). Daily average $PM_{2.5}$ concentrations (Sept. 1 – 29, 2013) were measured using a tapered element oscillating microbalance and were received from TCEQ upon request (personal communication with Jim Price, TCEQ). Wind speed and wind direction data for MT and MC sites were also retrieved from the Texas Air Monitoring Information System web interface (TCEQ, 2018).

Organic and Elemental Carbon

All collected filters were analyzed for OC and EC by a thermal optical transmission instrument (Lab OC-EC Analyzer; Sunset Laboratory Inc., Tigard, OR, USA) using the NIOSH 5040 method (Birch and Cary, 1996). Triplicate analysis was completed every tenth sample run with an average relative standard deviation of 3.03%. Samples were blank corrected using site- and sampler-specific filter blanks. Average

blank subtraction was 14.4 ± 11.6% of OC concentration. There was no EC contribution in the blanks.

Day and night OC and EC measurements are reported here. When a daytime filter was not available, OC and EC masses from morning (06:30 – 10:00) and afternoon (10:00 – 20:00) samples were summed and volume normalized to represent daytime measurements. When a nighttime sample was not available, daytime masses (06:30 – 20:00) were subtracted from 24-h masses (06:00 – 05:30) and then volume normalized to represent nighttime measurements.

Detailed Analyses

Radiocarbon analysis. The filter-based TOC (i.e. OC + EC) was analyzed for ^{14}C abundance as described previously (Barrett et al., 2015). Briefly, a fraction of each filter corresponding to ~100 µg of TOC was acid fumigated in a desiccator over 1N HCl and then dried at 60 °C for 1 h. The samples were shipped on ice to the National Sciences Accelerator Mass Spectrometry facility in Woods Hole Oceanographic Institution (Woods Hole, MA, USA) for ^{14}C analysis. Field and laboratory blanks were handled and analyzed in the same manner to allow for blank correction.

Once received by the facility, these filter samples were analyzed using accelerator mass spectrometry to determine the fraction of modern carbon (F_M). F_M is the ^{14}C to ^{12}C ratio of the sample to a "Modern" reference sample (i.e. NBS Oxalic Acid I).

$$F_M = \frac{(^{14}C/^{12}C)_{sample}}{(^{14}C/^{12}C)_{AD1950}} \quad (1)$$

The F_M was blank corrected using field blanks collected during the sampling campaign. The averaged blank concentration of 1.12 ± 0.50 μg C cm^{-2} had a F_M value of 0.38 ± 0.01.

Organic Tracer Analysis

The MT samples from week 2 and MT and MC samples from week 4 were analyzed for organic tracers by solvent extraction followed by analysis on a gas chromatograph – mass spectrometer (GC-MS). These samples were analyzed for a suite of non-polar combustion (alkanes, PAHs, hopanes and steranes), polar combustion (levoglucosan), and secondary biogenic (2-methyltetrols, pinic and pinonic acids) organic tracer compounds. An adapted version of a previously published pressurized liquid extraction method was used for tracer analysis (Clark et al., 2015). For this method, a portion of each filter sample representing ~400 μg of OC was utilized. Filters were spiked with a known amount of isotopically-labelled internal standards (IS; tetracosane-d^{50}, triacontane-d^{58}, dotriacontane-d^{66}, fluoranthene-d^{10}, pyrene-d^{10}, benz(a)anthracene-d^{12}, chrysene-d^{12}, benzo(b)fluoranthene-d^{12}, benzo(e)pyrene-d^{12}, benzo(k)fluoranthene-d^{12}, indeno(1,2,3-cd)pyrene-d^{14}, dibenz(ah)anthracene-d^{14} , coronene-d^{12}, cholestane-d^{4}, levoglucosan-C^{13}). Filters were extracted using an accelerated solvent extractor (Dionex 350, Sunnyvale, CA, USA) with a solvent mixture of 2:1 v/v dichloromethane and acetone. The extracts were concentrated to ~0.5 mL using a Caliper TurboVap II (Hopkinton, MA, USA). The extracts were then concentrated to a total volume of 125 μL using a gentle nitrogen stream and analyzed using a GC-MS with an electron ionization source (Agilent Technologies, Santa Clara, CA, USA). The organic tracers were quantified against prepared six- to seven-point external calibration solutions. A check

standard, generally the mid-point of the dilution standard series, was run before and after each sample batch for quality control on the calibration curve.

To analyze levoglucosan, a polar compound, a 25 µL aliquot of each sample extract was blown down to dryness using a gentle nitrogen stream. The samples were then reconstituted using 25 µL of pyridine (Fisher Chemical, Waltham, MA, USA) with 50 µL of *N,O*-bis(trimethylsilyl)trifluoroacetamide trimethylchlorosilane (BSTFA-TMCS; Sigma Aldrich, St. Louis, MO, USA) (Simoneit et al., 1999). Within 24 h, the derivatized samples were run on the GC-MS with a six-point calibration curve and check standards as mentioned before.

Source Apportionment Tools for Filter-based Measurements

Radiocarbon apportionment. The $\Delta^{14}C$ value is the relative difference between the ^{14}C measurement of the sample and standard reference material, corrected to account for decay that took place between collection and time of measurement. $\Delta^{14}C$ is calculated using the reported F_m, inverse of radiocarbon's half-life (λ), and the year of the sample collected (Y_c):

$$\Delta^{14}C = \left[F_m * e^{\lambda(1950-Y_c)} - 1\right] * 1000 \qquad (2)$$

The $\Delta^{14}C$ can then be used to apportion fractional contribution from fossil and contemporary sources in atmospheric PM (Hildemann et al., 1994). With known end-members for contemporary and fossil sources, the contribution of contemporary, f_{cont}, versus fossil sources, 1-f_{cont}, can be determined using a mass balance approach:

$$\Delta^{14}C_{sample} = \left(\Delta^{14}C_{cont}\right)\left(f_{cont}\right) + \left(\Delta^{14}C_{fossil}\right)(1 - f_{cont}) \qquad (3)$$

End-member values of +67.5‰ and -1000‰ were used to represent contemporary and fossil sources, respectively. The contemporary end-member is an averaged value of +107.5‰ to represent wood burning and +28‰ to represent emissions from annual growth (Zotter et al., 2014). A final combined uncertainty, u_c, was calculated for each sample measurement (equation 4) which included instrument standard error, σ_{ins}, relative difference of F_M blank correction, $d_{r_{blk}}$, and the standard deviation of using either of the two contemporary end-members (i.e. +28‰ and +107‰) for calculating the $\Delta^{14}C_{sample}$, σ_{endmem}. The σ_{endmem} accounted for the uncertainty when using an average (i.e. +67.5‰) of the two contemporary end-members.

$$u_c = \sqrt{\sigma_{ins}^2 + d_{r_{blk}}^{\ 2} + \sigma_{endmem}^2} \qquad (4)$$

Chemical Mass Balance

The CMB model is a receptor-based source apportionment model, which uses measured species concentration and known source profiles to calculate contributions of each source for each sample (Schauer et al., 1996). The model assumes that no change occurs in the emissions from source to receptor. However, this is an over-simplification, as oxidation and partitioning between gas- and particle-phases leads to changes in the plume during transport. For the purposes of the current study, the primary emissions apportioned by the CMB are assumed to be representative of the remaining primary plume which was collected on the filter during sampling. The current study used the EPA CMBv8.2 model (Coulter, 2004). The CMB source profiles, f_{ij}, included primary sources from vegetative detritus (Rogge et al., 1993), EPA Region 4 woodsmoke (Fine et al., 2002; Sheesley et al., 2007), diesel-powered motor vehicle exhaust, gasoline-powered

motor vehicle exhaust, and lubricating oil-impacted motor vehicle exhaust (Lough et al., 2007). The motor vehicle sources are combined and presented as "motor vehicle exhaust" (MVE). The CMB model outputs were accepted if the χ-square < 4 and $r^2 > 0.80$. For all samples, the average χ-square and r^2 values are 1.97 ± 0.88 and 0.90 ± 0.04, respectively.

Combined ^{14}C and CMB Source Apportionment of TOC

The ^{14}C source apportionment distinguished contribution of fossil and contemporary carbon of TOC. The CMB source apportionment distinguished contribution from major primary sources from fossil (MVE) and contemporary (wood smoke and vegetative detritus) OC. The EC to OC ratios of each source profile was used to calculate the EC contribution for each primary source (Lough et al., 2007; Sheesley et al., 2007). The primary fossil and contemporary carbon concentration from the CMB analysis was subtracted from the respective ^{14}C apportioned fossil and contemporary TOC to calculate an upper estimate of secondary fossil and secondary contemporary carbon.

HYSPLIT Back Trajectory (BT) Analysis

The BT calculations were performed for the sampling sites using the NOAA Hybrid Single Particle Lagrangian Integrated Trajectory (HYSPLIT) model, v4, May 2012 release (Draxler and Rolph, 2010). The BTs were produced every 6-h starting at 00:00, 06:00, 12:00, and 18:00 each day from Sept. 4 – 28 during the sampling period. Individual BTs were run with an initial height of 0 m and 80 m AGL for MC and MT, respectively, using GDAS meteorological dataset. To understand the transport pathway and major sources of air masses impacting each site, the resulting BTs were clustered into

groups with similar transport patterns using the clustering function. The predominant cluster for each day was assigned (Table 4.1.). Final clustered BTs were plotted using ESRI's ArcGIS 10.1 mapping software (Figure 4.2). To model potential uncertainty in the HYSPLIT model BTs during DISCOVER-AQ, a sensitivity study was performed for MT at 10 km north and south the site. MT was plotted at 0, 80, and 100 m AGL. The sensitivity study results show that the HYSPLIT model is robust and reproducible, producing relatively similar BT pathways even when varying the locations and heights from the initial sampling site. The cluster analysis was run for the 0 m AGL and the 80 m AGL BTs separately.

Results and Discussion

Bulk carbon measurement was used as the initial characterization tool to identify trends of Houston's the carbonaceous aerosols during DISCOVER-AQ (Figure 4.3). These trends were also observed in the $PM_{2.5}$ and O_3 measurement made at the TCEQ monitoring sites across the HGB area (Figure 4.4). Based on these plots, two periods of interest were determined: week 2 (Sept. 8 – 15) with peaks in OC and PM and week 4 (Sept. 21 – 28) with peaks in OC, PM and O_3 (Figure 4.4). The two periods were separated by a week of intermittent precipitation (Figure 4.3 and 4.4).

Table 4.1. September 2013 Daily Back Trajectory Cluster. The daily cluster was assigned based on the predominant 6-h BT cluster for each day.

Day	Moody Tower Daily Cluster	Manvel Croix Daily Cluster
4-Sept.	**ESE**	**S**
5-Sept.	**ESE**	**ESE**
6-Sept.	**ESE**	**ESE**
7-Sept.	**ESE**	**ESE**
8-Sept.	**ESE**	**ESE**
9-Sept.	**ESE**	**ESE**
10-Sept.	**ESE – SE**	**ESE**
11-Sept.	**ESE – SE**	**ESE**
12-Sept.	**ESE**	**ESE**
13-Sept.	**ALL – 3**	**ESE**
14-Sept.	**ESE**	**ESE**
15-Sept.	**ESE**	**ESE**
16-Sept.	**SE**	**ESE**
17-Sept.	**ESE – SE**	**ESE**
18-Sept.	**ESE**	**ESE**
19-Sept.	**SE**	**ESE**
20-Sept.	**SE**	**ESE**
21-Sept.	**NNE**	**All – 3**
22-Sept.	**NNE**	**NNE**
23-Sept.	**ESE**	**NNE**
24-Sept.	**ESE**	**NNE**
25-Sept.	**NNE**	**NNE – S**
26-Sept.	**ESE**	**S**
27-Sept.	**ESE**	**ESE**
28-Sept.	**SE**	**ESE**

*North-northeast (NNE), East-southeast (ESE), Southeast (SE), Northeast (NE), South (S)

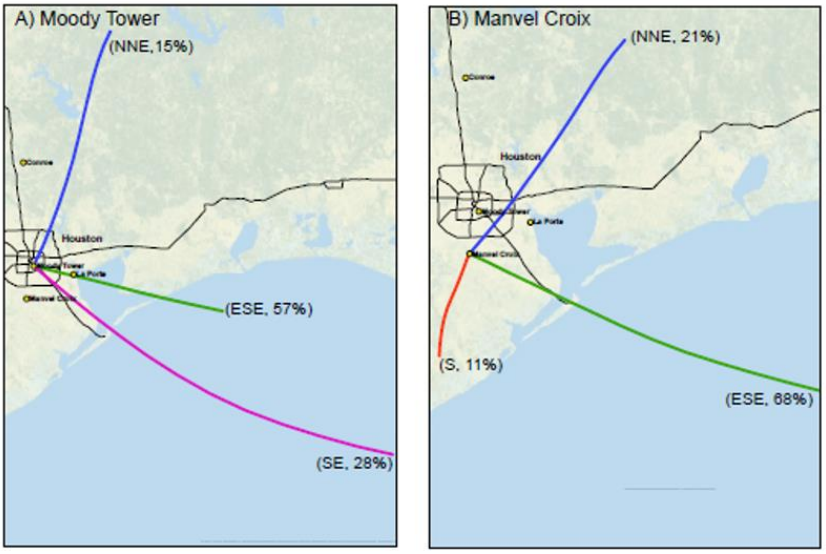

Figure 4.2. HYSPLIT 12 h clustered back trajectories were performed to display percentages of air masses that traveled to the sampling sites during DISCOVER-AQ.

The two weeks of interest were chosen for comparison with co-located measurements and for more detailed chemical analysis, including organic tracer and ^{14}C analysis. To better understand relationships between O_3 and PM in Houston, this detailed analysis focused on daytime samples at MT, the downtown Houston site, during both weeks 2 and 4. The detailed analysis of MC samples during week 4 were also daytime samples. Discussion of the results of the detailed analysis will follow the overview of the bulk carbon measurements.

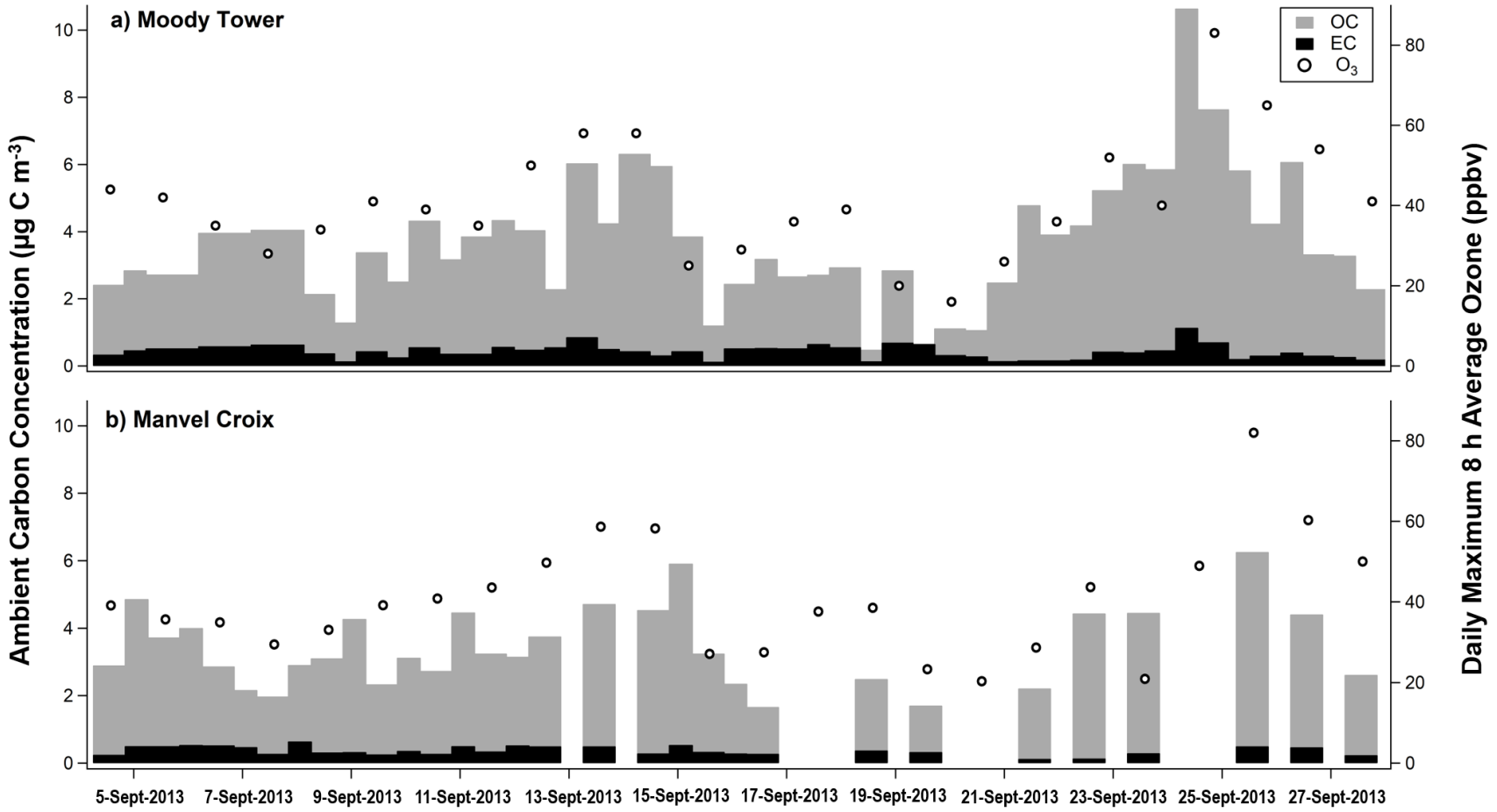

Figure 4.3. Day and night $PM_{2.5}$ OC (grey) and EC (black) measurements at a) Moody Tower and b) Manvel Croix during full sampling campaign. Daily maximum 8 h average ozone concentration on right y-axis.

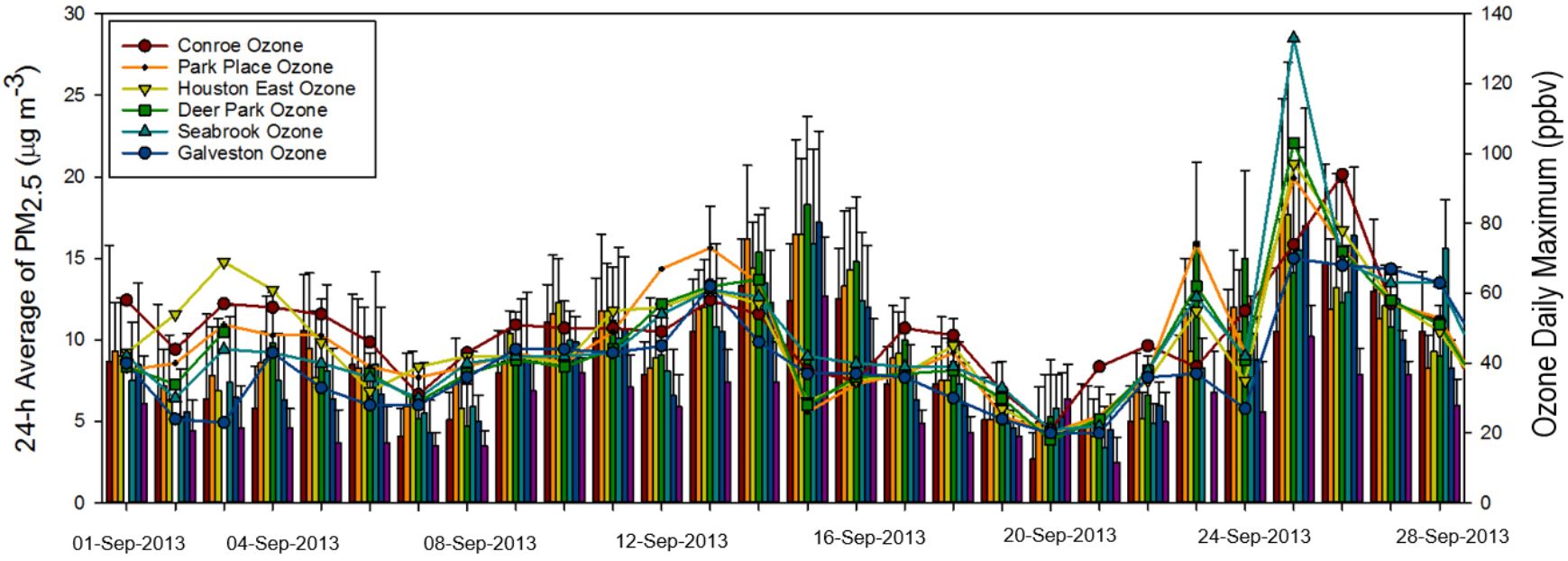

Figure 4.4. TCEQ Monitoring Sites O_3 and $PM_{2.5}$ concentrations across the southeastern regions of Texas. The $PM_{2.5}$ measurements were 24 h (06:00 - 5:30) averages and O_3 data are daily maximum concentrations provided from Houston-network of Environmental Towers (http://www.hnet.uh.edu).

Trends in Carbonaceous Aerosol and O_3 During DISCOVER-AQ

Average ambient concentration of daytime TOC during the full sampling period at MT and MC was 3.74 ± 1.65 and 3.36 ± 1.29, µg C m^{-3}, respectively. Of these samples, fractional contribution of OC at MT and MC was 0.87 ± 0.06 and 0.89 ± 0.04, respectively, while EC was 0.13 ± 0.06 and 0.11 ± 0.04, respectively. The OC and EC concentrations were highest at MT, the most urban site (Figure 3a and b). Ambient OC concentrations varied during the sampling period (Figure 3a), where OC was significantly enhanced during the high pollution weeks (weeks 2 and 4) compared to the rest of the sampling days (Mann-Whitney Rank Sum test; $p < 0.001$). Ambient EC concentrations observed similar trends as the OC (e.g. peak EC concentrations on Sept. 24 night) (Figure 3a), however, the EC was not significantly enhanced during the high pollution weeks (Mann-Whitney Rank Sum test; $p < 0.05$). Although both weeks had building concentrations of OC, the peak concentration was higher for week 4 at both MT and MC (Figure 4.3). For example, the OC concentration at MT dramatically peaked on Sept. 24 night (9.5 ± 1.1 µg C m) followed by Sept. 25 day (6.9 ± 0.7 µg C m^{-3}) when a peak O_3 event had occurred (Figure 3a). The EC concentration was comparable during both weeks 2 and 4 at both MT (avg: 0.50 ± 0.16 and 0.34 ± 0.19 µg C m^{-3}, respectively) and MC (average: 0.35 ± 0.09 and 0.29 ± 0.15 µg C m^{-3} , respectively).

Carbonaceous aerosols are a significant fraction of $PM_{2.5}$ based on previous Houston studies (Allen and Fraser, 2006; Fraser et al., 2002). As observed by the TCEQ monitoring sites, the $PM_{2.5}$ concentrations (Figure 4.4) and measured bulk carbon concentrations (Figure 4.3) had very similar trends. TOC was an important component of the increasing $PM_{2.5}$ concentrations during both weeks (excluding Sept. 15 when $PM_{2.5}$

peaks while TOC concentration drops). Over the full sampling campaign, TOC concentrations at MT and MC ranged between 0.62 – 10.44 µg C m^{-3} and 1.67 – 6.34 µg C m^{-3}, respectively.

The trends and concentration of O_3 were relatively consistent throughout the Houston metropolitan area based on the O_3 daily maximum concentrations measured at the TCEQ monitoring sites (Figure 4.4). The average O_3 concentration during the full campaign at MT and MC were both 41 ± 14 ppbv. The highest O_3 concentration was on Sept. 25 during week 4 with concentrations of 83 and 82 ppbv at MT and MC, respectively (Figure 4.3). The lowest O_3 concentration was on Sept. 20 during the intermittent precipitation period between weeks 2 and 4 with concentrations of 16 and 20 ppbv at MT and MC, respectively. The O_3 concentrations were well correlated with OC at MT and MC (r^2: 0.56 and 0.50, respectively).

Sources of Air Masses Based on BTs, Wind Direction and Speed

The clustered BTs and wind rose plots were used to evaluate air mass transport to MT and MC during the sampling period. The BTs were clustered into five groups: north-northeast, east-southeast, southeast, northeast, and south (Table 4.1 and Figure 4.2.). The BT clusters at MT and MC were mainly from onshore east-southeast (59 – 72%) and offshore north-northeast (12%) winds (Table 4.1). Earlier in the campaign, winds were generally from the east-southeast direction at MT and MC (Table 4.1, Figure C.1). A shift in wind direction occurred during week 4 where a combination of northern continental (e.g. north-north east) and onshore marine (e.g. east-southeast) air masses were observed (Table 4.1, Figure C.1). During week 4, lowest wind speeds were observed on Sept. 25 at both MT and MC with average speeds of 3.8 ± 2.9 and 3.2 ± 1.6 miles/h, respectively,

relative to average speeds of 8.2 ± 2.1 and 7.0 ± 1.4 miles/h, respectively, for the full campaign.

In or near coastal regions, shifting wind directions and lower wind speeds during the daytime is indicative of converging onshore and offshore winds due to the sea/bay breeze phenomenon (Banta et al., 2005; Banta et al., 2011; Caicedo et al., 2019; Stauffer and Thompson, 2015). During these periods, stagnant atmospheric conditions are produced allowing buildup of O_3 and pollutant concentrations (Banta et al., 2005; Loughner et al., 2011; Stauffer and Thompson, 2015); this was the case for the Houston metropolitan area on Sept. 25, 2013 (Baier et al., 2015; Caicedo et al., 2019). The lower wind speeds on Sept. 25 were accompanied by shifting wind directions during the day (Figure 4.5b). In comparison to Sept. 9, which had relatively lower O_3 levels, the wind direction was consistently from east-southeast with stronger wind speeds during the day (Figure 4.5a). The progression of change in the wind conditions during week 4 at MT followed observed pollutant trends (i.e. OC, $PM_{2.5}$, and O_3 concentrations) where the week began with consistent wind direction/high wind speeds then transitioned to varying wind direction/low wind speeds (i.e. stagnant conditions on Sept. 25) and then back. The sea/bay breeze on Sept. 25 caused recirculation of air masses transporting pollutants from the HSC out to the Gulf and then back to Houston; this circulation pattern was considered an important factor in reaching peak O_3 concentrations during this period (Baier et al., 2015; Li et al., 2016). Additionally, on Sept. 25, measurement and analysis of direct O_3 production rates at MT and at Smith Point (mouth of the HSC) indicated high O_3 production around MT with advection to Smith Point and outlying areas in Houston (Baier et al., 2015). The recirculation pattern coupled with the high O_3 production makes

Sept. 24 – 25 a time of high interest in understanding the major influences on aerosol formation across the Houston Metropolitan area.

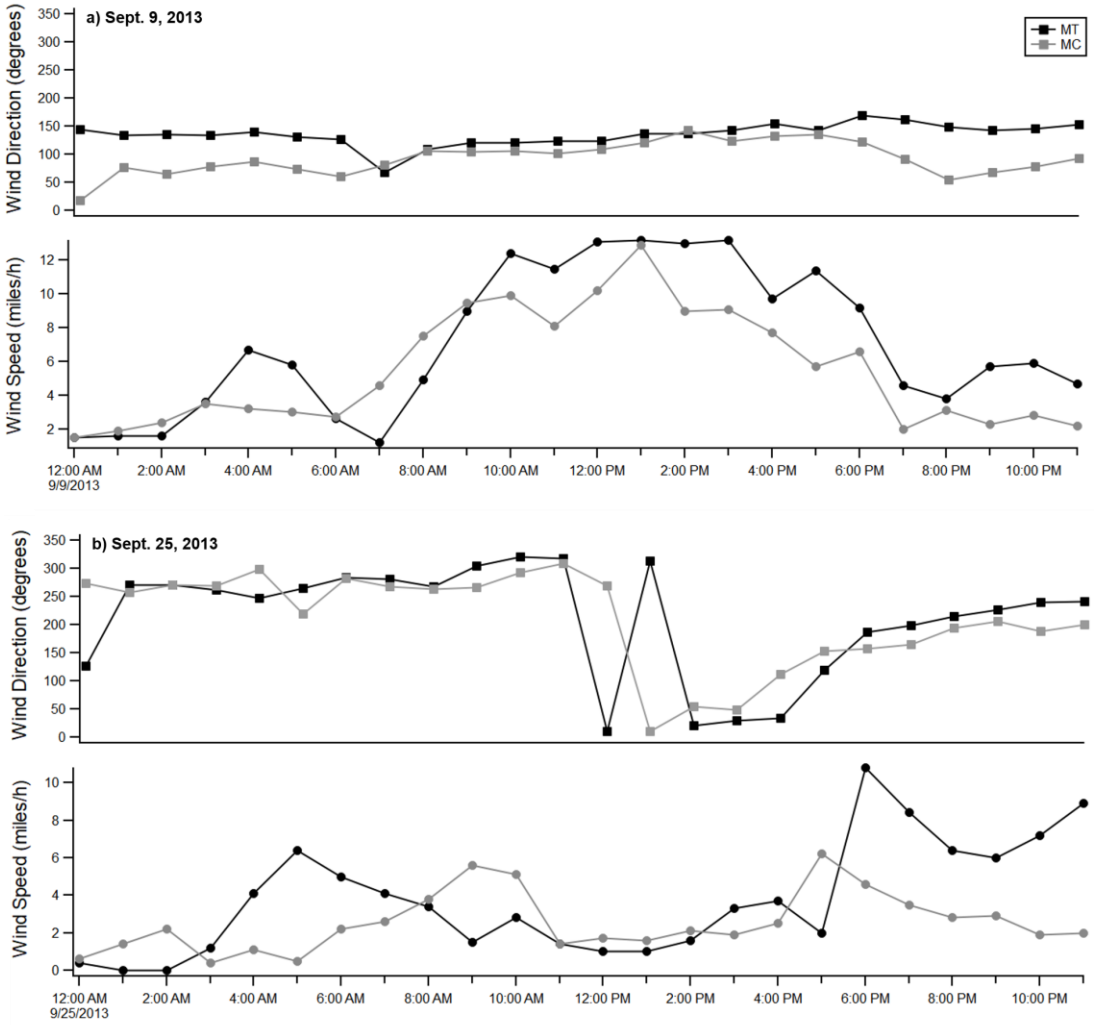

Figure 4.5. Hourly averaged wind speed and wind direction on a) Sept. 9, 2013 and b) Sept. 25, 2013 at Moody Tower (MT) and Manvel Croix (MC).

Detailed Analysis of Two High PM Weeks

To better characterize sources and potential atmospheric chemistry driving the buildup of PM in weeks 2 and 4 during DISCOVER-AQ, chemical and source apportionment analysis was conducted. Results of this analysis were compared to co-located measurements of O_3 and real-time OA by HR-ToF-AMS. The ^{14}C-based analysis

apportions TOC either as contemporary or fossil carbon, while molecular marker analysis indicates specific emission sources for the two weeks with building periods of PM during DISCOVER-AQ. Carbonaceous aerosols at both sites had larger contributions of contemporary than of fossil carbon. The MT measurements provide a comparison between weeks 2 and 4 to understand drivers of high PM in the Houston urban core. Analysis of week 4 provided comparisons of sources at both sites during a period of high PM.

Week-to-week comparison of contemporary and fossil carbon at Moody Tower. The detailed analysis of MT provided comparison of apportioned fossil and contemporary TOC during a week with high PM (week 2) and a week with high PM and a peak O_3 event (week 4). During week 2, contribution of contemporary carbon was relatively consistent until Sept. 14, when an increase in contemporary carbon contribution was observed (Figure 4.6). During week 4, contribution of contemporary carbon had strong day-to-day variability with a sharp decrease in contemporary contribution on Sept. 25, the day of peak OC and O_3 concentrations (Figure 4.4. and 4.6.). A closer look at ambient concentrations of contemporary and fossil TOC for week 4 reveals that the apparent decrease in contribution of contemporary TOC was driven by an increase in the ambient fossil TOC concentration (Figure 4.6). Contribution of fossil carbon at MT for week 2 (average 45 ± 8%) and week 4 (average: 39 ± 10%) were not statistically different (Mann-Whitney Rank Sum test; $p > 0.50$).

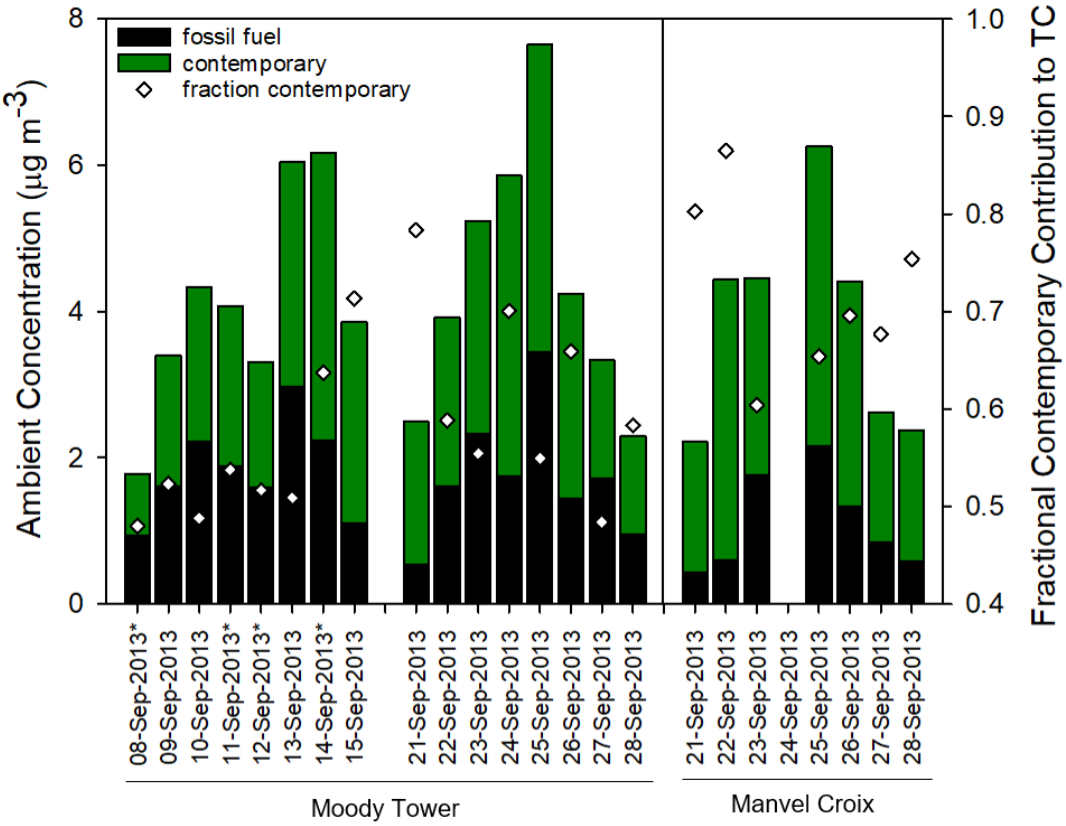

Figure 4.5. Contemporary and fossil carbon concentration from radiocarbon-based source apportionment (left y-axis). Fraction contemporary contribution are included (right y-axis). *These are of 24 h (06:30 – 06:00) samples.

Comparison of contemporary and fossil carbon by site. Based on ^{14}C-based source apportionment, contemporary sources contributed a majority of the TOC at both sites. During week 4, MT had smaller contribution and concentration of contemporary carbon than MC. Contemporary carbon contribution at MT ranged from 48 – 78% with an average of 61 ± 10%, while MC ranged from 60 – 86% with an average of 72 ± 9%. The average contemporary and fossil carbon concentration at MT was of 2.65 ± 1.01 and 1.73 ± 0.89 µg C m^{-3}, respectively, while MC was 2.72 ± 0.99 and 1.11 ± 0.66 µg C m^{-3}, respectively. Contribution from fossil carbon was significantly larger at MT than MC (t-

test; $p > 0.05$). These results are expected as MT is located at the urban core of Houston and is often impacted by more traffic and industrial emission sources than MC.

The apportioned contemporary carbon contribution from the current study can be compared to measurements made in southeastern U.S. cities from a previous decade, though it is important to note differences due to improved emissions control technology and geography. The contribution of contemporary carbon from DISCOVER-AQ are similar to Centreville, AL (85%), Nashville, TN (56-80%), and Tampa, FL (52 – 89%), but have a higher contribution than Birmingham, AL (37%) and Aldine, TX (another suburban city in the Houston metropolitan area: 34-68%) (Lemire et al., 2002; Lewis et al., 2004; Lewis and Stiles, 2006; Weber et al., 2007; Zheng et al., 2006). Studies have observed enhanced biogenic SOA production, particularly isoprene and monoterpene-derived SOA, under influence of urban air masses – representative of both MT and MC sites (Edney et al., 2005; Gunsch et al., 2018; Shilling et al., 2013; Surratt et al., 2010; Zhang et al., 2018).

Molecular marker source apportionment modeling. The CMB model is a receptor-based model which was used to apportion carbonaceous aerosols to primary sources including vegetative detritus, wood smoke, and MVE (sum of diesel exhaust, gasoline exhaust and lubricating oil contribution). The ^{14}C measurements were combined with the CMB results to calculate an upper estimate of SOC from secondary fossil and biogenic carbon precursors (Figure 4.7.). This apportionment method provides an upper estimate of SOC due to potential exclusion of other, likely minor, primary carbon sources. On average, the CMB apportioned 33 ± 14% of the TOC with the larger contribution from primary sources at MT (38 ± 13%) than MC (21 ± 7%). When

comparing weeks 2 and 4, the contributions of fossil and biogenic SOC were higher during week 4 when the peak O_3 event occurred (Figure 4.7.).

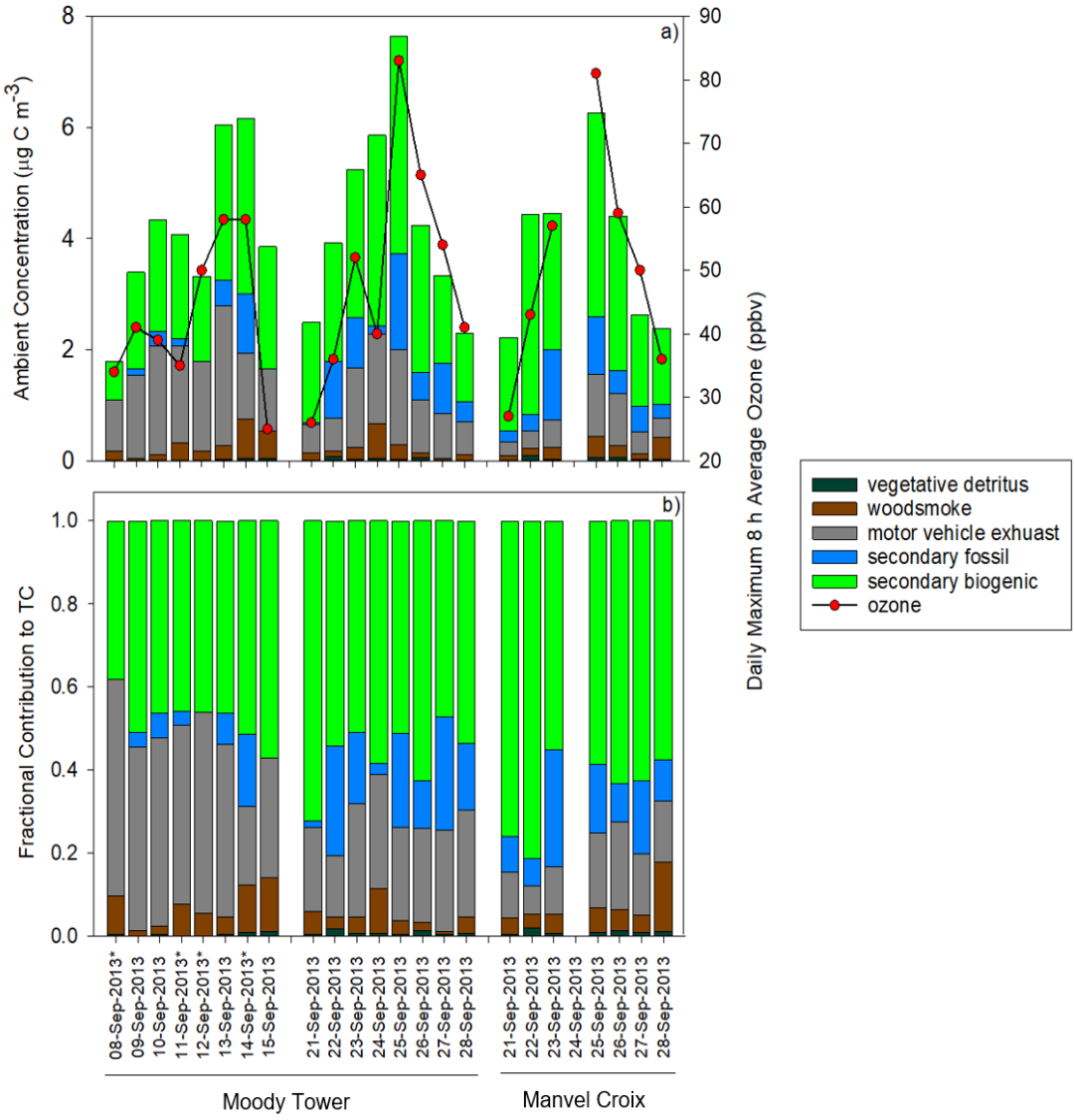

Figure 4.6. Apportionment of TOC using the CMB and ^{14}C analysis. Primary sources include vegetative detritus, wood smoke, and motor vehicle exhaust and secondary sources include fossil and biogenic precursors. Apportioned a) concentration and daily maximum 8-h average O_3 concentrations are included (right-axis) and b) fractional contribution. *These are of 24 h (06:30 – 06:00) samples.

Week-to-week comparison of Moody Tower by CMB + ^{14}C. Weeks 2 and 4 are of particular interest, as both weeks exhibited build up and peak concentrations of OC and EC, with different atmospheric oxidation conditions. Week 2 at MT was significantly more impacted by primary sources (t-test; $p < 0.001$), with an average TC apportionment to primary sources of 48 ± 10% compared to 28 ± 6% in week 4. For both weeks, the majority of the apportioned primary TOC at MT was from MVE, followed by wood smoke, then vegetative detritus. The average ambient concentration of MVE during the weeks 2 and 4 was 1.59 ± 0.50 and 1.02 ± 0.49 μg C m^{-3}, respectively, while average ambient concentration of wood smoke was 0.28 ± 0.22 and 0.19 ± 0.19 μg C m^{-3}, respectively. Although the relative contribution of MVE to total apportioned primary TC during each week was the same, the ambient concentration varied. The differences in ambient concentrations was likely more influenced by meteorological/environmental conditions than by large changes in local MVE emissions. This is in agreement with Glen et al. (1996), in which meteorological factors were a large driver of variability in MVE emissions in urban atmospheres.

Contribution of secondary biogenic and fossil carbon to TOC were significantly larger (t-test; $p < 0.05$) during week 4 (56 ± 8% and 16 ± 10%, respectively) compared to the week 2 (48 ± 6% and 5 ± 6%, respectively). However, the ambient concentration between the two weeks for both secondary biogenic and fossil carbon at MT were not statistically different (t-test; $p > 0.05$), due to the high standard deviation; the average ambient concentration for secondary biogenic carbon was 2.00 ± 0.23 and 2.42 ± 0.70 μg C m^{-3}, while secondary fossil carbon was 0.25 ± 0.37 and 0.70 ± 0.56 μg C m^{-3} for weeks

2 and 4, respectively. Secondary fossil carbon and O_3 concentrations peaked on Sept. 14 and Sept. 25, which were also peak days for OC and $PM_{2.5}$.

Comparison of the sites by CMB + ^{14}C. Direct comparison of the two sites is possible from the detailed chemical analysis and source apportionment of aerosol samples collected during the week 4 of the campaign. Both sites observed a building of fossil TOC (i.e. primary MVE and secondary fossil) concentration with the increasing peak O_3 concentration (Figure 4.7). EC was correlated with MVE ($r^2 = 0.65$) at both sites. The MVE concentration at MT (average: 1.02 ± 0.49 µg C m^{-3}) was not significantly larger than at MC (average: 0.55 ± 0.34 µg C m^{-3}) (t-test; $p < 0.05$). The ambient concentration of wood smoke at MT and MC was 0.19 ± 0.19 and 0.22 ± 0.12 µg C m^{-3}, respectively. The ambient concentration of vegetative detritus was 0.04 ± 0.02 and ± 0.03 µg C m^{-3} at MT and MC, respectively. Both primary TOC concentrations from wood smoke and vegetative detritus at MT and MC were minimal.

As mentioned previously, the CMB apportioned 31 ± 13% of the TOC, with larger contribution from primary sources at MT (weeks 2 and 4; 38 ± 13%), than MC (21 ± 7%). These values are comparable to the results of Dunker et al. (2019) using the CAMx model, which showed the primary to total OA ratios at Park Place (C416; most similar to the MT site) 40 ± 9%. However, for MC the CAMx value (35 ± 8%) was larger than the CMB estimate for MC. Differences in the values can be due to the source apportionment of either TC (CMB + ^{14}C) or OA (CAMx) where the TC accounts for just carbon mass while OA includes oxygen, hydrogen, nitrogen, and other elements associated with organic matter (OM). The OM/OC ratio measured previously range from 1.1 to 2.1 while contribution of secondary species are at the higher end of the range (El-

Zanan et al., 2005; Russell, 2003). For sites more impacted by secondary processes (e.g. MC), the difference between apportioned TC and OA will likely be greater. Another potential reason for the difference in apportioned TC and OA can be due to the sampling period, as the CAMx modeled values were 24-h averages, while the measured values at MT and MC were averages during the daytime (6:30 to 20:00). The exclusion of the nighttime in the measured data at MC can also contribute to driving a lower primary to total TC compared to the modeled 24-h average primary to total OA.

For both sites, the largest contribution of TOC was unapportioned, likely from SOC (average all sites: 67 ± 14%) or aged emissions (oxidized POC). With improvement in MVE technology, studies have observed a decrease of primary emissions (Gentner et al., 2017; Gordon et al., 2014). Secondary processes of carbonaceous aerosols previously have been demonstrated to be important during DISCOVER-AQ 2013 Houston studies (Bean et al., 2016; Dunker et al., 2019; Leong et al., 2017). The largest fraction of TOC at both sites was from secondary biogenic carbon, which could also include secondary or aged BB, with an average contribution of 65 ± 10% at MC and 52 ± 8% (week 2 and 4) at MT. During the week a peak O_3 event (i.e. week 4), the average ambient concentration of secondary biogenic TOC at both sites was 2.29 ± 0.86 µg C m^{-3} which is higher than other southeastern U.S. cities including Atlanta, GA (0.95 µg C m^{-3}); Pensacola, FL (1.15 µg C m^{-3}); and Birmingham (2.03 µg C m^{-3}) and Centreville (2.04 µg C m^{-3}), AL (Lewandowski et al., 2013). The biogenic SOC concentrations of these four southeastern cities were summer averages, while the current study reflects an average during a high pollution period for O_3 and PM. A previous study using molecular-tracer based source apportionment of biogenic SOC in Research Triangle Park, NC in 2003 included high

particulate pollution days (Kleindienst et al., 2007). The September average (1.48 ± 0.27 μg C m^{-3}) at Research Triangle Park was lower than the current study, while average biogenic SOC concentrations during August (2.75 ± 0.67 μg C m^{-3}) was more similar to the average concentration at the Houston sites (2.42 ± 0.89 μg C m^{-3}) (Kleindienst et al., 2007).

Contribution from secondary fossil sources was quite variable at both sites, ranging from 3-27% at MT and 9-18% at MC. The largest day-to-day variability and largest average contribution of secondary fossil carbon was observed at MT with an average contribution and concentration of 16 ± 10% and 0.70 ± 0.56 μg C m^{-3}, respectively. Contribution of gas-phase SOA precursors from MVE emissions would contribute to the secondary fossil carbon in the Houston metropolitan area (Gentner et al., 2017). MT also is influenced by emissions from the heavily industrialized HSC (Bahreini et al., 2009; Wallace et al., 2018). Dechapanya et al. (2004), utilizing emission inventory data for 2000, estimated that 53% of projected anthropogenic SOA in the Houston area was from industrial precursors, i.e. aromatics and terpenes from pulp and paper processing. These industrially produced terpene emissions, if biologically derived, would be apportioned as contemporary carbon and/or biogenic SOC; while petroleum-derived terpenes would be apportioned to fossil SOC. Since the metropolitan area is greatly impacted by biogenic sources of terpenes from the piney woods just north east of the city (Figure 4.1), it would take significant emissions to supplant this natural source (Nowak et al., 2017). Current studies of these point sources are needed to understand the impact of the industrially produced VOCs. Dunker et al. (2019) suggested that point sources could enhance both the yield of biogenic SOA and the production of O_3 in the HGB area via co-

emission of NO_x. The current study observed peak secondary fossil and biogenic carbon concentrations during peak PM and O_3 days at MT. Thus, Houston industrial point sources may be the drivers for the observed peak in both SOC and O_3 concentrations during DISCOVER-AQ. The recirculation pattern was observed on Sept. 25 where air masses passed through HSC out to the Gulf and then back onshore. This circulation pattern would allow the air mass to pick up potential anthropogenic emissions including HDD, industrial, and ship emissions (Schulze et al., 2018). While the more stagnant conditions during the daytime (i.e. lower wind speeds) (Figure C.1b) allowed the emissions to build during periods of high photochemical activity ultimately contributing to increased levels of SOC and O_3.

Positive Matrix Factorization of PM_1 organic aerosols. The HR-ToF-AMS operated in the MAQL with mobile measurements on-road transects near the MC site during DISCOVER-AQ. During week 4, the MAQL operated at or near MC, which provided opportunity to compare with the filter-based TOC source apportionment. The PMF analysis of the HR-ToF-AMS data resolved four factors: biomass burning organic aerosol (BBOA), hydrocarbon-like organic aerosol (HOA), less oxidized OOA (LO-OOA), and MO-OOA (Figure 4.8). As seen in the filter-based analysis, oxidized aerosol dominated the HR-ToF-AMS dataset; MO-OOA was the dominant constituent with 68% (Figure 4.8a). Determination of these factors is detailed in S1.The CMB – wood smoke contribution at MC had an average contribution of 4%, which is comparable to contribution of BBOA (8%) (Figure 4.8a and b). The CMB – wood smoke apportions the primary contribution of wood smoke based on the ratio of levoglucosan to OC. The PMF – BBOA includes OA (both primary and secondary) produced from biomass burning

events. The difference in contribution and concentration of CMB – wood smoke and BBOA measurements are due to difference in source apportionment methods including exclusion of possible SOC from wood smoke which would be apportioned as secondary biogenic contribution in the CMB + ^{14}C analysis. The other sources and factors including biogenic and fossil SOC closely matches the MO-OOA and LO-OOA while the HOA closely matches primary SOC from MVE and vegetative detritus (Figure 4.8a and b).

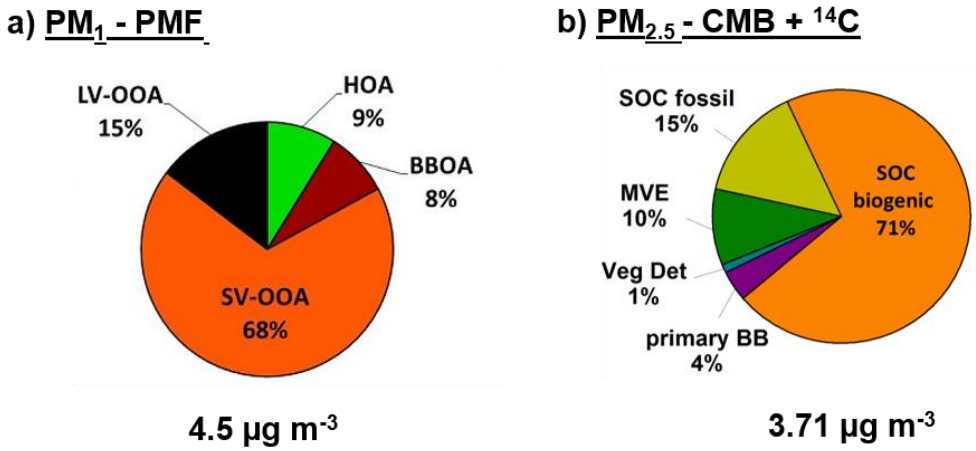

Figure 4.8. Apportioned a) OA of PM_1, and b) TOC of $PM_{2.5}$ at Manvel Croix from September 21 – 23. PM_1 OA was apportioned either as hydrocarbon-like OA (HOA), biomass burning OA (BBOA), less-oxidized oxygenated OA (LO-OOA), and more-oxidized oxygenated OA (MO-OOA). Below each pie chart includes average ambient concentration.

Carbonaceous Aerosols and Ozone

During the current study period, O_3 daily maximum and 24 h average $PM_{2.5}$ concentrations demonstrated similar trends across the HGB region (Figure 4.3), with r^2 values ranging from 0.52 – 0.68 (Figure C.3) for the different TCEQ monitoring sites. The sites nearest to Texas City (Galveston and Seabrook), a port city by the Gulf with heavy petroleum-refining and petrochemical-manufacturing activities, had the highest correlations (r^2 = 0.57 – 0.68) for O_3 and $PM_{2.5}$ (Figure C.3). This finding supports that

point sources are significant drivers for PM and O_3 formation in the Houston metropolitan area. Of the DISCOVER-AQ sites, MT had a similar correlation to the TCEQ sites in Houston ($r^2 = 0.54$), however, $PM_{2.5}$ mass concentration was not measured at MC. To better understand the relationship between PM and O_3, correlations with components of OC were also investigated. A strong correlation between $PM_{2.5}$ and OC, for both 24 h and daytime concentration, was observed at MT. However, when the OC concentrations are compared to O_3 daily maximum concentrations, a stronger correlation was observed with the daytime ($r^2 = 0.56$) compared to the 24 h average ($r^2 = 0.37$) measurement (Figure C.4c – e). For these reasons, daytime measurements at MT and MC were utilized for more detailed analysis and comparison with O_3.

Apportioned Primary and Secondary Organic Carbon, Meteorology and Ozone

Ozone is a secondary pollutant and was significantly more correlated to SOC ($r^2 = 0.57$) than to primary OC ($r^2 = 0.10$). Although PM chemistry is complex, the same key species (i.e. NO_x and VOCs) which enhance oxidation processes to form SOA are also precursors for O_3 formation (Mazzuca et al., 2016). Amongst the apportioned fossil and contemporary TC, O_3 was more strongly correlated to fossil carbon ($r^2 = 0.55$) than contemporary carbon ($r^2 = 0.34$) while comparable to fossil SOC($r^2 = 0.53$) (Figure 4.9a and b). Previous studies have found that emission of NOx and light olefins from petrochemical facilities led to high O_3 production in Houston (Kleinman et al., 2005). During DISCOVER-AQ, the O_3 production rate was greatest near areas with high emissions of NO_x and VOCs which included Houston's urban regions with hotspots measured over the HSC (Mazzuca et al., 2016). Based on measurements at MT and MC, a stronger correlation of O_3 to fossil carbon was observed at the more urban site () than

the suburban site (). The Sept. 25 day was when both peak O3 and PM concentration was observed across the Houston metropolitan area. During this day, MT and MC observed relatively large contribution and concentration of fossil carbon and fossil SOC at MT and MC (Figure 6).

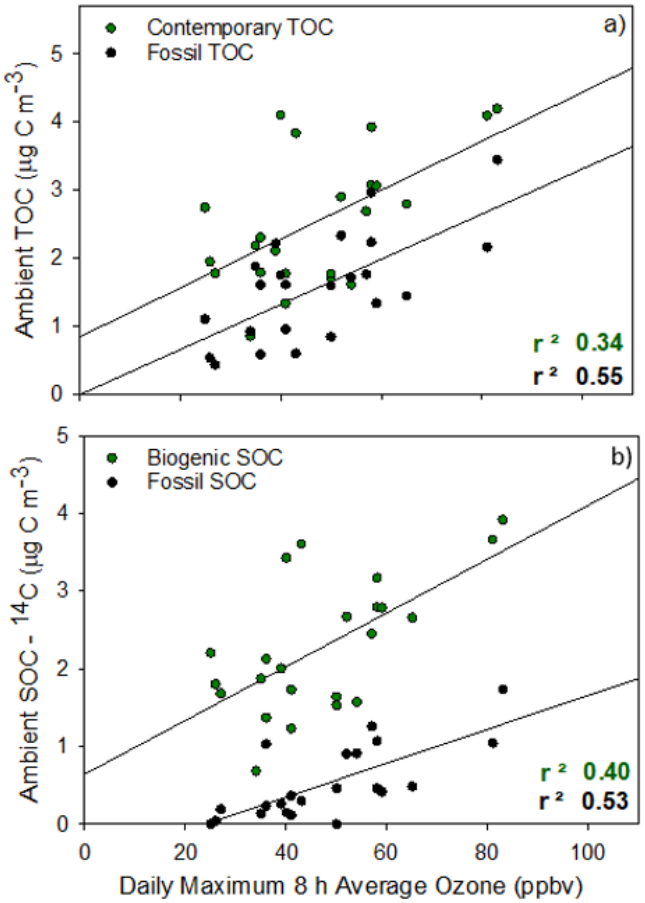

Figure 4.9. Correlation between daily maximum 8 h O_3 average and a) apportioned contemporary and fossil TOC from ^{14}C analysis and c) biogenic and fossil SOC.

Dunker et al. (2019) suggested that point sources greatly impacted production of both SOA and O_3 in Houston. The HSC area of Houston has a high density of point sources, but the BT analysis combined with the chemical speciation reveals that the peak O_3 events require specific meteorology as well. The wind conditions during week 2 had

relatively consistent wind direction (i.e. east-southeast and southeast) and wind speeds throughout the day (Figure C.1a and b). During this period, the sites were likely impacted from HDD, industrial, and ship emissions from the HSC, however, this was not the week with peak O_3. It was during week 4 where peak O_3 and largest carbonaceous aerosols concentrations were observed. Wind direction and wind speeds were more variable during week 4 producing periods of stagnant wind conditions (Figure C.1c and d; Figure C.2). On Sept. 25, a day with stagnant conditions (Figure 4.5 and C.2), a recirculation of air brought polluted HSC air masses out to the Bay and back to downtown Houston area, which was followed by the high PM and peak O_3 event (Baier et al., 2015; Caicedo et al., 2019). These patterns have been observed in previous peak O_3 events in Houston (Banta et al., 2005). While additional study is needed to better understand the mechanisms of the potential SOA production associated with fossil point sources, these results strongly indicate the importance of these sources to O_3 production in Houston metropolitan area.

Conclusion

The current study provided the first in-depth analysis of source apportioned daytime TOC and its relation to O_3 during the DISCOVER-AQ Houston campaign. A novel source apportionment method combining molecular marker CMB and ^{14}C analysis proved to be adept at apportioning both primary and secondary carbon sources. Based on these results, the carbonaceous aerosols in the Houston metropolitan area were dominated by biogenic SOC during DISCOVER-AQ. This finding supports previous DISCOVER-AQ studies which observed highly oxygenated OA (Dunker et al., 2019; Leong et al., 2017).

Though the composition of aerosol had consistent contributions from biogenic SOC and MVE, the fossil SOC had the greatest association with peak O_3. While fossil SOC concentrations were quite variable, they were enhanced at all sites during the high PM and peak O_3 event. Based on wind conditions and apportionment results, point source emissions from the HSC in conjunction with on- and off-shore wind cycling contributed to this peak event. This finding is in support of Dunker et al. (2019), who concluded that point source emissions were major contributors to OA and O_3 formation in the Houston metropolitan area.

The MT site (urban core) exhibited the largest and most consistent contribution from MVE and secondary fossil sources compared to the suburban MC site. Overall findings from the current study improve understanding of spatial trends (i.e. urban core and suburbs of the Houston metropolitan area) and identify key sources and factors that drive both O_3 and $PM_{2.5}$ production in the HGB region. Results from the current study highlight the need for continued high-intensity, multi-site studies to better understand impact of point sources from the HSC on air quality in the urban, suburb, and exurb regions of Houston. This will assist in effective regulation as the metropolitan area is still marginal nonattainment for O_3 amidst continual growth and spread of population into its suburbs and exurbs.

Acknowledgments

The preparation of this manuscript was financed through a grant from the Texas Commission on Environmental Quality (TCEQ), administered by the University of Texas at Austin, Center for Energy and Environmental Resources (CEER) through the Air Quality Research Program (AQRP)(12-032 and 14-029). The contents findings, opinions

and conclusions are the work of the author(s) and do not necessarily represent findings, opinions or conclusions of the TCEQ.

This project was also supported by the C. Gus Glasscock, Jr. Endowed Fund for Excellence in Environmental Sciences. The authors would like to thank the U.S. Environmental Protection Agency for providing two Tisch Hi Vol+ $PM_{2.5}$ samplers which were used at MT and CR. In addition, the authors would like to thank Raj B. Nadkarni and Jim Thomas at TCEQ for site access and support. We are also grateful to Greg Yarwood (Ramboll) for providing us with the CAMx modeled OA data from the Houston DISCOVER-AQ and Michael Lewandowski (U.S. Environmental Protection Agency) for providing us with apportioned SOC data from Research Triangle Park, NC from 2003.

References

2015. Houston-Galveston-Brazoria (HGB) PM2.5 Advance Path Forward Update, in: Council, H.-G.A. (Ed.), H-GAC Regional Air Quality Planning Advisory Committee.

2019. Estimates of the Components of Resident Population Change: April 1, 2010 to July 1, 2018. U.S. Census Bureau, Population Division.

AAPA, 2019. 2018 U.S. Port Rankings by Cargo Tonnage. American Association of Port Authorities.

Allen, D.T., Fraser, M., 2006. An overview of the gulf coast aerosol research and characterization study: The Houston fine particulate matter supersite. Journal of the Air & Waste Management Association 56, 456-466.

Allen, D.T., McDonald-Buller, E.C., McGaughey, G., 2018. State of the Science of Air Quality in Texas: Summary of Scientific Projects and Findings from the Texas Air Quality Research Program (AQRP) 2010-2017, in: Estes, M. (Ed.), Texas Commission on Environmental Quality.

Bahreini, R., Ervens, B., Middlebrook, A., Warneke, C., De Gouw, J., DeCarlo, P., Jimenez, J., Brock, C., Neuman, J., Ryerson, T., 2009. Organic aerosol formation in urban and industrial plumes near Houston and Dallas, Texas. J. Geophys. Res. Atmos. 114.

Baier, B.C., Brune, W.H., Lefer, B.L., Miller, D.O., Martins, D.K., 2015. Direct ozone production rate measurements and their use in assessing ozone source and receptor regions for Houston in 2013. Atmos. Environ. 114, 83-91.

Banta, R., Senff, C., Nielsen-Gammon, J., Darby, L., Ryerson, T., Alvarez, R., Sandberg, S., Williams, E., Trainer, M., 2005. A bad air day in Houston. Bull. Am. Meteorol. Soc. 86, 657-669.

Banta, R.M., Senff, C.J., Alvarez, R.J., Langford, A.O., Parrish, D.D., Trainer, M.K., Darby, L.S., Hardesty, R.M., Lambeth, B., Neuman, J.A., 2011. Dependence of daily peak O3 concentrations near Houston, Texas on environmental factors: Wind speed, temperature, and boundary-layer depth. Atmos. Environ. 45, 162-173.

Barrett, T.E., Robinson, E.M., Usenko, S., Sheesley, R.J., 2015. Source Contributions to Wintertime Elemental and Organic Carbon in the Western Arctic Based on Radiocarbon and Tracer Apportionment. Environ. Sci. Technol.

Bean, J.K., Faxon, C.B., Leong, Y.J., Wallace, H.W., Cevik, B.K., Ortiz, S., Canagaratna, M.R., Usenko, S., Sheesley, R.J., Griffin, R.J., 2016. Composition and Sources of Particulate Matter Measured near Houston, TX: Anthropogenic-Biogenic Interactions. Atmosphere 7, 73.

Birch, M., Cary, R., 1996. Elemental carbon-based method for monitoring occupational exposures to particulate diesel exhaust. Aerosol Sci. Technol. 25, 221-241.

Caicedo, V., Rappenglueck, B., Cuchiara, G., Flynn, J., Ferrare, R., Scarino, A., Berkoff, T., Senff, C., Langford, A., Lefer, B., 2019. Bay Breeze and Sea Breeze Circulation Impacts on the Planetary Boundary Layer and Air Quality From an Observed and Modeled DISCOVER-AQ Texas Case Study. J. Geophys. Res. Atmos. 124, 7359-7378.

Clark, A.E., Yoon, S., Sheesley, R.J., Usenko, S., 2015. Pressurized liquid extraction technique for the analysis of pesticides, PCBs, PBDEs, OPEs, PAHs, alkanes, hopanes, and steranes in atmospheric particulate matter. Chemosphere 137, 33-44.

Coulter, T.C., 2004. EPA-CMB8.2 Users Manual, in: Agency, U.S.E.P. (Ed.), Air Quality Modeling Group.

Czader, B.H., Choi, Y., Li, X., Alvarez, S., Lefer, B., 2015. Impact of updated traffic emissions on HONO mixing ratios simulated for urban site in Houston, Texas. Atmos. Chem. Phys. 15, 1253-1263.

Dechapanya, W., Russell, M., Allen, D.T., 2004. Estimates of anthropogenic secondary organic aerosol formation in Houston, Texas special issue of aerosol science and technology on findings from the fine particulate matter supersites program. Aerosol Sci. Technol. 38, 156-166.

Draxler, R., Rolph, G., 2010. HYSPLIT (HYbrid Single-Particle Lagrangian Integrated Trajectory), in: Laboratory, A.R. (Ed.), Silver Spring, MD. NOAA, p. 26.

Dunker, A.M., Koo, B., Yarwood, G., 2019. Source apportionment of organic aerosol and ozone and the effects of emission reductions. Atmos. Environ. 198, 89-101.

Edney, E., Kleindienst, T., Jaoui, M., Lewandowski, M., Offenberg, J., Wang, W., Claeys, M., 2005. Formation of 2-methyl tetrols and 2-methylglyceric acid in secondary organic aerosol from laboratory irradiated isoprene/NOx/SO2/air mixtures and their detection in ambient PM2. 5 samples collected in the eastern United States. Atmos. Environ. 39, 5281-5289.

El-Zanan, H.S., Lowenthal, D.H., Zielinska, B., Chow, J.C., Kumar, N., 2005. Determination of the organic aerosol mass to organic carbon ratio in IMPROVE samples. Chemosphere 60, 485-496.

EPA, 2019. Texas Nonattainment/Maintenance Status for Each County by Year for All Criteria Pollutants, United States Environmental Protection Agency.

Fine, P.M., Cass, G.R., Simoneit, B.R., 2002. Chemical characterization of fine particle emissions from the fireplace combustion of woods grown in the southern United States. Environ. Sci. Technol. 36, 1442-1451.

Fraser, M., Yue, Z., Tropp, R., Kohl, S., Chow, J., 2002. Molecular composition of organic fine particulate matter in Houston, TX. Atmospheric Environment 36, 5751-5758.

Gentner, D.R., Jathar, S.H., Gordon, T.D., Bahreini, R., Day, D.A., El Haddad, I., Hayes, P.L., Pieber, S.M., Platt, S.M., de Gouw, J., Goldstein, A.H., Harley, R.A., Jimenez, J.L., Prévôt, A.S.H., Robinson, A.L., 2017. Review of Urban Secondary Organic Aerosol Formation from Gasoline and Diesel Motor Vehicle Emissions. Environ. Sci. Technol. 51, 1074-1093.

Glen, W.G., Zelenka, M.P., Graham, R.C., 1996. Relating meteorological variables and trends in motor vehicle emissions to monthly urban carbon monoxide concentrations. Atmospheric Environment 30, 4225-4232.

Gordon, T., Presto, A., May, A., Nguyen, N., Lipsky, E., Donahue, N., Gutierrez, A., Zhang, M., Maddox, C., Rieger, P., 2014. Secondary organic aerosol formation exceeds primary particulate matter emissions for light-duty gasoline vehicles. Atmospheric Chemistry and Physics 14, 4661-4678.

Gunsch, M.J., Schmidt, S.A., Gardner, D.J., Bondy, A.L., May, N.W., Bertman, S.B., Pratt, K.A., Ault, A.P., 2018. Particle growth in an isoprene-rich forest: Influences of urban, wildfire, and biogenic air masses. Atmos. Environ. 178, 255-264.

Hildemann, L.M., Klinedinst, D.B., Klouda, G.A., Currie, L.A., Cass, G.R., 1994. Sources of urban contemporary carbon aerosol. Environ. Sci. Technol. 28, 1565-1576.

Kleindienst, T.E., Jaoui, M., Lewandowski, M., Offenberg, J.H., Lewis, C.W., Bhave, P.V., Edney, E.O., 2007. Estimates of the contributions of biogenic and anthropogenic hydrocarbons to secondary organic aerosol at a southeastern US location. Atmos. Environ. 41, 8288-8300.

Kleinman, L.I., Daum, P., Imre, D., Lee, Y.N., Nunnermacker, L., Springston, S., Weinstein-Lloyd, J., Rudolph, J., 2002. Ozone production rate and hydrocarbon reactivity in 5 urban areas: A cause of high ozone concentration in Houston. Geophysical Research Letters 29, 105-101-105-104.

Kleinman, L.I., Daum, P.H., Lee, Y.N., Nunnermacker, L.J., Springston, S.R., Weinstein-Lloyd, J., Rudolph, J., 2005. A comparative study of ozone production in five US metropolitan areas. J. Geophys. Res. Atmos. 110.

Lefer, B., Rappenglück, B., Flynn, J., Haman, C., 2010. Photochemical and meteorological relationships during the Texas-II Radical and Aerosol Measurement Project (TRAMP). Atmos. Environ. 44, 4005-4013.

Lemire, K.R., Allen, D.T., Klouda, G.A., Lewis, C.W., 2002. Fine particulate matter source attribution for Southeast Texas using 14C/13C ratios. J. Geophys. Res. Atmos. 107, ACH 3-1-ACH 3-7.

Leong, Y., Sanchez, N., Wallace, H., Karakurt Cevik, B., Hernandez, C., Han, Y., Flynn, J., Massoli, P., Floerchinger, C., Fortner, E., 2017. Overview of surface measurements and spatial characterization of submicrometer particulate matter during the DISCOVER-AQ 2013 campaign in Houston, TX. J. Air Waste Manag. Assoc. 67, 854-872.

Lewandowski, M., Piletic, I.R., Kleindienst, T.E., Offenberg, J.H., Beaver, M.R., Jaoui, M., Docherty, K.S., Edney, E.O., 2013. Secondary organic aerosol characterisation at field sites across the United States during the spring–summer period. International journal of environmental analytical chemistry 93, 1084-1103.

Lewis, C.W., Klouda, G.A., Ellenson, W.D., 2004. Radiocarbon measurement of the biogenic contribution to summertime PM-2.5 ambient aerosol in Nashville, TN. Atmos. Environ. 38, 6053-6061.

Lewis, C.W., Stiles, D.C., 2006. Radiocarbon content of PM2. 5 ambient aerosol in Tampa, FL. Aerosol Sci. Technol. 40, 189-196.

Li, X., Choi, Y., Czader, B., Roy, A., Kim, H., Lefer, B., Pan, S., 2016. The impact of observation nudging on simulated meteorology and ozone concentrations during DISCOVER-AQ 2013 Texas campaign. Atmos. Chem. Phys 16, 3127-3144.

Lough, G.C., Christensen, C.G., Schauer, J.J., Tortorelli, J., Mani, E., Lawson, D.R., Clark, N.N., Gabele, P.A., 2007. Development of molecular marker source profiles for emissions from on-road gasoline and diesel vehicle fleets. J. Air Waste Manag. Assoc. 57, 1190-1199.

Loughner, C.P., Allen, D.J., Pickering, K.E., Zhang, D.-L., Shou, Y.-X., Dickerson, R.R., 2011. Impact of fair-weather cumulus clouds and the Chesapeake Bay breeze on pollutant transport and transformation. Atmos. Environ. 45, 4060-4072.

Lubertino, G., 2019. Transportation Air Quality Conformity Report for the Houston-Brazoria-Galveston Region: 2045 Regional Transportation Plan. Houston-Galveston Area Council.

Mazzuca, G.M., Ren, X., Loughner, C.P., Estes, M., Crawford, J.H., Pickering, K.E., Weinheimer, A.J., Dickerson, R.R., 2016. Ozone production and its sensitivity to NOx and VOCs: Results from the DISCOVER-AQ field experiment, Houston 2013. Atmos. Chem. Phys. 16, 14463–14474.

NASA, 2019. DISCOVER-AQ, National Aeronautics and Space Administration.

Nowak, D.J., Bodine, A.R., Hoehn, R.E.I., Edgar, C.B., Riely, G., Hartel, D.R., Dooley, K.J., Stanton, S.M., Hatfield, M.A., Brandeis, T.J., Lister, T.W., 2017. Houston's Urban Forest, 2015. United States Department of Agriculture, U.S. Forest Service.

Olaguer, E.P., Kolb, C.E., Lefer, B., Rappenglück, B., Zhang, R., Pinto, J.P., 2014. Overview of the SHARP campaign: motivation, design, and major outcomes. J. Geophys. Res. Atmos. 119, 2597-2610.

Parrish, D., Allen, D., Bates, T., Estes, M., Fehsenfeld, F., Feingold, G., Ferrare, R., Hardesty, R., Meagher, J., Nielsen-Gammon, J., 2009. Overview of the second Texas air quality study (TexAQS II) and the Gulf of Mexico atmospheric composition and climate study (GoMACCS). J. Geophys. Res. Atmos. 114.

Rogge, W.F., Hildemann, L.M., Mazurek, M.A., Cass, G.R., Simoneit, B.R., 1993. Sources of fine organic aerosol. 4. Particulate abrasion products from leaf surfaces of urban plants. Environ. Sci. Technol. 27, 2700-2711.

Russell, L.M., 2003. Aerosol organic-mass-to-organic-carbon ratio measurements. Environ. Sci. Technol. 37, 2982-2987.

Ryerson, T., Trainer, M., Angevine, W., Brock, C., Dissly, R., Fehsenfeld, F., Frost, G., Goldan, P., Holloway, J., Hübler, G., 2003. Effect of petrochemical industrial emissions of reactive alkenes and NOx on tropospheric ozone formation in Houston, Texas. J. Geophys. Res. Atmos. 108.

Schauer, J.J., Rogge, W.F., Hildemann, L.M., Mazurek, M.A., Cass, G.R., Simoneit, B.R.T., 1996. Source apportionment of airborne particulate matter using organic compounds as tracers. Atmos.Environ. 30, 3837-3855.

Schulze, B.C., Wallace, H.W., Bui, A.T., Flynn, J.H., Erickson, M.H., Alvarez, S., Dai, Q., Usenko, S., Sheesley, R.J., Griffin, R.J., 2018. The impacts of regional shipping emissions on the chemical characteristics of coastal submicron aerosols near Houston, TX. Atmos. Chem. Phys. 18, 14217-14241.

Sheesley, R.J., Schauer, J.J., Zheng, M., Wang, B., 2007. Sensitivity of molecular marker-based CMB models to biomass burning source profiles. Atmos. Environ. 41, 9050-9063.

Shilling, J.E., Zaveri, R.A., Fast, J.D., Kleinman, L., Alexander, M., Canagaratna, M.R., Fortner, E., Hubbe, J.M., Jayne, J.T., Sedlacek, A., 2013. Enhanced SOA formation from mixed anthropogenic and biogenic emissions during the CARES campaign. Atmos. Chem. Phys. 13, 2091-2113.

Simoneit, B.R.T., Schauer, J.J., Nolte, C.G., Oros, D.R., Elias, V.O., Fraser, M.P., Rogge, W.F., Cass, G.R., 1999. Levoglucosan, a tracer for cellulose in biomass burning and atmospheric particles. Atmos. Environ. 33, 173-182.

Stauffer, R.M., Thompson, A.M., 2015. Bay breeze climatology at two sites along the Chesapeake bay from 1986–2010: Implications for surface ozone. Journal of atmospheric chemistry 72, 355-372.

Sullivan, D.W., Price, J.H., Lambeth, B., Sheedy, K.A., Savanich, K., Tropp, R.J., 2013. Field study and source attribution for PM2.5 and PM10 with resulting reduction in concentrations in the neighborhood north of the Houston Ship Channel based on voluntary efforts. J. Air Waste Manage. Assoc. 63, 1070-1082.

Surratt, J.D., Chan, A.W., Eddingsaas, N.C., Chan, M., Loza, C.L., Kwan, A.J., Hersey, S.P., Flagan, R.C., Wennberg, P.O., Seinfeld, J.H., 2010. Reactive intermediates revealed in secondary organic aerosol formation from isoprene. Proc. Natl. Acad. Sci. 107, 6640-6645.

TCEQ, 2018. Texas Air Monitoring Information System (TAMIS) Web Interface, Texas Commission on Environmental Quality.

Tucker, S.C., Banta, R.M., Langford, A.O., Senff, C.J., Brewer, W.A., Williams, E.J., Lerner, B.M., Osthoff, H.D., Hardesty, R.M., 2010. Relationships of coastal nocturnal boundary layer winds and turbulence to Houston ozone concentrations during TexAQS 2006. J. Geophys. Res. Atmos. 115.

Wallace, H.W., Sanchez, N.P., Flynn, J.H., Erickson, M.H., Lefer, B.L., Griffin, R.J., 2018. Source apportionment of particulate matter and trace gases near a major refinery near the Houston Ship Channel. Atmos. Environ. 173, 16-29.

Wang, Y., Jia, B., Wang, S.-C., Estes, M., Shen, L., Xie, Y., 2016. Influence of the Bermuda High on interannual variability of summertime ozone in the Houston–Galveston–Brazoria region. Atmospheric Chemistry and Physics 16, 15265-15276.

Weber, R.J., Sullivan, A.P., Peltier, R.E., Russell, A., Yan, B., Zheng, M., De Gouw, J., Warneke, C., Brock, C., Holloway, J.S., 2007. A study of secondary organic aerosol formation in the anthropogenic-influenced southeastern United States. J. Geophys. Res. Atmos. 112.

Wong, K., Tsai, C., Lefer, B., Haman, C., Grossberg, N., Brune, W., Ren, X., Luke, W., Stutz, J., 2012. Daytime HONO vertical gradients during SHARP 2009 in Houston, TX. Atmos. Chem. Phys. 12, 635-652.

Zhang, H., Yee, L.D., Lee, B.H., Curtis, M.P., Worton, D.R., Isaacman-VanWertz, G., Offenberg, J.H., Lewandowski, M., Kleindienst, T.E., Beaver, M.R., 2018. Monoterpenes are the largest source of summertime organic aerosol in the southeastern United States. Proc. Natl. Acad. Sci. 115, 2038-2043.

Zheng, M., Ke, L., Edgerton, E.S., Schauer, J.J., Dong, M., Russell, A.G., 2006. Spatial distribution of carbonaceous aerosol in the southeastern United States using molecular markers and carbon isotope data. J. Geophys. Res. Atmos. 111.

Zhou, W., Cohan, D., Henderson, B., 2014. Slower ozone production in Houston, Texas following emission reductions: evidence from Texas Air Quality Studies in 2000 and 2006. Atmos. Chem. Phys. 14, 2777-2788.

Zotter, P., El-Haddad, I., Zhang, Y., Hayes, P.L., Zhang, X., Lin, Y.H., Wacker, L., Schnelle-Kreis, J., Abbaszade, G., Zimmermann, R., 2014. Diurnal cycle of fossil and nonfossil carbon using radiocarbon analyses during CalNex. J. Geophys. Res. Atmos. 119, 6818-6835.

CHAPTER FIVE

Conclusions and Future Work

Conclusions and Scientific Significance

The carbonaceous aerosols are a significant contributor to PM, however, based on current available analytical methods, chemical speciation of this fraction is quite difficult. This dissertation work utilized multiple tools for chemical speciation and source apportionment models to better understand major sources, trends and drivers of carbonaceous aerosol formation at two major U.S. metropolitan areas: San Francisco Bay Area and Houston metropolitan area. These coastal regions have complex and dynamic meteorological conditions (e.g. bay breeze phenomenon) making air quality investigations challenging. For these reasons, the studies in this dissertation have also included meteorological data (e.g. wind direction, speed, air mass transport) to better understand formation and transport of organic aerosols.

San Francisco Bay Area

The San Francisco Bay Area has implemented highly progressive regulations for lowering elemental (EC) and black (BC) carbon concentrations the last several decades. Lowering emissions of these light absorbing carbonaceous aerosols is of great interest due to the particles' negative impact to human and environmental health and for its climate-forcing abilities. The two main objectives for this study was to (1) harvest EC from filter-based PM_{10} samples and (2) analyze and apportion EC using ^{14}C abundances. The method of harvesting or isolating EC was accomplished by driving off the organic

carbon (OC) and pyrolytic carbon (PyrC) from the filter sample using the pre-determined split-time and removal of calcium carbonate (CC) by acid fumigation. However, this EC isolation method has many uncertainties, most importantly the potential inclusion of PyrC and CC. A separate CC test identified minimal contribution of CC in the samples. Sensitivity tests were completed to account for potential inclusion of PyrC and carbon contamination from shipping and handling of the harvested EC samples. Results from both sensitivity tests were included in the sample uncertainty calculation.

Results from the San Francisco Bay Area study identified seasonal variations across all sites where carbonaceous aerosol concentrations were greater during the winter compared to the non-winter. For several of these sites, the enhancement of aerosols in the winter were driven my meteorological conditions (e.g. temperature inversion) rather than changes in emissions. The seasonal differences observed at San Francisco, the most urban site, was likely due to meteorological conditions rather than changes in emissions as fossil carbon contribution for EC and total organic carbon (TOC; OC+EC) were similar during winter (62% and 48%, respectively) and non-winter (68% and 48%, respectively) season. However, in Napa the enhancement in the winter season was likely due to increased agricultural and biomass burning (e.g. wood smoke) activities rather than meteorological influences as there was a significant difference in contemporary carbon contribution for EC and TOC during the winter (63% and 78%, respectively) and non-winter (43% and 59%, respectively) season.

This dissertation work identified major source contribution of carbonaceous aerosols at each site. Of the seven sites, the most distinctive were Napa and San Francisco where both sites had the largest aerosol concentrations but continuously proved

to be at two extremes: Napa with significant contribution of contemporary emissions while San Francisco was mainly from fossil fuel emissions for both seasons. Bethel Island, which was the smallest city amongst the sampling sites had a relatively large TOC concentration during the winter especially as local emissions were expected to be small. The enhanced concentration at Bethel Island is likely from long-range transport of emissions from the Central Valley, the most productive agricultural region in California. Based on the study's findings, site specific regulations for certain cities like Napa and San Francisco will be most effective in reducing EC emissions.

The results from the source apportioned EC (CMB-EC and ^{14}C-EC) was compared to BC emissions inventory data. The BC emissions inventories included one from California Air Resource Board and another from the Bay Area Air Quality Management District. Both emissions inventories over estimated diesel contribution but underestimated wood smoke and cooking (i.e. biomass burning) contribution. The differences observed between the EI and observation-based receptor method is partially due to differences in methodology of the bottom-up (i.e. EI models) and top-down (receptor-based) approaches.

Houston Metropolitan Area

Houston is an ideal location to study secondary processes as the metropolitan area has a myriad of fossil fuel and contemporary sources all within a highly oxidizing urban atmosphere. Aside from the different organic aerosol emissions, meteorological conditions were an important factor when determining air quality in Houston. For this reason, the source apportioned data was coupled with wind speed, wind direction and HYSPLIT back trajectory data.

Strong diurnal trends of enhanced primary OC, EC and BC concentrations were observed in the morning followed by increased secondary processing of aerosols in the day and nighttime periods. The increase of carbonaceous aerosols in the morning was due to a combination of increased motor vehicle exhaust (MVE) emissions and a lower boundary layer. These increased EC concentrations in the morning periods was driven by fine rather than coarse EC, consistent with MVE exhaust EC emissions. Interestingly, large concentration of coarse EC was measured at the urban Houston site. Coarse EC is produced from less efficient/older industrial combustion processes or agricultural burning. Higher concentrations of coarse EC have been measured in developing countries rather than European and U.S. cities. A likely source of coarse EC measured at the urban Houston site is likely from industrial processes (e.g. coke ovens) near the Houston Ship Channel.

Two weeks of interest were identified based on the bulk carbon and ozone measurement: September 8 – 15 (week 2) and Sept 21 – 25 (week 4). These weeks observed multi day increases in TOC with low ozone concentration (week 2) and multi-day increases in TOC with high ozone concentrations (week 4). During these two weeks, the increase in OC was driven in the fine rather than coarse fraction and the OC to EC ratio (OC/EC) was also significantly larger than other sampling days, both indicative of increased secondary processes. The day $PM_{2.5}$ filter samples collected during weeks 2 and 4 were further speciated and utilized in ^{14}C+CMB source apportionment. Results from this combined model distinguished contributions of TOC to its primary (i.e. MVE, wood smoke and vegetative detritus) and secondary (i.e. secondary fossil and biogenic sources) sources.

In Houston, the MVE was the greatest contributor of primary sources while there was minimal contribution from wood smoke and vegetative detritus at both sites. The Houston metropolitan area was highly impacted by SOA with largest contribution from contemporary sources. Contribution of biogenic SOC was significant and consistent throughout the two weeks and at both sites, ranging from 48 to 81% of TOC. Fossil SOC was highly variable but was enhanced at all sites during periods of poor air quality. The largest contribution of fossil SOC was at the urban Houston site during week 4: the week with highest ozone concentrations. The fossil SOC had the greatest association with daily maximum 8 h average ozone concentration with largest concentration of both fossil SOC and ozone on Sept. 25. Aside from emission sources, the bay breeze phenomenon was an important factor for poor air quality on Sept. 25 where it created favorable conditions for aerosol and ozone formation. Based on the HYSPLIT back trajectory data, the initially strong onshore marine winds shifted to combination of weaker continental and onshore marine winds starting week 4. On Sept. 25, the varying wind directions and slower wind speeds created stagnant atmospheric conditions allowing for buildup of pollutants concentration over Houston.

Future Work

Based on our findings, SOA is a significant contributor to carbonaceous aerosols in the Houston metropolitan area. Analysis of SOA was completed by ^{14}C and CMB analysis apportioning SOC either as contemporary or fossil carbon. Additional analysis including OC to EC ratio and OC size distribution were utilized to identify periods of enhanced secondary processes. Even so, continual work for better speciation of the SOA fraction and methods for source apportionment is needed, especially fossil SOA where

increased fossil SOA coincided with periods of high PM and ozone concentration. Based on air mass transport analysis and previous studies, this fossil SOC was assumed to be from point sources in the HSC. Further studies including volatile organic carbon (VOC) and aerosol measurement near the HSC and downwind sites in Houston city and further downwind to suburban/exurb sites will provide a more complete understanding of the SOA formation processes in the Houston metropolitan area. Aside for photooxidation processes, nighttime oxidation was also important in this region, however, only daytime samples were analyzed for the ^{14}C+CMB source apportionment. Future studies providing extensive analysis and characterization of nighttime samples from the Houston metropolitan area is highly recommended. Additionally, further study of the coarse EC and its potential sources would also be of interest. Lastly, additional meteorological conditions including boundary layer heights would also be beneficial to better understand their impacts to the resultant air quality.

The San Francisco Bay Area study provided source apportioned EC and TOC for composited winter and non-winter samples. Results identified varying contribution of fossil and contemporary/biomass burning sources by site. Instead of composited seasonal samples, this study will benefit to analyze carbonaceous aerosols from higher frequency samples (e.g. day and night). Like the Houston study, a combined ^{14}C and organic tracer-based source apportionment analysis will provide better insight into major OA sources and will distinguish aerosol contributions from primary and secondary sources. Identifying more specific sources at sites like Napa and San Francisco would be beneficial for regulation purposes as carbonaceous aerosols at these sites had significant contribution from either biomass burning or fossil sources year round. Inclusion of

meteorological data including wind direction, wind speed, humidity, boundary layer heights, etc. would also be beneficial in further understanding their impact on aerosol chemistry/formation, improving the ability to identify the major drivers for poor air quality in complex urban coastal regions.

APPENDICES

APPENDIX A

Supplemental Information for "Biomass and Fossil Fuel Combustion Contributions to Elemental Carbon across the San Francisco Bay Area"

^{14}C of Organic Carbon

The ^{14}C measurement of organic carbon (OC) is an estimate based on results from ^{14}C of total organic carbon(TOC) and elemental carbon(EC) analysis. Using a mass-balance approach, the fraction modern (F_M) of OC, $F_{M\ of\ OC}$ was estimated by the following equation:

$$F_{M\ of\ OC} = \frac{\left(M_{TOC} * F_{M\ of\ TOC}\right) - \left(M_{EC} * F_{M\ of\ EC}\right)}{\left(M_{TOC} - M_{EC}\right)}$$

using F_M values of EC and TOC samples from ^{14}C results and M_{TOC} and M_{EC} which are the mass concentrations of TOC and EC.

Table A.1.: Sampler and Sampling Site Description

Site	Latitude and Longitude	Sampler Location	County	Statistical Area	Sampler Type	Ground Cover
Bethel Island	38.006311, 121.641918	Trailer in parking lot.	Contra Costa	San Francisco-Oakland-Fremont	Andersen GUV-16HBLA	Gravel surrounded by grassy fields
Concord	37.936013, 122.026154	One-story commercial building.	Contra Costa	San Francisco-Oakland-Fremont	Andersen HiVol 1200	Paved
San Pablo	37.960400, 122.356811	One-story commercial building	Contra Costa	San Francisco-Oakland-Fremont	Tisch Env. HiVol TE-60	Paved
San Rafael	37.972310, 122.520004	Second floor of two-story commercial building	Marin	San Francisco-Oakland-Fremont	Andersen HiVol 1200	Paved
San Francisco	37.765946, 122.399044	One-story commercial building	San Francisco	San Francisco-Oakland-Fremont	Andersen HiVol 1200	Paved
Napa	38.310942, 122.296189	One-story commercial building	Napa	Napa	Tisch Env. HiVol TE-6000	Paved
Cupertino	37.318435, 122.069705	Trailer in parking lot	Santa Clara	San Jose-Sunnyvale-Santa Clara	Andersen HiVol 1200	Paved

Table A.2: Sample Composite Description

Date	Day of Week	Composite Type
November 11, 2011	Friday	
December 5, 2011	Monday	
December 23, 2011	Friday	
January 4, 2012	Wednesday	Winter Samples
January 22, 2012	Sunday	
February 9, 2012	Thursday	
February 21, 2012	Tuesday	
March 22, 2012	Thursday	
April 21, 2012	Saturday	
May 9, 2012	Wednesday	
June 26, 2012	Tuesday	Non-Winter Samples
July 8, 2012	Sunday	
August 13, 2012	Monday	
October 12, 2012	Friday	

Composites from each site (BI, Con, SP, SR, SF, Nap, Cup) for both EC and TOC samples included 24hr TSP samples for the above dates

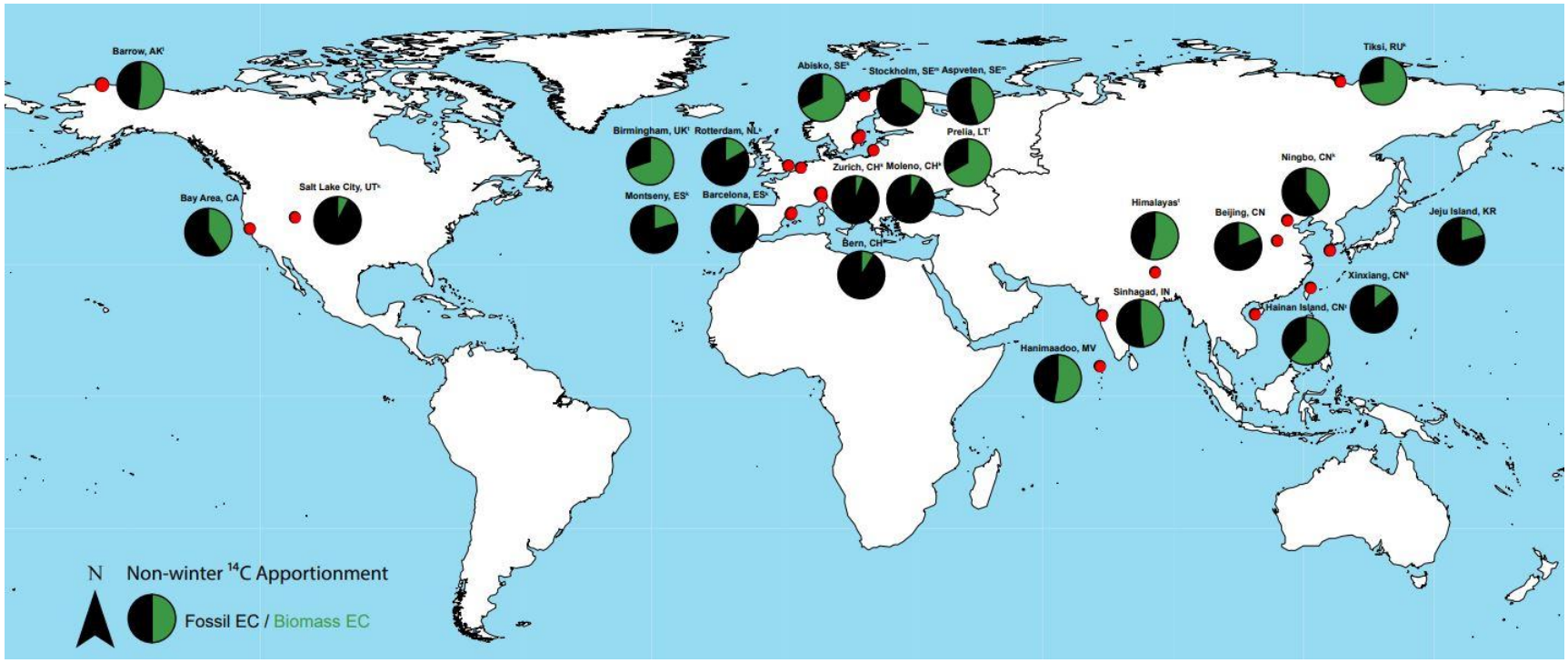

Figure A.1.: Global map of biomass burning and fossil fuel contribution of non-winter EC/BC values from radiocarbon-based source apportionment studies. The studies included in the figure have reported average non-winter values. [k] summer season [l] spring or late winter season [m] autumn season [t] annual. Table 2.2 includes all references.

APPENDIX B

Supplemental Information for "Fine and Coarse Carbonaceous Aerosol in Houston, TX during DISCOVER-AQ"

B.1. Detailed Calculation for BC Correction

Based on Schmid et al. (Schmid et al., 2006) absorption coefficient correction (equation 1), calculation for light scattering (*C*) (Schmid et al., 2006) and shadowing effect (R(ATN) (Weingartner et al., 2003) are needed:

$$\mathrm{R(ATN)} = \left(\frac{1}{f} - 1\right)\left(\frac{\ln ATN - \ln 10}{\ln 50 - \ln 10}\right) + 1, \quad \text{(B.1.)}$$

$$\frac{C}{C_{ref}} = \frac{\lambda^{A\ln(\lambda/\mathrm{nm})+B}}{\lambda_{ref}{}^{A\ln(\lambda\mathrm{ref/nm})+B}}, \quad \text{(B.2.)}$$

The shadowing effect is negligible when the ATN < 10. The correction was made only when ATN > 10. For the equation B.1., the *f* shadowing factor is devised by the linear fit equation for the attenuation of pure internally and externally mixed diesel soot:

$$f = a\,(1 - \omega_0) + 1, \quad \text{(B.3.)}$$

where the ω_0 is the single scattering albedo (SSA). An SSA value of 0.80 was used for the correction. This 0.80 value was an averaged SSA value based on measurements made at several sites across the Houston metropolitan area (Massoli et al., 2009).

The light scattering correction, *C* value (equation B.2.), is normalized to the C_{ref} value, at wavelength 552 nm, which is determined by the following equation:

$$C_{ref} = C^* + m_s \frac{\omega_O}{1 - \omega_O}, \quad \text{(B.4.)}$$

where $C^* = C_{532} = 2.1$ for pure or externally mixed soot (Schmid et al., 2006) and m_s is non-negligible aerosol scattering correction factor. The m_s is a relationship factor to directly compare C and C^* which is 0.0523 (Arnott et al., 2003).

The values for *A* and *B* for equation B.2. are derived using a quadratic fit of *A* and *B* with respect to the absorption Angstrom exponent (α), and given by:

$$A = 0.102\ \alpha_a^2 - 0.187\ \alpha_a - 0.141, \quad \text{(B.5.)}$$

$$B = -1.275\ \alpha_a^2 + 2.564\ \alpha_a + 1.827, \quad \text{(B.6.)}$$

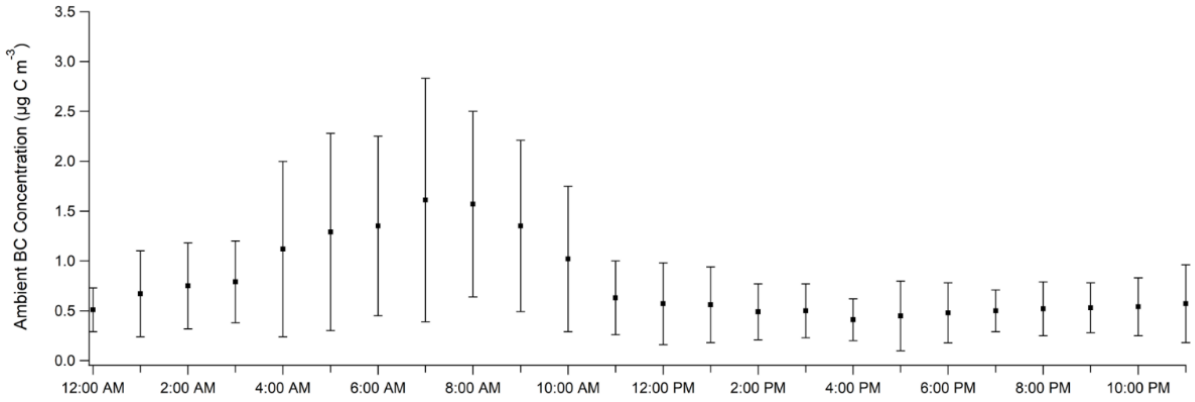

Figure B.1. Hourly averaged ambient BC concentration including 1 standard deviation error bars.

Table B.1. Bulk carbon including OC and EC (and respectively uncertainty) ambient concentration for all $PM_{2.5}$ and TSP samples from MT. Each sample is identified by the sample date (YYMMDD) followed by the sampling period which includes morning (M), afternoon (A), day (D), night (N) and 24 h samples.

Sample Type	Sample (YYMMDD_ period)	OC (µg m^{-3})	OC unc (µg m^{-3})	EC (µg m^{-3})	EC unc (µg m^{-3})
$PM_{2.5}$	130904_M	1.43	0.44	0.67	0.34
	130904_A	2.89	0.27	0.34	0.12
	130904_N	2.38	0.24	0.47	0.12
	130905_M	6.90	0.71	1.94	0.40
	130906_24h	3.38	0.27	0.59	0.11
	130907_24h	3.43	0.27	0.64	0.12
	130908_D	1.77	0.18	0.38	0.10
	130908_24h	1.51	0.18	0.27	0.10
	130909_D	2.95	0.24	0.44	0.10
	130909_24h	2.65	0.23	0.36	0.10
	130910_D	3.77	0.28	0.56	0.11
	130910_24h	3.36	0.27	0.48	0.11
	130911_D	3.49	0.27	0.37	0.10

	130911_24h	3.62	0.28	0.46	0.11
	130912_D	3.56	0.27	0.49	0.10
	130912_24h	2.79	0.24	0.52	0.11
	130913_D	5.18	0.35	0.86	0.12
	130913_24h	4.59	0.33	0.72	0.12
	130914_D	5.88	0.39	0.44	0.10
	130914_24h	5.78	0.39	0.39	0.10
	130915_D	3.41	0.27	0.44	0.10
	130915_24h	2.43	0.23	0.31	0.10
	130916_D	1.92	0.19	0.53	0.10
	130916_24h	2.22	0.21	0.54	0.11
	130917_M	3.47	0.49	1.25	0.33
	130917_A	1.62	0.21	0.24	0.12
	130917_24h	2.11	0.21	0.58	0.11
	130918_D	2.38	0.21	0.56	0.10
	130918_24h	1.56	0.18	0.39	0.10
	130919_M	3.34	0.49	1.36	0.33
	130919_A	1.68	0.22	0.43	0.13
	130919_24h	1.23	0.16	0.69	0.12
	130920_D	0.79	0.13	0.33	0.09
	130920_24h	0.79	0.14	0.32	0.10
	130921_D	2.34	0.21	0.15	0.08
	130921_24h	3.27	0.27	0.16	0.09
	130922_D	3.75	0.28	0.17	0.08
	130922_24h	3.85	0.30	0.18	0.09
	130923_D	4.81	0.33	0.43	0.10
	130923_24h	5.13	0.36	0.42	0.11
	130924_D	5.38	0.36	0.47	0.10
	130924_24h	7.06	0.46	0.75	0.12
	130925_D	6.94	0.44	0.71	0.11
	130925_24h	6.41	0.42	0.51	0.11
	130926_D	3.93	0.29	0.31	0.09
	130926_24h	4.63	0.33	0.35	0.10
	130927_D	3.03	0.24	0.31	0.09
	130927_24h	3.02	0.25	0.29	0.10
	130928_D	2.10	0.20	0.19	0.09
	130928_24h	2.04	0.20	0.24	0.09
TSP	130904_M	5.60	0.64	0.97	0.38
	130904_A	6.57	0.45	0.76	0.15
	130904_N	5.37	0.39	0.97	0.16
	130905_M	15.98	1.14	2.32	0.44
	130905_N	4.43	0.34	0.80	0.15
	130906_N	2.84	0.26	0.73	0.15
	130907_D	6.78	0.43	1.03	0.14
	130907_N	7.64	0.50	1.02	0.16
	130908_D	4.55	0.32	0.48	0.11
	130908_N	3.10	0.27	0.62	0.14
	130909_D	6.71	0.43	1.08	0.14
	130909_N	4.97	0.36	0.71	0.14
	130910_D	5.84	0.38	1.07	0.14
	130910_N	5.55	0.39	0.86	0.15
	130911_D	7.69	0.48	1.10	0.14
	130911_N	6.39	0.46	1.34	0.20
	130912_D	8.52	0.52	1.40	0.16
	130913_M	14.98	1.05	3.49	0.46
	130913_A	10.69	0.78	0.83	0.28
	130914_D	10.92	0.64	1.31	0.15
	130914_N	8.06	0.53	0.80	0.16
	130915_D	6.13	0.40	0.91	0.13

130915_N	2.62	0.25	0.22	0.12
130916_M	10.35	0.82	1.92	0.38
130916_N	4.68	0.35	0.81	0.15
130917_M	11.30	0.88	2.13	0.40
130917_A	3.36	0.29	0.48	0.14
130917_N	5.29	0.39	0.87	0.16
130918_24h	4.12	0.26	0.94	0.10
130919_24h	3.04	0.20	0.89	0.09
130921_D	4.06	0.29	0.19	0.09
130922_D	7.29	0.45	0.25	0.09
130923_D	9.92	0.58	0.92	0.13
130923_N	8.78	0.56	0.87	0.16
130924_D	8.49	0.51	0.77	0.12
130924_N	13.95	0.83	1.33	0.19
130925_D	10.29	0.60	1.03	0.13
130925_N	7.22	0.51	0.90	0.18
130926_D	8.17	0.49	0.91	0.13
130926_N	6.24	0.46	0.67	0.17
130927_D	6.70	0.42	0.93	0.13
130928_D	3.77	0.27	0.59	0.11
130916_N	4.68	0.35	0.81	0.15
130917_M	11.30	0.88	2.13	0.40
130917_A	3.36	0.29	0.48	0.14
130917_N	5.29	0.39	0.87	0.16
130918_24h	4.12	0.26	0.94	0.10
130919_24h	3.04	0.20	0.89	0.09
130921_D	4.06	0.29	0.19	0.09
130922_D	7.29	0.45	0.25	0.09
130923_D	9.92	0.58	0.92	0.13
130923_N	8.78	0.56	0.87	0.16
130924_D	8.49	0.51	0.77	0.12
130924_N	13.95	0.83	1.33	0.19
130925_D	10.29	0.60	1.03	0.13
130925_N	7.22	0.51	0.90	0.18
130926_D	8.17	0.49	0.91	0.13
130926_N	6.24	0.46	0.67	0.17
130927_D	6.70	0.42	0.93	0.13
130928_D	3.77	0.27	0.59	0.11

Table B.2. Contemporary and fossil carbon (and respective uncertainty) ambient concentration of TOC from ^{14}C analysis and its uncertainty for all $PM_{2.5}$ and TSP samples from MT. Samples from Moody Tower (MT) and La Porte (LP) are included. Each sample is identified by the sample date (YYMMDD) followed by the sampling period which includes day (D), night (N) and 24 h samples.

Site - Sample Type	Sample (YYMMDD_ period)	Contemporary Carbon (µg m^{-3})	Contemporary Carbon unc (µg m^{-3})	Fossil Carbon (µg m^{-3})	Fossil Carbon unc (µg m^{-3})
MT-$PM_{2.5}$	130921_D	1.95	0.24	0.54	0.24
	130922_D	2.30	0.15	1.61	0.15
	130923_D	2.90	0.19	2.33	0.19
	130923_24h	3.38	0.23	2.18	0.23
	130924_D	4.11	0.29	1.75	0.29
	130924_24h	5.09	0.32	2.72	0.32
	130925_D	4.20	0.26	3.45	0.26
	130925_24h	4.14	0.27	2.77	0.27
	130926_D	2.80	0.21	1.45	0.21

	130926_24h	3.32	0.25	1.66	0.25
	130927_D	1.61	0.11	1.72	0.11
	130928_D	1.34	0.12	0.96	0.12
	130925_24h	4.14	0.27	2.77	0.27
	130926_D	2.80	0.21	1.45	0.21
	130926_24h	3.32	0.25	1.66	0.25
	130927_D	1.61	0.11	1.72	0.11
	130928_D	1.34	0.12	0.96	0.12
MT-TSP	130923_D	5.54	0.34	5.30	0.34
	130923_N	6.06	0.35	3.60	0.35
	130924_D	5.69	0.33	3.57	0.33
	130924_N	8.67	0.52	6.61	0.52
	130925_D	6.02	0.36	5.31	0.36
	130925_N	5.25	0.31	2.87	0.31
LP-TSP	130921_24h	6.41	0.36	1.35	0.36
	130922_24h	8.45	0.47	1.76	0.47
	130923_24h	5.64	0.33	3.08	0.33
	130924_24h	8.44	0.49	4.13	0.49
	130925_24h	8.41	0.51	8.01	0.51
	130926_24h	5.01	0.30	3.90	0.30

Table B.3. Hourly-averaged ambient BC concentration during sampling period. Dates are formatted as YYMMDD.

	Date						
Time	130903	130904	130905	130906	130907	130908	130909
0:00	0.39	0.66	0.79	0.58	0.86	0.95	0.40
1:00	0.19	0.60	0.64	1.66	1.09	1.99	0.87
2:00	0.26	0.57	1.30	1.35	1.27	1.33	0.86
3:00	0.21	0.98	1.51	0.80	0.82	1.26	0.59
4:00	0.24	0.68	1.58	1.30	1.35	1.03	0.66
5:00	0.39	0.59	3.29	2.87	1.66	1.30	1.08
6:00	0.81	0.78	2.62	3.87	1.62	1.37	0.77
7:00	0.62	0.93	3.31	5.30	2.62	1.25	2.50
8:00	0.62	1.51	2.44	2.72	2.94	0.94	3.28
9:00	0.57	1.67	1.59	1.48	2.15	0.78	2.40
10:00	0.60	0.71	0.98	1.71	0.38	0.86	0.59
11:00	0.66	1.58	0.94	0.53	1.02	0.39	0.37
12:00	0.35	1.98	1.38	1.13	0.50	0.18	0.47
13:00	0.53	0.78	0.83	1.45	0.89	0.27	0.47
14:00	0.38	0.65	0.76	1.41	0.41	0.36	0.40
15:00	0.41	0.59	0.98	0.75	0.73	0.30	0.65
16:00	0.41	0.37	1.06	0.23	0.83	0.25	0.42
17:00	0.30	0.51	0.69	0.34	0.95	0.23	0.59
18:00	0.27	0.75	0.43	0.35	0.43	0.48	0.78
19:00	0.32	0.42	0.40	0.32	0.57	0.45	0.41
20:00	0.34	0.44	0.37	0.48	0.66	0.61	1.01
21:00	0.24	0.64	0.42	0.51	0.84	0.36	0.68
22:00	0.49	0.66	0.51	0.77	0.63	0.55	0.29
23:00	0.52	0.57	0.49	1.96	0.87	1.22	0.44
	Date						
Time	130910	130911	130912	130913	130914	130915	130916
0:00	0.49	0.51	0.42	0.31	0.62	0.65	0.68
1:00	0.33	0.56	0.65	0.59	0.82	0.96	0.64
2:00	0.37	0.54	0.65	0.90	0.63	1.61	0.49
3:00	0.67	1.48	1.38	0.64	0.92	1.11	0.73

4:00	1.23	2.18	2.96	2.34	3.03	1.00	0.86
5:00	1.91	1.36	3.04	2.14	2.25	0.95	0.99
6:00	2.49	1.34	2.09	2.65	2.04	1.74	1.05
7:00	3.47	2.01	1.94	3.39	1.97	2.40	1.58
8:00	2.45	1.78	1.48	3.30	0.97	2.51	1.61
9:00	3.02	1.81	1.13	2.54	1.02	2.49	1.46
10:00	2.75	1.37	0.90	1.37	0.77	1.37	1.74
11:00	0.52	0.61	0.58	1.00	0.90	0.40	1.25
12:00	0.52	0.59	0.50	0.47	0.91	0.29	1.15
13:00	1.16	0.65	0.41	0.31	0.99	0.21	1.67
14:00	0.68	0.47	0.36	0.41	0.61	0.31	1.29
15:00	0.51	0.60	0.37	0.49	0.70	0.32	1.44
16:00	0.47	0.58	0.45	0.49	0.69	0.29	0.61
17:00	0.36	0.53	0.26	0.41	0.62	0.31	1.99
18:00	0.33	0.44	0.28	0.36	0.64	0.34	1.78
19:00	0.43	0.43	0.44	0.47	0.96	1.28	0.72
20:00	0.41	0.29	0.45	0.42	1.07	0.25	0.68
21:00	0.51	0.35	0.52	0.42	0.48	0.38	0.83
22:00	1.55	0.60	0.48	0.45	0.50	0.32	0.84
23:00	0.52	0.51	0.40	0.47	0.50	0.64	0.54

	Date						
Time	130917	130918	130919	130920	130921	130922	130923
0:00	0.48	0.51	0.14	0.26	0.37	0.41	0.34
1:00	0.43	0.43	0.21	1.06	0.30	0.50	0.38
2:00	1.81	0.56	0.21	0.89	0.32	0.41	0.35
3:00	1.56	1.37	0.23	0.78	0.22	0.58	0.26
4:00	1.86	2.68	0.19	1.91	0.30	0.22	0.30
5:00	1.34	3.31	0.67	2.29	0.20	0.15	0.35
6:00	1.96	2.28	1.14	1.56	0.28	0.19	0.49
7:00	1.81	1.70	1.24	0.23	0.26	0.25	0.71
8:00	2.90	1.46	1.71	1.32	0.37	0.30	0.88
9:00	3.37	1.56	1.74	0.45	0.39	0.24	0.83
10:00	3.37	0.86	1.14	0.44	0.47	0.23	0.96
11:00	0.50	0.42	0.56	0.28	0.28	0.22	0.84
12:00	0.23	0.41	0.24	0.20	0.37	0.18	0.75
13:00	0.24	0.34	0.33	0.21	0.30	0.22	0.74
14:00	0.26	0.45	0.49	0.22	0.29	0.13	0.41
15:00	0.29	0.30	0.58	0.16	0.33	0.14	0.58
16:00	0.30	0.15	0.28	0.10	0.32	0.10	0.51
17:00	0.29	0.16	0.33	0.16	0.26	0.13	0.54
18:00	0.26	0.18	0.60	0.29	0.36	0.22	0.62
19:00	0.40	0.21	0.55	0.35	0.50	0.51	0.64
20:00	0.53	0.21	1.05	0.41	0.48	0.31	0.82
21:00	0.51	0.17	0.70	0.32	0.20	0.41	0.81
22:00	0.55	0.27	0.33	0.27	0.40	0.41	0.63
23:00	0.71	0.15	0.13	0.23	0.25	0.42	0.48

	Date						
Time	130924	130925	130926	130927	130928	130929	130930
0:00	0.35	1.14	0.46	0.47	0.40	0.39	0.39
1:00	0.42	1.31	0.56	0.75	0.41	0.23	0.23
2:00	0.63	1.09	0.49	0.65	0.39	0.55	0.55
3:00	0.57	0.80	0.47	0.75	0.35	0.50	0.50
4:00	0.64	0.85	0.43	0.68	0.30	0.28	0.28
5:00	0.74	0.64	0.45	1.02	0.63	0.23	0.23
6:00	0.68	1.01	0.74	0.87	0.81	0.23	0.23
7:00	0.88	1.30	0.55	1.51	1.01	0.21	0.21
8:00	1.12	1.77	0.95	1.22	0.86	0.24	0.24
9:00	1.40	1.26	0.77	0.77	0.40	0.28	0.28
10:00	1.30	1.42	0.80	0.59	0.39	0.19	0.19

11:00	0.82	1.38	0.36	0.55	0.24	0.23	0.23
12:00	0.46	0.86	0.40	0.52	0.44	0.27	0.27
13:00	0.39	0.42	0.22	0.50	0.31	0.38	0.38
14:00	0.45	0.43	0.28	0.50	0.63	0.33	0.33
15:00	0.29	0.38	0.40	0.60	0.48	0.32	0.32
16:00	0.26	0.37	0.30	0.57	0.42	0.32	0.32
17:00	0.25	0.37	0.25	0.40	0.34	0.53	0.53
18:00	0.34	0.59	0.31	0.44	0.58	0.54	0.54
19:00	0.60	0.50	0.39	0.37	0.51	0.43	0.43
20:00	1.18	0.32	0.43	0.42	0.47	0.30	0.30
21:00	1.38	0.87	0.38	0.40	0.68	0.46	0.46
22:00	1.18	0.81	0.36	0.41	0.36	0.30	0.30
23:00	1.45	0.48	0.56	0.47	0.37	0.34	0.34

References

Arnott, W., Moosmüller, H., Sheridan, P., Ogren, J., Raspet, R., Slaton, W., Hand, J., Kreidenweis, S., Collett Jr, J., 2003. Photoacoustic and filter-based ambient aerosol light absorption measurements: Instrument comparisons and the role of relative humidity. J. Geophys. Res. Atmos. 108, AAC 15-11-AAC 15-11.

Massoli, P., Bates, T., Quinn, P., Lack, D., Baynard, T., Lerner, B., Tucker, S., Brioude, J., Stohl, A., Williams, E., 2009. Aerosol optical and hygroscopic properties during TexAQS-GoMACCS 2006 and their impact on aerosol direct radiative forcing. J. Geophys. Res. Atmos. 114.

Schmid, O., Artaxo, P., Arnott, W., Chand, D., Gatti, L.V., Frank, G., Hoffer, A., Schnaiter, M., Andreae, M., 2006. Spectral light absorption by ambient aerosols influenced by biomass burning in the Amazon Basin. I: Comparison and field calibration of absorption measurement techniques. Atmos. Chem. Phys. 6, 3443-3462.

Weingartner, E., Saathoff, H., Schnaiter, M., Streit, N., Bitnar, B., Baltensperger, U., 2003. Absorption of light by soot particles: determination of the absorption coefficient by means of aethalometers. J. Aerosol Sci. 34, 1445-1463.

APPENDIX C

Supplemental Data for "Apportioned Primary and Secondary Organic Aerosol during Pollution Events of DISCOVER-AQ Houston"

S1. PMF Methodology for PM_1 (HR-ToF-AMS)

The analysis discussed here focused of measurements during the late week of September 2013, due to the elevated OA concentrations Positive matrix factorization is a bilinear unmixing model that assumes that the fitted HR-ToF-AMS time series (with *i* number of mass spectra (MS) measured at each time step) is a linear combination of *p* number of factors that have constant mass spectral profiles but varying relative contributions to the total fitted MS signal (Ulbrich et al., 2009). The assumption of constant MS (with time) is key to this technique. The PMF model is explained by:

$$x_{ij} = \sum_p g_{ip} f_{pj} + e_{ij} \qquad \text{(a)}$$

where *i* and *j* refer to indices of rows (time stamps) and columns (mass-to-charge ratios (m/z) of fragments fitted and chosen for PMF analysis) respectively; *p* refers to total number of factors in each solution; x_{ij} is an element of the *m x n* matrix *X*; and matrix *X* consists of the *m x n* (*m* = m/z fitted in each MS; *n* = number of MS collected) data elements to be fit by PMF. The data matrix *X* here can be modeled as the sum of f_{ip} (an element of the mass contribution *p x n* matrix *F* for each factor) multiplied by g_{pj} (an element of the factor time series *m x p* matrix *G*), plus e_{ij} (an element of the residual *m x n* matrix *E*; residual refers to the MS signals not fit by the model). PMF also constrains matrices *G* and *F* to be positive because negative MS signals in factor/source profiles do not have real physical meaning. The model iteratively solves for matrices *G* and *F* with a

weighted least-squares algorithm used to minimize Q (quality of fit parameter), as given by:

$$Q = \sum_{i=1}^{m} \sum_{j=1}^{n} (e_{ij}/\sigma_{ij})^2 \qquad \text{(b)}$$

where σ_{ij} is an element of the *m x n* error matrix that corresponds to the 1-sigma estimated signal errors (uncertainties in the HR-ToF-AMS ion count rate) of each element in matrix *X*.

The PMF2 algorithm v.4.2 (Paatero and Tapper, 1994) was used to solve for matrices *G* and *F* assuming different number of factors (p = 1 to 10), while the PMF Evaluation Tool (PET, v2.06b) (Ulbrich et al., 2009) software was utilized for the selection of the optimized solution. An optimized solution entails the selection of the correct number of physically meaningful factors (e.g., factors with distinct time trends that correlate with internal/external tracers) that minimizes $Q/Q_{expected}$, where $Q_{expected}$ is calculated from the degrees of freedom of the data matrix = $mn - p(m+n)$ or ~mn since $mn >> p(m+n)$ in HR-ToF-AMS datasets. Consecutively, different fPeak parameters in the PMF model were chosen for each model run to explore a subset of the rotational ambiguity of the chosen solutions (Paatero and Tapper, 1994; Ulbrich et al., 2009). Selecting a non-zero fPeak parameter imposes distorted positive (fPeak > 0) or negative (fPeak < 0) rotations (or linear transformations) on the solution matrices and increases $Q/Q_{expected}$. A range of fPeak values were tested in PMF2 such that $Q/Q_{expected}$ increases by more than 10%, as recommended by Ulbrich et al. (2009)).

To determine the qualitative uncertainties in the chosen PMF solution, different starting pseudorandom values in the PMF2 algorithm (Paatero, 1997), known as SEED values, were tested to rule out local minima in the optimized solution produced by the

fitting algorithm (integer SEED values tested were 1 to 50). Bootstrapping analysis (Norris et al., 2008) (50 iterations) also was employed to determine quantitatively 1-σ statistical uncertainties in the factor MS and time series (Ulbrich et al., 2009).

The HR dataset obtained from DISCOVER-AQ required additional processing to yield meaningful PMF results. Standard data pre-treatment and weighting procedures were used (Ulbrich et al., 2009; Zhang et al., 2011), and the appropriate diagnostic tools in addition to those mentioned above were used to choose the optimized PMF solution for this particular dataset. Briefly, the data and 1σ error matrices were produced from the PIKA software. A minimum error corresponding to the signal uncertainties from sampling a single ion during one sampling period in the HR-ToF-AMS was calculated using PIKA and applied to the error matrix (Ulbrich et al., 2009). Next, spiky time periods corresponding to bad MS sampling (e.g., due to electronic noise) were removed from these matrices. Certain ions (m/z) were removed or down-weighted from the data and error matrices when low S/N were observed (Ulbrich et al., 2009). As recommended by Paatero and Hopke (2003), ions with S/N < 0.2 were considered bad and were removed entirely, while ions with S/N < 2 but larger than 0.2 were down-weighted by increasing their associated errors in the error matrix by a factor of 2. Several ions (e.g., CO^+) in the HR spectrum were estimated based on proportionality with the CO_2^+ signal using a fragmentation table (Allan et al., 2004) and were down-weighted accordingly to avoid "over-weighting" the errors from the CO_2^+ ion. An error diagnostics tool was used as a supplement to the PIKA software to determine if errors for particular ions were underestimated; these were adjusted accordingly. Finally, by iterating several model runs using PMF, several additional data points in the time series were removed due to extreme

plume events (likely from very fresh local emissions) that were badly under-fit by the model.

Upon PMF analysis of the HR-ToF-AMS data, the resolved OA factors were compared to other co-located external tracer measurements as well as internal tracers (specific species or tracer ions measured by the HR-ToF-AMS). This not only facilitates the identification of distinct factors but also ensures that the resolved factors represent physically real aerosol sources/types. The component MS for each factor have been compared to those from an online database of published studies, as component MS obtained from different locations are fairly similar and have matching characteristics (e.g., HOA factors show high signals of saturated alkane, alkene, and cycloalkane ions).

In addition to being used as external tracers for comparison with OA components, the inorganic species and their fragments from HR-ToF-AMS data have been included in PMF to resolve more components of OA (Sun et al., 2012) because the inorganic portion can be internally mixed with OA and can provide additional information when included in the PMF analysis. In particular, Hao et al. (2014) and Xu et al. (2015) successfully have included the HR-ToF-AMS nitrate (NO_3) signal (with mixed contributions from organic and inorganic forms) into PMF analysis, resolving for certain datasets a nitrate inorganic aerosol (NIA) factor dominated by inorganic NO_3 and simultaneously apportioning the remaining NO_3 into different PMF factors.

In order to utilize PMF as an independent NO_3 source apportionment technique and to improve the characterization of the resolved PMF factors in this study, two sets of HR-ToF-AMS matrices (matrix X_{Org} *and matrix* $X_{Org+NO3}$) were analyzed using the PMF model. The first matrix consists only of organic fragments from m/z 1-120; the PMF

analysis of this matrix will be referred to as PMF_{Org}. On the other hand, the second matrix contains NO_x^+ ions ($NO^+ + NO_2^+$) in addition to the same organic fragments; this PMF analysis will be referred to as $PMF_{Org+NO3}$. Both PMF analyses follow the identical, standard analysis procedures outlined in Zhang et al. (2011).

An optimal 4-factor $PMF_{Org+NO3}$ was derived from a 5-factor solution (P=5), whereby two of the factors (factor 2 and factor 3) were combined using a "mass-weighted combination" method established in Hao et al. (2014):

$$m/z_{combined,\,j} = ((m/z_{factor2,\,j})^2 + (m/z_{factor3,\,j})^2) / (m/z_{factor2,\,j} + m/z_{factor3,\,j}) \qquad (c)$$

The $m/z_{factor,\,j}$ variable in this equation refers to the scaled mass contributions at each m/z (column j) for each factor (combined, factor 2, or factor 3). This approach was chosen because the P=5 solution clearly resolves a new factor – later identified as the important biomass burning OA (BBOA) factor – which was mixed between all other factors in the P=3 and P=4 solutions. The original factors 2 and 3 had MS profiles and time series that indicated they were real and not "split" factors, but they did not correlate consistently with internal/external factors to allow identification as meaningful factors. Upon application of equation c, the combined factor is highly representative of the well established LO-OOA. Other factors identified include HOA and MO-OOA.

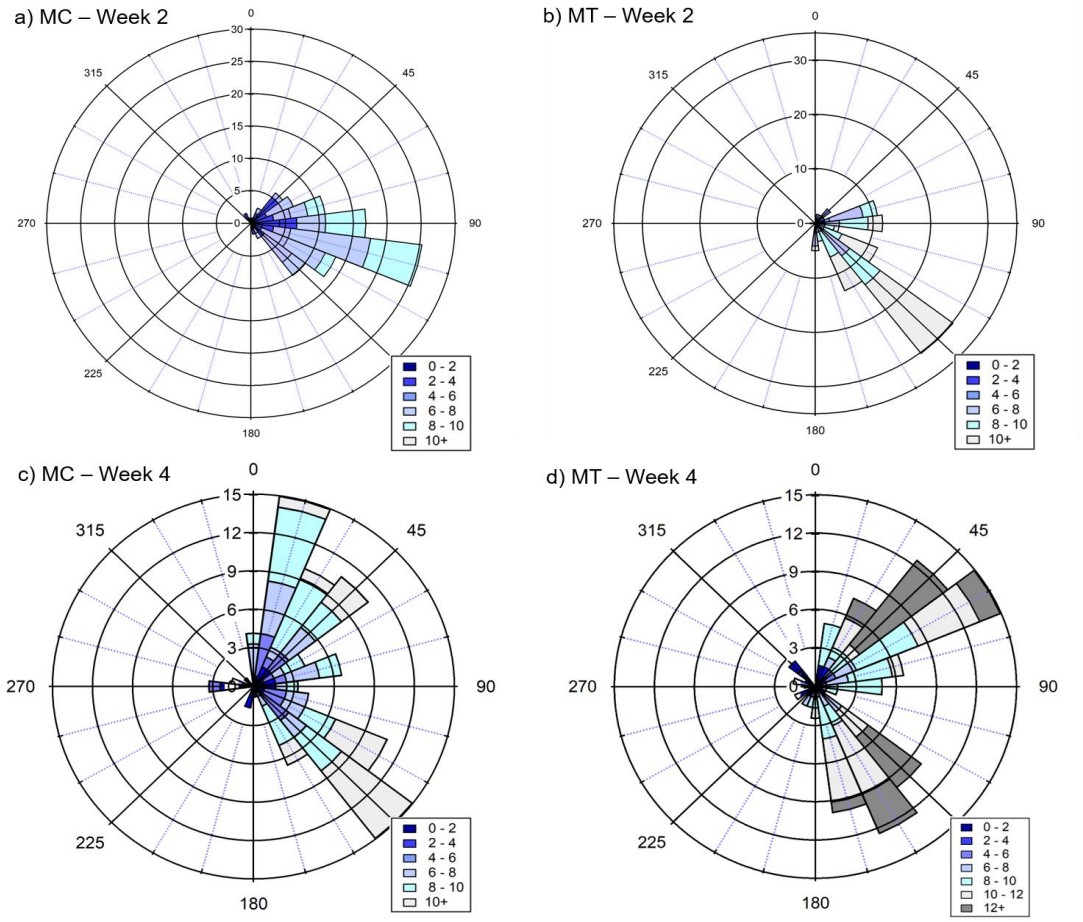

Figure C.7. Wind rose plots of daytime periods during week 2 at a) MC and b) MT, and during week 4 at c) MC and d) MT.

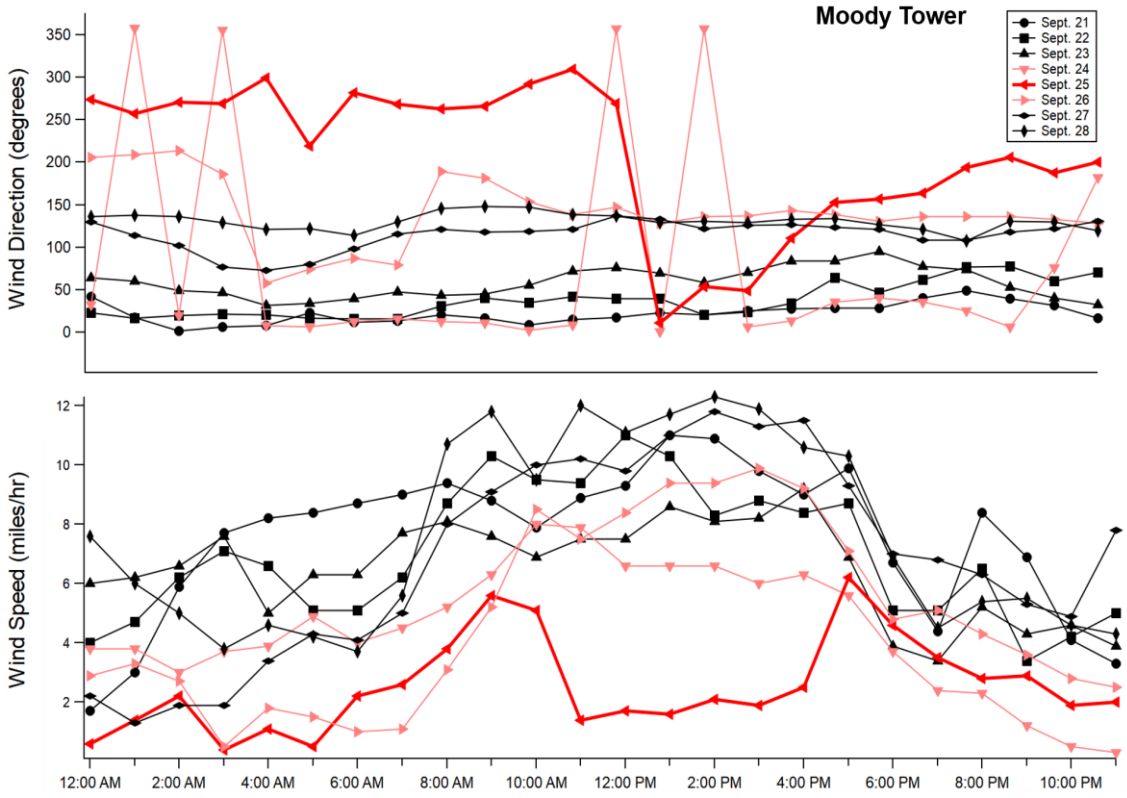

Figure C.8. Wind direction and speed during Week 4 (Sept. 21 to 28) at Moody Tower.

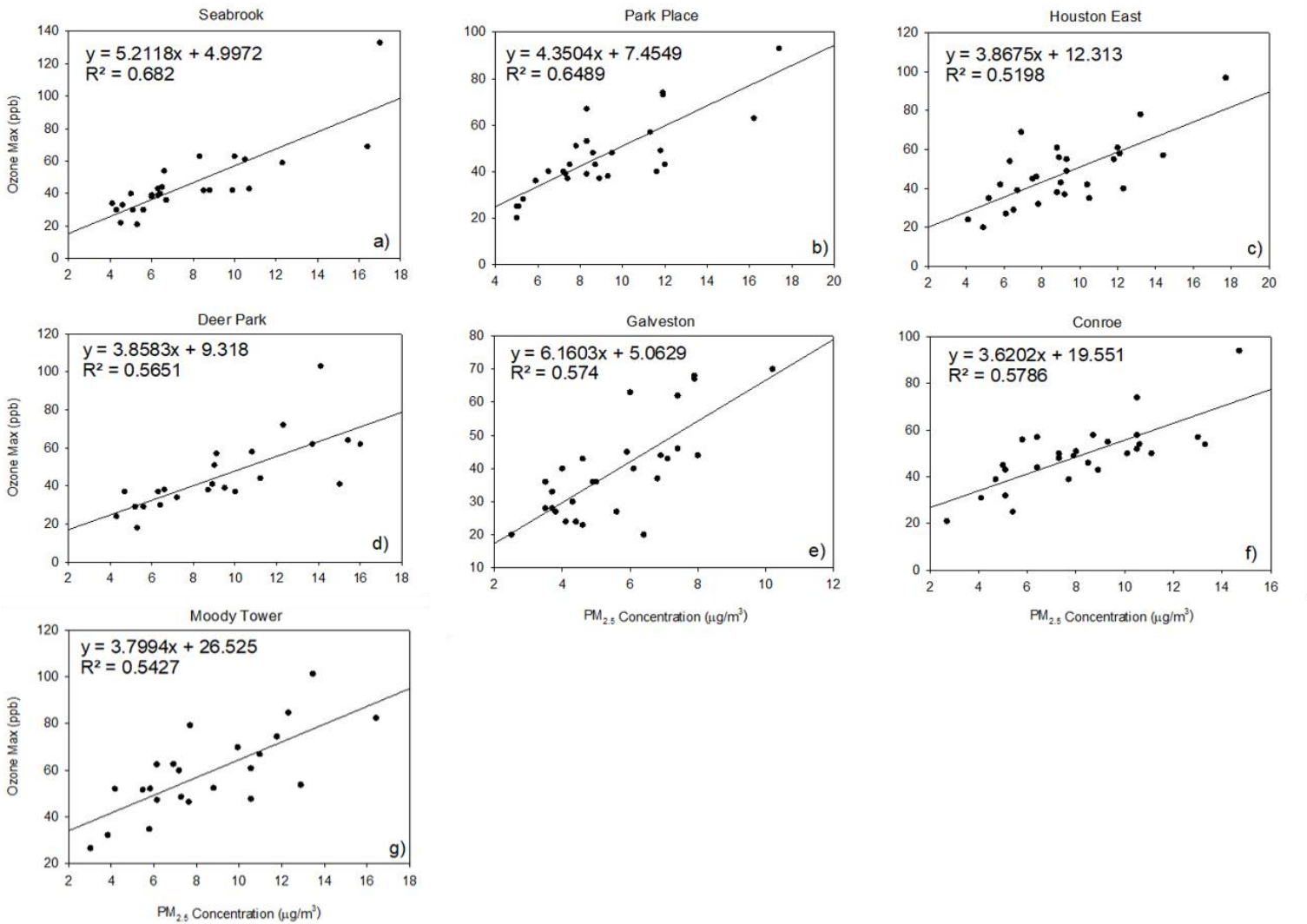

Figure C.3. Comparison of O_3 daily maximum to $PM_{2.5}$ concentration at the CAMS sites (a-g) in September 2013.

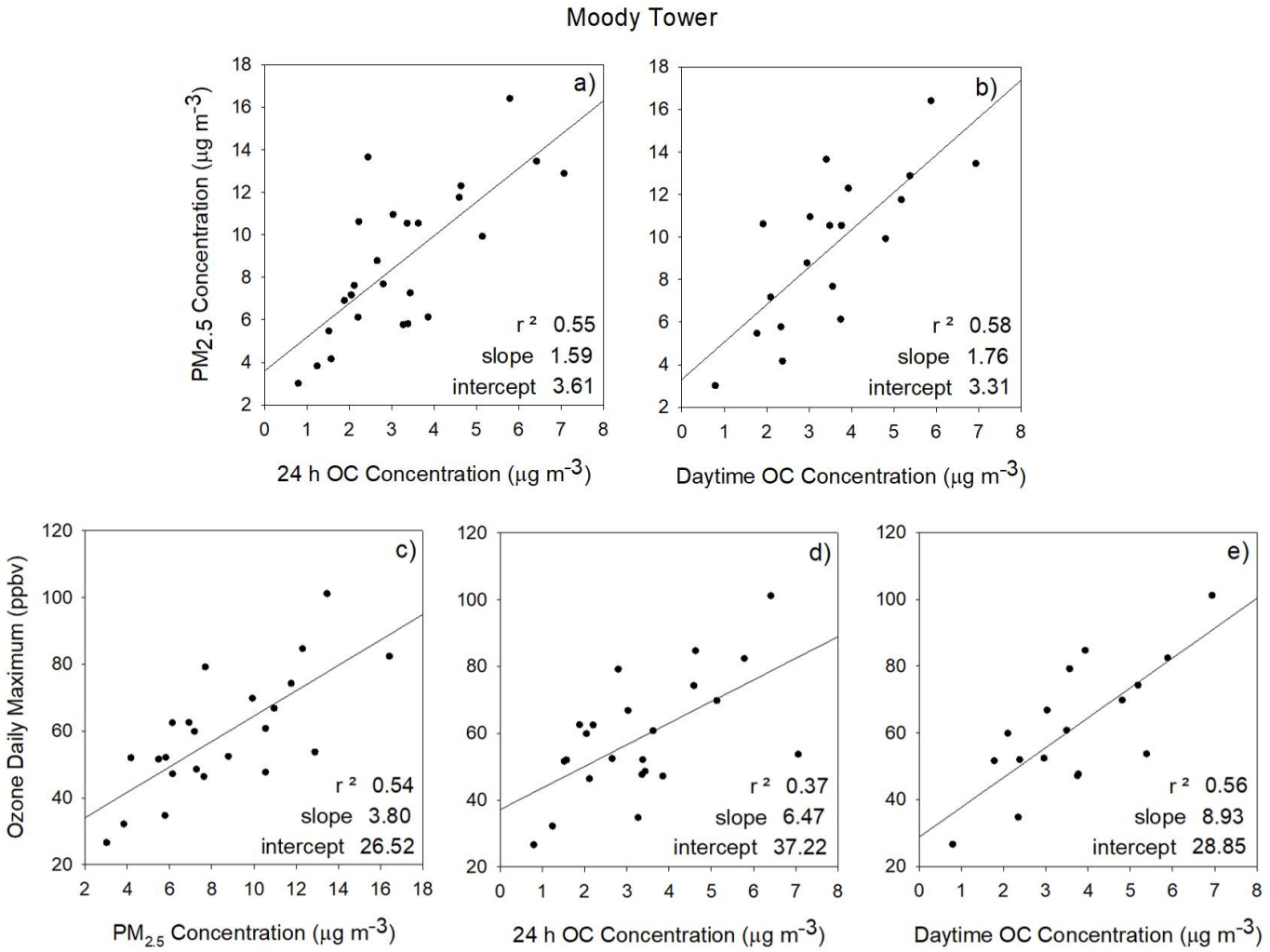

Figure C.4. Comparison of $PM_{2.5}$, organic carbon (OC), and O_3 concentrations at Moody Tower. Comparison of 24-h average $PM_{2.5}$ concentration to a) 24-h and b) daytime OC concentrations. Comparison of ozone daily maximum concentration to c) 24 h average $PM_{2.5}$ concentration, d) OC concentration measured from 24-h filters, and e) daytime OC concentration at Moody Tower

References

Allan, J.D., Delia, A.E., Coe, H., Bower, K.N., Alfarra, M.R., Jimenez, J.L., Middlebrook, A.M., Drewnick, F., Onasch, T.B., Canagaratna, M.R., Jayne, J.T., Worsnop, D.R., 2004. A generalised method for the extraction of chemically resolved mass spectra from Aerodyne aerosol mass spectrometer data. Journal of Aerosol Science 35, 909-922.

Hao, L.Q., Kortelainen, A., Romakkaniemi, S., Portin, H., Jaatinen, A., Leskinen, A., Komppula, M., Miettinen, P., Sueper, D., Pajunoja, A., Smith, J.N., Lehtinen, K.E.J., Worsnop, D.R., Laaksonen, A., Virtanen, A., 2014. Atmospheric submicron aerosol composition and particulate organic nitrate formation in a boreal forestland–urban mixed region. Atmos. Chem. Phys. 14, 13483-13495.

Norris, G., Vedantham, R., Wade, K., Brown, S., Prouty, J., Foley, C., 2008. EPA Positive Matrix Factorization (PMF) 3.0 Fundamentals and User Guide, in: EPA (Ed.).

Paatero, P., 1997. Least squares formulation of robust non-negative factor analysis. Chemometrics and Intelligent Laboratory Systems 37, 23-35.

Paatero, P., Hopke, P.K., 2003. Discarding or downweighting high-noise variables in factor analytic models. Analytica Chimica Acta 490, 277-289.

Paatero, P., Tapper, U., 1994. Positive matrix factorization - a nonnegative factor model with optimal utilization of error-estimates of data values. Environmetrics 5, 111-126.

Sun, Y.L., Zhang, Q., Schwab, J.J., Yang, T., Ng, N.L., Demerjian, K.L., 2012. Factor analysis of combined organic and inorganic aerosol mass spectra from high resolution aerosol mass spectrometer measurements. Atmospheric Chemistry and Physics 12, 8537-8551.

Ulbrich, I.M., Canagaratna, M.R., Zhang, Q., Worsnop, D.R., Jimenez, J.L., 2009. Interpretation of organic components from Positive Matrix Factorization of aerosol mass spectrometric data. Atmospheric Chemistry and Physics 9, 2891-2918.

Xu, L., Suresh, S., Guo, H., Weber, R.J., Ng, N.L., 2015. Aerosol characterization over the southeastern United States using high-resolution aerosol mass spectrometry: spatial and seasonal variation of aerosol composition and sources with a focus on organic nitrates. Atmospheric Chemistry and Physics 15, 7307-7336.

Zhang, Q., Jimenez, J.L., Canagaratna, M.R., Ulbrich, I.M., Ng, N.L., Worsnop, D.R., Sun, Y.L., 2011. Understanding atmospheric organic aerosols via factor analysis of aerosol mass spectrometry: a review. Anal. Bioanal. Chem. 401, 3045-3067.

BIBLIOGRAPHY

2012. 2012 Wildfire Activity Statistics, California Department of Forestry and Fire Protection (CAL FIRE), pp. 20-21.

2015. Houston-Galveston-Brazoria (HGB) PM2.5 Advance Path Forward Update, in: Council, H.-G.A. (Ed.), H-GAC Regional Air Quality Planning Advisory Committee.

2016. CARB Black Carbon Emission Inventory Technical Support Document, California Air Resources Board (CARB).

2019a. Estimates of the Components of Resident Population Change: April 1, 2010 to July 1, 2018. U.S. Census Bureau, Population Division.

2019b. United States Census Burea: QuickFacts Houston city, Texas, United States Census Bureau.

AAPA, 2019. 2018 U.S. Port Rankings by Cargo Tonnage. American Association of Port Authorities.

Allan, J.D., Delia, A.E., Coe, H., Bower, K.N., Alfarra, M.R., Jimenez, J.L., Middlebrook, A.M., Drewnick, F., Onasch, T.B., Canagaratna, M.R., Jayne, J.T., Worsnop, D.R., 2004. A generalised method for the extraction of chemically resolved mass spectra from Aerodyne aerosol mass spectrometer data. Journal of Aerosol Science 35, 909-922.

Allen, D.T., Fraser, M., 2006. An overview of the gulf coast aerosol research and characterization study: The Houston fine particulate matter supersite. Journal of the Air & Waste Management Association 56, 456-466.

Allen, D.T., McDonald-Buller, E.C., McGaughey, G., 2018. State of the Science of Air Quality in Texas: Summary of Scientific Projects and Findings from the Texas Air Quality Research Program (AQRP) 2010-2017, in: Estes, M. (Ed.), Texas Commission on Environmental Quality.

Arnott, W., Moosmüller, H., Sheridan, P., Ogren, J., Raspet, R., Slaton, W., Hand, J., Kreidenweis, S., Collett Jr, J., 2003. Photoacoustic and filter-based ambient aerosol light absorption measurements: Instrument comparisons and the role of relative humidity. J. Geophys. Res. Atmos. 108, AAC 15-11-AAC 15-11.

Bahreini, R., Ervens, B., Middlebrook, A., Warneke, C., De Gouw, J., DeCarlo, P., Jimenez, J., Brock, C., Neuman, J., Ryerson, T., 2009. Organic aerosol formation in urban and industrial plumes near Houston and Dallas, Texas. J. Geophys. Res. Atmos. 114.

Baier, B.C., Brune, W.H., Lefer, B.L., Miller, D.O., Martins, D.K., 2015. Direct ozone production rate measurements and their use in assessing ozone source and receptor regions for Houston in 2013. Atmos. Environ. 114, 83-91.

Banta, R., Senff, C., Nielsen-Gammon, J., Darby, L., Ryerson, T., Alvarez, R., Sandberg, S., Williams, E., Trainer, M., 2005. A bad air day in Houston. Bull. Am. Meteorol. Soc. 86, 657-669.

Banta, R.M., Senff, C.J., Alvarez, R.J., Langford, A.O., Parrish, D.D., Trainer, M.K., Darby, L.S., Hardesty, R.M., Lambeth, B., Neuman, J.A., 2011. Dependence of daily peak O3 concentrations near Houston, Texas on environmental factors: Wind speed, temperature, and boundary-layer depth. Atmos. Environ. 45, 162-173.

Barbero, R., Abatzoglou, J., Larkin, N., Kolden, C., Stocks, B., 2015. Climate change presents increased potential for very large fires in the contiguous United States. International Journal of Wildland Fire 24, 892-899.

Barrett, T.E., Robinson, E.M., Usenko, S., Sheesley, R.J., 2015. Source Contributions to Wintertime Elemental and Organic Carbon in the Western Arctic Based on Radiocarbon and Tracer Apportionment. Environ. Sci. Technol.

Barrett, T.E., Sheesley, R.J., 2014. Urban impacts on regional carbonaceous aerosols: Case study in central Texas. J. Air Waste Manag. Assoc. 64, 917-926.

Bean, J.K., Faxon, C.B., Leong, Y.J., Wallace, H.W., Cevik, B.K., Ortiz, S., Canagaratna, M.R., Usenko, S., Sheesley, R.J., Griffin, R.J., 2016. Composition and Sources of Particulate Matter Measured near Houston, TX: Anthropogenic-Biogenic Interactions. Atmosphere 7, 73.

Benetello, F., Squizzato, S., Hofer, A., Masiol, M., Khan, M.B., Piazzalunga, A., Fermo, P., Formenton, G.M., Rampazzo, G., Pavoni, B., 2017. Estimation of local and external contributions of biomass burning to PM 2.5 in an industrial zone included in a large urban settlement. Environ. Sci. Pollut. Res. 24, 2100-2115.

Birch, M., Cary, R., 1996. Elemental carbon-based method for monitoring occupational exposures to particulate diesel exhaust. Aerosol Sci. Technol. 25, 221-241.

Blanchard, C.L., Hidy, G.M., Tanenbaum, S., Edgerton, E., Hartsell, B., Jansen, J., 2008. Carbon in southeastern US aerosol particles: Empirical estimates of secondary organic aerosol formation. Atmos. Environ. 42, 6710-6720.

Bond, T.C., Streets, D.G., Yarber, K.F., Nelson, S.M., Woo, J.H., Klimont, Z., 2004. A technology-based global inventory of black and organic carbon emissions from combustion. J. Geophys. Res. Atmos. 109.

Brook, R.D., Rajagopalan, S., Pope, C.A., Brook, J.R., Bhatnagar, A., Diez-Roux, A.V., Holguin, F., Hong, Y., Luepker, R.V., Mittleman, M.A., 2010. Particulate matter air pollution and cardiovascular disease: an update to the scientific statement from the American Heart Association. Circulation 121, 2331-2378.

Cachier, H., Bremond, M.-P., Buat-Menard, P., 1989. Determination of atmospheric soot carbon with a simple thermal method. Tellus B. 41, 379-390.

Caicedo, V., Rappenglueck, B., Cuchiara, G., Flynn, J., Ferrare, R., Scarino, A., Berkoff, T., Senff, C., Langford, A., Lefer, B., 2019. Bay Breeze and Sea Breeze Circulation Impacts on the Planetary Boundary Layer and Air Quality From an Observed and Modeled DISCOVER-AQ Texas Case Study. J. Geophys. Res. Atmos. 124, 7359-7378.

Cao, J.-j., Chow, J.C., Tao, J., Lee, S.-c., Watson, J.G., Ho, K.-f., Wang, G.-h., Zhu, C.-s., Han, Y.-m., 2011. Stable carbon isotopes in aerosols from Chinese cities: Influence of fossil fuels. Atmos. Environ. 45, 1359-1363.

Chen, R., Zhao, Z., Kan, H., 2013. Heavy smog and hospital visits in Beijing, China. Am. J. Respir. Crit. Care Med. 188, 1170-1171.

Chow, J.C., Watson, J.G., Crow, D., Lowenthal, D.H., Merrifield, T., 2001. Comparison of IMPROVE and NIOSH carbon measurements. Aerosol Science & Technology 34, 23-34.

Chow, J.C., Watson, J.G., Fujita, E.M., Lu, Z., Lawson, D.R., Ashbaugh, L.L., 1994. Temporal and spatial variations of PM2. 5 and PM10 aerosol in the Southern California air quality study. Atmos. Environ. 28, 2061-2080.

Chung, C.E., Ramanathan, V., Decremer, D., 2012. Observationally constrained estimates of carbonaceous aerosol radiative forcing. Proc. Natl. Acad. Sci. 109, 11624-11629.

Claire, S.J., Dinh, T. M., Fanai, A. K., Nguyen, M. H., Schultz, S. A., 2015. Bay Area Emissions Inventory Summary Report: Greenhouse Gases. Base Year 2011. Bay Area Air Quality Management District.

Clark, A.E., Yoon, S., Sheesley, R.J., Usenko, S., 2015. Pressurized liquid extraction technique for the analysis of pesticides, PCBs, PBDEs, OPEs, PAHs, alkanes, hopanes, and steranes in atmospheric particulate matter. Chemosphere 137, 33-44.

Coulter, T.C., 2004. EPA-CMB8.2 Users Manual, in: Agency, U.S.E.P. (Ed.), Air Quality Modeling Group.

Czader, B.H., Choi, Y., Li, X., Alvarez, S., Lefer, B., 2015. Impact of updated traffic emissions on HONO mixing ratios simulated for urban site in Houston, Texas. Atmos. Chem. Phys. 15, 1253-1263.

Dechapanya, W., Russell, M., Allen, D.T., 2004. Estimates of anthropogenic secondary organic aerosol formation in Houston, Texas special issue of aerosol science and technology on findings from the fine particulate matter supersites program. Aerosol Sci. Technol. 38, 156-166.

Delfino, R.J., Murphy-Moulton, A.M., Becklake, M.R., 1998. Emergency room visits for respiratory illnesses among the elderly in Montreal: association with low level ozone exposure. Environ. Res. 76, 67-77.

Dockery, D.W., Pope, C.A., 1994. Acute respiratory effects of particulate air pollution. Ann. Rev. Pubic Health 15, 107-132.

Draxler, R., Rolph, G., 2010. HYSPLIT (HYbrid Single-Particle Lagrangian Integrated Trajectory), in: Laboratory, A.R. (Ed.), Silver Spring, MD. NOAA, p. 26.

Dunker, A.M., Koo, B., Yarwood, G., 2019. Source apportionment of organic aerosol and ozone and the effects of emission reductions. Atmos. Environ. 198, 89-101.

Edgerton, E.S., Casuccio, G.S., Saylor, R.D., Lersch, T.L., Hartsell, B.E., Jansen, J.J., Hansen, D.A., 2009. Measurements of OC and EC in coarse particulate matter in the southeastern United States. J. Air Waste Manag. Assoc. 59, 78-90.

Edney, E., Kleindienst, T., Jaoui, M., Lewandowski, M., Offenberg, J., Wang, W., Claeys, M., 2005. Formation of 2-methyl tetrols and 2-methylglyceric acid in secondary organic aerosol from laboratory irradiated isoprene/NOx/SO2/air mixtures and their detection in ambient PM2. 5 samples collected in the eastern United States. Atmos. Environ. 39, 5281-5289.

El-Zanan, H.S., Lowenthal, D.H., Zielinska, B., Chow, J.C., Kumar, N., 2005. Determination of the organic aerosol mass to organic carbon ratio in IMPROVE samples. Chemosphere 60, 485-496.

EPA, 2019. Texas Nonattainment/Maintenance Status for Each County by Year for All Criteria Pollutants, United States Environmental Protection Agency.

Fine, P.M., Cass, G.R., Simoneit, B.R., 2002. Chemical characterization of fine particle emissions from the fireplace combustion of woods grown in the southern United States. Environ. Sci. Technol. 36, 1442-1451.

Fraser, M., Yue, Z., Tropp, R., Kohl, S., Chow, J., 2002. Molecular composition of organic fine particulate matter in Houston, TX. Atmospheric Environment 36, 5751-5758.

Gentner, D.R., Jathar, S.H., Gordon, T.D., Bahreini, R., Day, D.A., El Haddad, I., Hayes, P.L., Pieber, S.M., Platt, S.M., de Gouw, J., Goldstein, A.H., Harley, R.A., Jimenez, J.L., Prévôt, A.S.H., Robinson, A.L., 2017. Review of Urban Secondary Organic Aerosol Formation from Gasoline and Diesel Motor Vehicle Emissions. Environ. Sci. Technol. 51, 1074-1093.

Glen, W.G., Zelenka, M.P., Graham, R.C., 1996. Relating meteorological variables and trends in motor vehicle emissions to monthly urban carbon monoxide concentrations. Atmospheric Environment 30, 4225-4232.

Gordon, T., Presto, A., May, A., Nguyen, N., Lipsky, E., Donahue, N., Gutierrez, A., Zhang, M., Maddox, C., Rieger, P., 2014. Secondary organic aerosol formation exceeds primary particulate matter emissions for light-duty gasoline vehicles. Atmospheric Chemistry and Physics 14, 4661-4678.

Gunsch, M.J., Schmidt, S.A., Gardner, D.J., Bondy, A.L., May, N.W., Bertman, S.B., Pratt, K.A., Ault, A.P., 2018. Particle growth in an isoprene-rich forest: Influences of urban, wildfire, and biogenic air masses. Atmos. Environ. 178, 255-264.

Gustafsson, Ö., Kruså, M., Zencak, Z., Sheesley, R.J., Granat, L., Engström, E., Praveen, P., Rao, P., Leck, C., Rodhe, H., 2009. Brown clouds over South Asia: biomass or fossil fuel combustion? Science 323, 495-498.

Hansen, A., Rosen, H., Novakov, T., 1983. Aethalometer-an instrument for the real-time measurement of optical absorption by aerosol particles. Lawrence Berkeley Lab., CA (USA).

Hao, L.Q., Kortelainen, A., Romakkaniemi, S., Portin, H., Jaatinen, A., Leskinen, A., Komppula, M., Miettinen, P., Sueper, D., Pajunoja, A., Smith, J.N., Lehtinen, K.E.J., Worsnop, D.R., Laaksonen, A., Virtanen, A., 2014. Atmospheric submicron aerosol composition and particulate organic nitrate formation in a boreal forestland–urban mixed region. Atmos. Chem. Phys. 14, 13483-13495.

Hildemann, L.M., Klinedinst, D.B., Klouda, G.A., Currie, L.A., Cass, G.R., 1994. Sources of urban contemporary carbon aerosol. Environ. Sci. Technol. 28, 1565-1576.

Hong, L., Liu, G., Zhou, L., Li, J., Xu, H., Wu, D., 2017. Emission of organic carbon, elemental carbon and water-soluble ions from crop straw burning under flaming and smoldering conditions. Particuology 31, 181-190.

Huang, R.-J., Zhang, Y., Bozzetti, C., Ho, K.-F., Cao, J.-J., Han, Y., Daellenbach, K.R., Slowik, J.G., Platt, S.M., Canonaco, F., 2014. High secondary aerosol contribution to particulate pollution during haze events in China. Nature 514, 218.

Kanakidou, M., Seinfeld, J., Pandis, S., Barnes, I., Dentener, F., Facchini, M., Dingenen, R.V., Ervens, B., Nenes, A., Nielsen, C., 2005. Organic aerosol and global climate modelling: a review. Atmos. Chem. Phys. 5, 1053-1123.

Kavouras, I.G., Stephanou, E.G., 2002. Particle size distribution of organic primary and secondary aerosol constituents in urban, background marine, and forest atmosphere. J. Geophys. Res. Atmos. 107, AAC 7-1-AAC 7-12.

Kim, B.M., Teffera, S., Zeldin, M.D., 2000. Characterization of PM25 and PM10 in the South Coast air basin of Southern California: part 1—spatial variations. J. Air Waste Manag. Assoc. 50, 2034-2044.

Kirchstetter, T.W., Preble, C.V., Hadley, O.L., Bond, T.C., Apte, J.S., 2017. Large reductions in urban black carbon concentrations in the United States between 1965 and 2000. Atmos. Environ. 151, 17-23.

Kleindienst, T.E., Jaoui, M., Lewandowski, M., Offenberg, J.H., Lewis, C.W., Bhave, P.V., Edney, E.O., 2007. Estimates of the contributions of biogenic and anthropogenic hydrocarbons to secondary organic aerosol at a southeastern US location. Atmos. Environ. 41, 8288-8300.

Kleinman, L.I., Daum, P., Imre, D., Lee, Y.N., Nunnermacker, L., Springston, S., Weinstein-Lloyd, J., Rudolph, J., 2002. Ozone production rate and hydrocarbon reactivity in 5 urban areas: A cause of high ozone concentration in Houston. Geophysical Research Letters 29, 105-101-105-104.

Kleinman, L.I., Daum, P.H., Lee, Y.N., Nunnermacker, L.J., Springston, S.R., Weinstein-Lloyd, J., Rudolph, J., 2005. A comparative study of ozone production in five US metropolitan areas. J. Geophys. Res. Atmos. 110.

Laden, F., Neas, L.M., Dockery, D.W., Schwartz, J., 2000. Association of fine particulate matter from different sources with daily mortality in six US cities. Environ. Health Perspect. 108, 941.

Lee, T., Yu, X.-Y., Ayres, B., Kreidenweis, S.M., Malm, W.C., Collett Jr, J.L., 2008. Observations of fine and coarse particle nitrate at several rural locations in the United States. Atmos. Environ. 42, 2720-2732.

Lefer, B., Rappenglück, B., Flynn, J., Haman, C., 2010. Photochemical and meteorological relationships during the Texas-II Radical and Aerosol Measurement Project (TRAMP). Atmos. Environ. 44, 4005-4013.

Lemire, K.R., Allen, D.T., Klouda, G.A., Lewis, C.W., 2002. Fine particulate matter source attribution for Southeast Texas using 14C/13C ratios. J. Geophys. Res. Atmos. 107, ACH 3-1-ACH 3-7.

Leong, Y., Sanchez, N., Wallace, H., Karakurt Cevik, B., Hernandez, C., Han, Y., Flynn, J., Massoli, P., Floerchinger, C., Fortner, E., 2017. Overview of surface measurements and spatial characterization of submicrometer particulate matter during the DISCOVER-AQ 2013 campaign in Houston, TX. J. Air Waste Manag. Assoc. 67, 854-872.

Levy, M.E., Zhang, R., Khalizov, A.F., Zheng, J., Collins, D.R., Glen, C.R., Wang, Y., Yu, X.Y., Luke, W., Jayne, J.T., 2013. Measurements of submicron aerosols in Houston, Texas during the 2009 SHARP field campaign. J. Geophys. Res. Atmos. 118, 10,518-510,534.

Lewandowski, M., Piletic, I.R., Kleindienst, T.E., Offenberg, J.H., Beaver, M.R., Jaoui, M., Docherty, K.S., Edney, E.O., 2013. Secondary organic aerosol characterisation at field sites across the United States during the spring–summer period. International journal of environmental analytical chemistry 93, 1084-1103.

Lewis, C.W., Klouda, G.A., Ellenson, W.D., 2004. Radiocarbon measurement of the biogenic contribution to summertime PM-2.5 ambient aerosol in Nashville, TN. Atmos. Environ. 38, 6053-6061.

Lewis, C.W., Stiles, D.C., 2006. Radiocarbon content of PM2. 5 ambient aerosol in Tampa, FL. Aerosol Sci. Technol. 40, 189-196.

Li, X., Choi, Y., Czader, B., Roy, A., Kim, H., Lefer, B., Pan, S., 2016. The impact of observation nudging on simulated meteorology and ozone concentrations during DISCOVER-AQ 2013 Texas campaign. Atmos. Chem. Phys 16, 3127-3144.

Lough, G.C., Christensen, C.G., Schauer, J.J., Tortorelli, J., Mani, E., Lawson, D.R., Clark, N.N., Gabele, P.A., 2007. Development of molecular marker source profiles for emissions from on-road gasoline and diesel vehicle fleets. J. Air Waste Manag. Assoc. 57, 1190-1199.

Loughner, C.P., Allen, D.J., Pickering, K.E., Zhang, D.-L., Shou, Y.-X., Dickerson, R.R., 2011. Impact of fair-weather cumulus clouds and the Chesapeake Bay breeze on pollutant transport and transformation. Atmos. Environ. 45, 4060-4072.

Lubertino, G., 2019. Transportation Air Quality Conformity Report for the Houston-Brazoria-Galveston Region: 2045 Regional Transportation Plan. Houston-Galveston Area Council.

Massoli, P., Bates, T., Quinn, P., Lack, D., Baynard, T., Lerner, B., Tucker, S., Brioude, J., Stohl, A., Williams, E., 2009. Aerosol optical and hygroscopic properties during TexAQS-GoMACCS 2006 and their impact on aerosol direct radiative forcing. J. Geophys. Res. Atmos. 114.

Mazzuca, G.M., Ren, X., Loughner, C.P., Estes, M., Crawford, J.H., Pickering, K.E., Weinheimer, A.J., Dickerson, R.R., 2016. Ozone production and its sensitivity to NOx and VOCs: Results from the DISCOVER-AQ field experiment, Houston 2013. Atmos. Chem. Phys. 16, 14463–14474.

Mouteva, G.O., Randerson, J.T., Fahrni, S.M., Bush, S.E., Ehleringer, J.R., Xu, X., Santos, G.M., Kuprov, R., Schichtel, B.A., Czimczik, C.I., 2017. Using radiocarbon to constrain black and organic carbon aerosol sources in Salt Lake City. J. Geophys. Res. Atmos. 122, 9843-9857.

NASA, 2019. DISCOVER-AQ, National Aeronautics and Space Administration.

Norris, G., Vedantham, R., Wade, K., Brown, S., Prouty, J., Foley, C., 2008. EPA Positive Matrix Factorization (PMF) 3.0 Fundamentals and User Guide, in: EPA (Ed.).

Novakov, T., Penner, J., 1993. Large contribution of organic aerosols to cloud-condensation-nuclei concentrations. Nature 365, 823.

Nowak, D.J., Bodine, A.R., Hoehn, R.E.I., Edgar, C.B., Riely, G., Hartel, D.R., Dooley, K.J., Stanton, S.M., Hatfield, M.A., Brandeis, T.J., Lister, T.W., 2017. Houston's Urban Forest, 2015. United States Department of Agriculture, U.S. Forest Service.

Offenberg, J.H., Baker, J.E., 2000. Aerosol size distributions of elemental and organic carbon in urban and over-water atmospheres. Atmos. Environ. 34, 1509-1517.

Olaguer, E.P., Kolb, C.E., Lefer, B., Rappenglück, B., Zhang, R., Pinto, J.P., 2014. Overview of the SHARP campaign: motivation, design, and major outcomes. J. Geophys. Res. Atmos. 119, 2597-2610.

Paatero, P., 1997. Least squares formulation of robust non-negative factor analysis. Chemometrics and Intelligent Laboratory Systems 37, 23-35.

Paatero, P., Hopke, P.K., 2003. Discarding or downweighting high-noise variables in factor analytic models. Analytica Chimica Acta 490, 277-289.

Paatero, P., Tapper, U., 1994. Positive matrix factorization - a nonnegative factor model with optimal utilization of error-estimates of data values. Environmetrics 5, 111-126.

Park, C., Schade, G.W., Boedeker, I., 2011. Characteristics of the flux of isoprene and its oxidation products in an urban area. J. Geophys. Res. Atmos. 116, D21303.

Parrish, D., Allen, D., Bates, T., Estes, M., Fehsenfeld, F., Feingold, G., Ferrare, R., Hardesty, R., Meagher, J., Nielsen-Gammon, J., 2009. Overview of the second Texas air quality study (TexAQS II) and the Gulf of Mexico atmospheric composition and climate study (GoMACCS). J. Geophys. Res. Atmos. 114.

Ram, K., Sarin, M., 2011. Day–night variability of EC, OC, WSOC and inorganic ions in urban environment of Indo-Gangetic Plain: implications to secondary aerosol formation. Atmos. Environ. 45, 460-468.

Rattigan, O.V., Felton, H.D., Bae, M.-S., Schwab, J.J., Demerjian, K.L., 2010. Multi-year hourly PM2. 5 carbon measurements in New York: Diurnal, day of week and seasonal patterns. Atmos. Environ. 44, 2043-2053.

Riley, K.L., Abatzoglou, J.T., Grenfell, I.C., Klene, A.E., Heinsch, F.A., 2013. The relationship of large fire occurrence with drought and fire danger indices in the western USA, 1984–2008: the role of temporal scale. International Journal of Wildland Fire 22, 894-909.

Rogge, W.F., Hildemann, L.M., Mazurek, M.A., Cass, G.R., Simoneit, B.R., 1993. Sources of fine organic aerosol. 4. Particulate abrasion products from leaf surfaces of urban plants. Environ. Sci. Technol. 27, 2700-2711.

Russell, L.M., 2003. Aerosol organic-mass-to-organic-carbon ratio measurements. Environ. Sci. Technol. 37, 2982-2987.

Ryerson, T., Trainer, M., Angevine, W., Brock, C., Dissly, R., Fehsenfeld, F., Frost, G., Goldan, P., Holloway, J., Hübler, G., 2003. Effect of petrochemical industrial emissions of reactive alkenes and NOx on tropospheric ozone formation in Houston, Texas. J. Geophys. Res. Atmos. 108.

Schauer, J.J., 2003. Evaluation of elemental carbon as a marker for diesel particulate matter. J. Expo. Sci. Environ. Epidemiol. 13, 443.

Schauer, J.J., Cass, G.R., 2000. Source apportionment of wintertime gas-phase and particle-phase air pollutants using organic compounds as tracers. Environ. Sci. Technol. 34, 1821-1832.

Schauer, J.J., Rogge, W.F., Hildemann, L.M., Mazurek, M.A., Cass, G.R., Simoneit, B.R.T., 1996. Source apportionment of airborne particulate matter using organic compounds as tracers. Atmos.Environ. 30, 3837-3855.

Schmid, O., Artaxo, P., Arnott, W., Chand, D., Gatti, L.V., Frank, G., Hoffer, A., Schnaiter, M., Andreae, M., 2006. Spectral light absorption by ambient aerosols influenced by biomass burning in the Amazon Basin. I: Comparison and field calibration of absorption measurement techniques. Atmos. Chem. Phys. 6, 3443-3462.

Schulze, B.C., Wallace, H.W., Bui, A.T., Flynn, J.H., Erickson, M.H., Alvarez, S., Dai, Q., Usenko, S., Sheesley, R.J., Griffin, R.J., 2018. The impacts of regional shipping emissions on the chemical characteristics of coastal submicron aerosols near Houston, TX. Atmos. Chem. Phys. 18, 14217-14241.

Shahid, I., Kistler, M., Mukhtar, A., Ghauri, B.M., Ramirez-Santa Cruz, C., Bauer, H., Puxbaum, H., 2016. Chemical characterization and mass closure of PM10 and PM2. 5 at an urban site in Karachi–Pakistan. Atmos. Environ. 128, 114-123.

Shakya, K.M., Louchouarn, P., Griffin, R.J., 2011. Lignin-derived phenols in Houston aerosols: Implications for natural background sources. Environ. Sci. Technol. 45, 8268-8275.

Sheesley, R.J., Schauer, J.J., Zheng, M., Wang, B., 2007. Sensitivity of molecular marker-based CMB models to biomass burning source profiles. Atmos. Environ. 41, 9050-9063.

Shilling, J.E., Zaveri, R.A., Fast, J.D., Kleinman, L., Alexander, M., Canagaratna, M.R., Fortner, E., Hubbe, J.M., Jayne, J.T., Sedlacek, A., 2013. Enhanced SOA formation from mixed anthropogenic and biogenic emissions during the CARES campaign. Atmos. Chem. Phys. 13, 2091-2113.

Shiraiwa, M., Yee, L.D., Schilling, K.A., Loza, C.L., Craven, J.S., Zuend, A., Ziemann, P.J., Seinfeld, J.H., 2013. Size distribution dynamics reveal particle-phase chemistry in organic aerosol formation. Proc. Natl. Acad. Sci. 110, 11746-11750.

Simoneit, B.R.T., Schauer, J.J., Nolte, C.G., Oros, D.R., Elias, V.O., Fraser, M.P., Rogge, W.F., Cass, G.R., 1999. Levoglucosan, a tracer for cellulose in biomass burning and atmospheric particles. Atmos. Environ. 33, 173-182.

Snyder, D.C., Schauer, J.J., 2007. An inter-comparison of two black carbon aerosol instruments and a semi-continuous elemental carbon instrument in the urban environment. Aerosol Sci. Technol. 41, 463-474.

Spracklen, D., Carslaw, K., Pöschl, U., Rap, A., Forster, P., 2011. Global cloud condensation nuclei influenced by carbonaceous combustion aerosol. Atmos. Chem. Phys. 11, 9067-9087.

Stauffer, R.M., Thompson, A.M., 2015. Bay breeze climatology at two sites along the Chesapeake bay from 1986–2010: Implications for surface ozone. Journal of atmospheric chemistry 72, 355-372.

Stone, E.A., Schauer, J.J., Pradhan, B.B., Dangol, P.M., Habib, G., Venkataraman, C., Ramanathan, V., 2010. Characterization of emissions from South Asian biofuels and application to source apportionment of carbonaceous aerosol in the Himalayas. Journal of Geophysical Research: Atmospheres 115.

Strader, R., Lurmann, F., Pandis, S.N., 1999. Evaluation of secondary organic aerosol formation in winter. Atmos. Environ. 33, 4849-4863.

Stuiver, M., Polach, H.A., 1977. Discussion; reporting of C-14 data. Radiocarbon 19, 355-363.

Sullivan, D.W., Price, J.H., Lambeth, B., Sheedy, K.A., Savanich, K., Tropp, R.J., 2013a. Field study and source attribution for PM2.5 and PM10 with resulting reduction in concentrations in the neighborhood north of the Houston Ship Channel based on voluntary efforts. J. Air Waste Manage. Assoc. 63, 1070-1082.

Sullivan, D.W., Price, J.H., Lambeth, B., Sheedy, K.A., Savanich, K., Tropp, R.J., 2013b. Field study and source attribution for PM2. 5 and PM10 with resulting reduction in concentrations in the neighborhood north of the Houston Ship Channel based on voluntary efforts. J. Air Waste Manag. Assoc. 63, 1070-1082.

Sun, Y.L., Zhang, Q., Schwab, J.J., Yang, T., Ng, N.L., Demerjian, K.L., 2012. Factor analysis of combined organic and inorganic aerosol mass spectra from high resolution aerosol mass spectrometer measurements. Atmospheric Chemistry and Physics 12, 8537-8551.

Surratt, J.D., Chan, A.W., Eddingsaas, N.C., Chan, M., Loza, C.L., Kwan, A.J., Hersey, S.P., Flagan, R.C., Wennberg, P.O., Seinfeld, J.H., 2010. Reactive intermediates revealed in secondary organic aerosol formation from isoprene. Proc. Natl. Acad. Sci. 107, 6640-6645.

TCEQ, 2018. Texas Air Monitoring Information System (TAMIS) Web Interface, Texas Commission on Environmental Quality.

Tian, S., Pan, Y., Liu, Z., Wen, T., Wang, Y., 2019. Reshaping the size distribution of aerosol elemental carbon by removal of coarse mode carbonates. Atmos. Environ. 214, 116852.

Tsigaridis, K., Daskalakis, N., Kanakidou, M., Adams, P., Artaxo, P., Bahadur, R., Balkanski, Y., Bauer, S., Bellouin, N., Benedetti, A., 2014. The AeroCom evaluation and intercomparison of organic aerosol in global models. Atmos. Chem. Phys. 14, 10845-10895.

Tucker, S.C., Banta, R.M., Langford, A.O., Senff, C.J., Brewer, W.A., Williams, E.J., Lerner, B.M., Osthoff, H.D., Hardesty, R.M., 2010. Relationships of coastal nocturnal boundary layer winds and turbulence to Houston ozone concentrations during TexAQS 2006. J. Geophys. Res. Atmos. 115.

Turpin, B.J., Huntzicker, J.J., 1995. Identification of secondary organic aerosol episodes and quantitation of primary and secondary organic aerosol concentrations during SCAQS. Atmos. Environ. 29, 3527-3544.

Turpin, B.J., Huntzicker, J.J., Larson, S.M., Cass, G.R., 1991. Los Angeles summer midday particulate carbon: primary and secondary aerosol. Environ. Sci. Technol. 25, 1788-1793.

Ulbrich, I.M., Canagaratna, M.R., Zhang, Q., Worsnop, D.R., Jimenez, J.L., 2009. Interpretation of organic components from Positive Matrix Factorization of aerosol mass spectrometric data. Atmospheric Chemistry and Physics 9, 2891-2918.

Viana, M., Maenhaut, W., Ten Brink, H., Chi, X., Weijers, E., Querol, X., Alastuey, A., Mikuška, P., Večeřa, Z., 2007. Comparative analysis of organic and elemental carbon concentrations in carbonaceous aerosols in three European cities. Atmos. Environ. 41, 5972-5983.

Wallace, H.W., Sanchez, N.P., Flynn, J.H., Erickson, M.H., Lefer, B.L., Griffin, R.J., 2018. Source apportionment of particulate matter and trace gases near a major refinery near the Houston Ship Channel. Atmos. Environ. 173, 16-29.

Wang, Y., Jia, B., Wang, S.-C., Estes, M., Shen, L., Xie, Y., 2016. Influence of the Bermuda High on interannual variability of summertime ozone in the Houston–Galveston–Brazoria region. Atmospheric Chemistry and Physics 16, 15265-15276.

Weber, R.J., Sullivan, A.P., Peltier, R.E., Russell, A., Yan, B., Zheng, M., De Gouw, J., Warneke, C., Brock, C., Holloway, J.S., 2007. A study of secondary organic aerosol formation in the anthropogenic-influenced southeastern United States. J. Geophys. Res. Atmos. 112.

Weingartner, E., Saathoff, H., Schnaiter, M., Streit, N., Bitnar, B., Baltensperger, U., 2003. Absorption of light by soot particles: determination of the absorption coefficient by means of aethalometers. J. Aerosol Sci. 34, 1445-1463.

Westerling, A.L., Hidalgo, H.G., Cayan, D.R., Swetnam, T.W., 2006. Warming and earlier spring increase western US forest wildfire activity. Science 313, 940-943.

Wong, K., Tsai, C., Lefer, B., Haman, C., Grossberg, N., Brune, W., Ren, X., Luke, W., Stutz, J., 2012. Daytime HONO vertical gradients during SHARP 2009 in Houston, TX. Atmos. Chem. Phys. 12, 635-652.

Xu, L., Suresh, S., Guo, H., Weber, R.J., Ng, N.L., 2015. Aerosol characterization over the southeastern United States using high-resolution aerosol mass spectrometry: spatial and seasonal variation of aerosol composition and sources with a focus on organic nitrates. Atmospheric Chemistry and Physics 15, 7307-7336.

Yoon, S., Ortiz, S., Clark, A.E., Barrett, T.E., Usenko, S., Duvall, R.M., Hildebrandt Ruiz, L., Bean, J.K., Faxon, C.B., Flynn, J., leong, Y.J., Griffin, R., Sheesley, R.J., under review. Apportioned primary and secondary organic aerosol during pollution events of DISCOVER-AQ Houston, Atmos. Environ.

Zeng, T., Wang, Y., 2011. Nationwide summer peaks of OC/EC ratios in the contiguous United States. Atmos. Environ. 45, 578-586.

Zhang, H., Yee, L.D., Lee, B.H., Curtis, M.P., Worton, D.R., Isaacman-VanWertz, G., Offenberg, J.H., Lewandowski, M., Kleindienst, T.E., Beaver, M.R., 2018. Monoterpenes are the largest source of summertime organic aerosol in the southeastern United States. Proc. Natl. Acad. Sci. 115, 2038-2043.

Zhang, Q., Jimenez, J.L., Canagaratna, M.R., Ulbrich, I.M., Ng, N.L., Worsnop, D.R., Sun, Y.L., 2011. Understanding atmospheric organic aerosols via factor analysis of aerosol mass spectrometry: a review. Anal. Bioanal. Chem. 401, 3045-3067.

Zhang, X., Craft, E., Zhang, K., 2017. Characterizing spatial variability of air pollution from vehicle traffic around the Houston Ship Channel area. Atmos. Environ. 161, 167-175.

Zhang, Y., Zotter, P., Perron, N., Prévôt, A., Wacker, L., Szidat, S., 2013. Fossil and non-fossil sources of different carbonaceous fractions in fine and coarse particles by radiocarbon measurement. Radiocarbon 55, 1510-1520.

Zheng, M., Ke, L., Edgerton, E.S., Schauer, J.J., Dong, M., Russell, A.G., 2006. Spatial distribution of carbonaceous aerosol in the southeastern United States using molecular markers and carbon isotope data. J. Geophys. Res. Atmos. 111.

Zhou, W., Cohan, D., Henderson, B., 2014. Slower ozone production in Houston, Texas following emission reductions: evidence from Texas Air Quality Studies in 2000 and 2006. Atmos. Chem. Phys. 14, 2777-2788.

Zotter, P., El-Haddad, I., Zhang, Y., Hayes, P.L., Zhang, X., Lin, Y.H., Wacker, L., Schnelle-Kreis, J., Abbaszade, G., Zimmermann, R., 2014. Diurnal cycle of fossil and nonfossil carbon using radiocarbon analyses during CalNex. J. Geophys. Res. Atmos. 119, 6818-6835.